Sclerostin Antibody as a Treatment for Osteogenesis Imperfecta

by

Benjamin P. Sinder

A dissertation submitted in partial fulfillment
of the requirements for the degree of
Doctor of Philosophy
(Biomedical Engineering)
in the University of Michigan
2014

Doctoral Committee:

Assistant Professor Kenneth M. Kozloff, Chair
Assistant Professor Michelle S. Caird
Professor David H. Kohn
Professor Laurie K. McCauley

To my Mom and Dad.

Acknowledgements

Thanks to Jason Kutch for being a great research mentor in the Summer of 2007, and setting an example that encouraged me to pursue graduate school.

I would like to thank my committee of Ken Kozloff, Michelle Caird, Dave Kohn, and Laurie McCauley for their contributions to this work. Although it seems like forever, it wasn't that long ago I was just another student in Ken's office asking him if OI was "kind of like osteoporosis". Since then, Ken has provided support, guidance, and an environment that are directly responsible for my development as a scientist. When Ken attempted to explain a set of osteoclast + bisphosphonate data I had produced in my first year of graduate school by making an analogy to the movie *Airplane!*, I had a feeling I had found the right lab.

"Other" members of my committee include Laurie McCauley, Dave Kohn, and Michelle Caird. I am not writing about them because I am supposed to - each contributed significantly to my development. In the name of youthful enthusiasm, I scanned a lot of microCT samples for members of the McCauley lab in my beginning years of graduate school. Inevitably, I learned a thing or two about microCT, but gained more by observing how an established lab operates and publishes papers.

It is true, Dr. Michelle Caird did provide the cliché "clinical" perspective. But I'm more appreciative of other things. As one example of many, although we only attended several conferences together, she dragged multiple established professors over to my poster or invited me to join them for lunch.

Dave Kohn probably doesn't know this, but he is a main reason that I wound up working for Ken. At the time, I was a bit scared of all things biology, but several comments he made during my graduate school visit to Michigan influenced my decision.

Mike Ominsky was not a committee member of mine, but I always enjoyed our discussions about data. His insight was often unique, but always on point.

Thanks to Joan Marini for her insightful comments about OI and the Brtl/+ mouse model.

Thanks to Bill Lloyd and Mike Morris for their Raman spectroscopy analysis related to Chapter 5 – it was a pleasure working with you.

Thanks to Mary Eddy, Logan White, and Joe Salemi. Each of you contributed significantly to this work, and moreover, were fun to work with.

I'd also like to thank my funding sources. In particular, Rackham provided early graduate funding and travel grants, NIH R01AR062522, and ASBMR for numerous awards and travel support to great meetings in cool locations that I wouldn't have otherwise been able to attend.

Thanks to the ORL for being a great place to do research. The resources, both in equipment and personal, are tremendous. In particular, Bonnie Nolan contributed a large amount of work towards data included in this dissertation, and even more to several studies beforehand. Not only did Bonnie make the animal work go faster and better, but we always had a good time doing it. All things administrative were always "magically" taken care of. That magic is Sharon and Peggy, who were always proactive and had things in order. To John Baker – thanks for all the histology assistance, and even more for the fun times working together. I wish you the best in your upcoming retirement! To tomkat (not celebrity couple) – I miss your funny emails and brand of humor. To Charles - a visit to the shop was always well worth it, and I often left with

much more than the single tool I needed. To Ed, Einor, and Rob, thanks for keeping the computers alive, and always providing an interesting conversation.

To prior trainees Jacque, Grant, Jason, Ethan, Connie, Jeff, Danese, and Erik – you set the bar high and made the lab a good place to be. I learned from each of you, appreciate advice you gave, and the example you set. To Joey and Neil – it was great working with together, and I always had fun with you at conferences or hanging out after work. To the current ORL generation of David, Diana, Steve, Lauren, Eugene, Erin, Laura, Shan and Christophe – I enjoyed working alongside all of you, keep the science alive.

To Mathieu. Whether it was carpooling to indoor soccer in a snowstorm, talking science, or karaoke at a conference – we always had a good time. Thanks for being a great lab mate.

To Dana. Thanks for being a good friend, making the lab fun, and showing me the wonder of froyo. To Reese - thanks for letting me be your other roommate on short notice.

To Danielle. These last several years have been much more enjoyable with you. Thanks for never making me feel guilty about staying late at lab, and always making me smile.

Finally, I'd like to thank my parents. Any success of mine is a direct result of your past and continued support.

Table of Contents

List of Figures

List of Tables

CHAPTER 1

Introduction

Osteogenesis Imperfecta

Osteogenesis imperfecta (OI), or "brittle bone disease", is a genetic disorder of collagen characterized by brittle bones [1]. Patients with OI have increased bone fragility and are susceptible to fracture from minimal force. In many cases, skeletal deformities and short stature are also observed. OI fragility symptoms tend to be most prominent in children, although the condition often persists throughout life. The increased bone fragility of OI can be related to reductions in tissue quality or tissue amount or both.

Classically, OI was identified as an autosomal dominant genetic disorder, and these account for approximately 90% of the genetic mutations in OI. More recently, recessive OI mutations have been found in proteins that participate in prolyl 3-hydroxylation or those responsible for proper folding of the collagen triple helix [2–4]. Collectively, recessive OI only accounts for ~10% of all cases.

The cause of OI is not singular, but rather arises from hundreds of different genetic mutations associated with Type I collagen [5]. As a result of this large number of mutations, there is a wide variety of clinical presentation. For example, some cases of autosomal dominant OI are a mild form caused by a deficient *COL1A1* allele. As the other functioning *COL1A1* allele remains in these patients, they can synthesize normal collagen heterotrimers, but do so at a

slower rate[6]. While patients with this mutation do exhibit increased bone fragility, they have relatively normal stature and minimal bone deformity. Conversely, patients with mutations that feature an amino acid substitution within either *COL1A1* or *COL1A2* allele can have a more severe phenotype. Every third amino acid on *COL1A1* or *COL1A2* allele is a glycine – the smallest of the 20 amino acids. OI mutations are commonly an amino acid substitutions for a single glycine residue [7]. The specific amino acid substitution, as well as specific position of this substitution along a *COL1A1* or *COL1A2* allele, influences the phenotype of the specific mutation. Patients with these substitutions can be perinatal lethal. Alternatively, depending on the specific mutation, many survive. The range of presentation includes wheelchair bound patients with progressive limb deformity and extremely high fracture risk, and patients who achieve ambulation with moderate fracture risk.

Before genetic technology allowed researchers the ability to determine the specific mutation in an OI patient, they were classified into groups based upon clinical presentation. These initial efforts were made by Sillence, and consist of a numerical classification scheme [8]. Briefly, Type I OI describes those with a single functioning *COL1A1* allele and present moderately [6]. Type II OI is characterized by perinatal lethality [9]. Of surviving OI types, Type III patients have the most severe form, with progressive severe limb deformity and extreme fracture risk. Type IV OI represents a less severe form of OI, and although patients suffer many fractures, they are typically able to achieve ambulation. Additional types exist, but these four comprise the bulk of OI cases, and include the specific type of OI studied in this dissertation. While efforts to correlate genotype to phenotype have revealed patterns and provided mechanistic insight for OI and collagen, clinical presentation and Sillence Type remain the standard way to categorize patients and treatment regimens.

OI is a highly variable disease, and what is true of a specific case of OI is not generalizable to all. However, several features frequently exist in OI. Most importantly, patients with OI have significantly reduced bone mass, and in many cases, altered bone material properties. At the cellular level, patients frequently have increased osteoclastic bone resorption [10, 11]. While greater remodeling also increases bone formation, the inferred bone formation per cell in OI is less than normal [11]. The phenotype of OI becomes less severe with time, and fracture rates often decrease after puberty [12]. In addition, patients with OI are frequently short in stature. Finally, a recent report in several OI mouse models suggests that elevated TGF-β levels may be a common factor in the pathology of OI [13].

The Brtl/+ Mouse Model of Osteogenesis Imperfecta

Brtl/+ is a mouse model of moderately severe Type IV OI. Brtl/+ is heterozygous for a glycine to cysteine substitution at the 349th position of one *col1a1* allele [14]. The Brtl/+ mouse was created to reproduce a mutation found in a child with Type IV OI and as such, reproduces many features of the typical OI phenotype. These include reduced bone mass and strength, particularly in young animals – which mimics the phenotypic reduction in OI fracture risk with age. The material properties of Brtl/+ matrix are also altered, and increased brittleness and mineralization have been observed [15, 16]. At the cellular level, Brtl/+ has increased osteoclast surface with a concomitant reduction, or no change, in bone formation, depending on animal age [17]. In culture, Brtl/+ osteoclasts demonstrate increased bone resorption similar to the *in vivo* phenotype [17, 18]. Interestingly, initial cell-matrix exchange experiments suggest that the Brtl/+ matrix may cause some of the observed osteoclast differences independent of intrinsic differences in Brtl/+ cells [16, 18]. In addition, increased endoplasmic reticulum size due to

retention of mutant collagen has been observed in Brtl/+ fibroblasts, and may relate to osteoblast differences [19]. In summary, the Brtl/+ mouse is appropriate for studying candidate OI treatments in young and adult mice because it recapitulates a clinically observed mutation as well as the adaptation of an OI skeleton over time.

Treatments for OI Patients

Presently, the most common drug therapy for the treatment of pediatric OI are anti-resorptive bisphosphonates. The anti-resorptive nature of bisphosphonates is appealing as increased bone turnover has been observed in OI [10, 11]. However, the results from controlled pediatric OI clinical trials suggest a mixed efficacy in reducing fractures [20–24]. While effective at increasing vertebral BMD and sometimes vertebral functional outcomes such as vertebral height, an effect on long bone fracture rate is often absent. Moreover, while bisphosphonates are generally well tolerated, there are several concerns about their application in a growing skeleton. These include retention of calcified cartilage, long term retention of bisphosphonates in the skeleton, and potential for altered growth dynamics [25–28]. On the anabolic side, growth hormone therapy has been shown to increase linear growth rates in *some* pediatric OI patients. However, in the ~50% patients where growth hormone does not have a discernible benefit, it may even exacerbate the OI phenotype by increasing osteoclast surface [29]. Parathyroid hormone, while an approved anabolic therapy for osteoporosis, is not available for use in pediatric OI patients with an open growth plate due to a risk of osteosarcoma [30].

In adult OI, bisphosphonates are also used in the clinic despite limited clinical trials. The data suggests bisphosphonates are effective at increasing BMD in the axial skeleton, but fracture rate benefits are inconclusive [31–34]. Unlike pediatric OI, anabolic parathyroid hormone is not

contraindicated due to risk of osteosarcoma for use in adult OI. Initial studies investigating teriparitide in adults with OI suggest that it is effective in patients with Type I OI, but not in Type III and IV [35].

More effective therapies are needed for both pediatric and adult OI and no consistently effective anabolic therapy has been established in either case.

Sclerostin and Early Use of Sclerostin Inhibiting Antibodies

Sclerostin is a potent inhibitor of bone formation, named after a mutation in the protein was found to cause the long-diagnosed clinical bone overgrowth condition sclerosteosis [36, 37]. An absence of sclerostin is observed in patients with bone overgrowth in sclerosteosis, implicating the protein as an inhibitor of bone formation. Physiologically, sclerostin is secreted by osteocytes and it is currently thought that sclerostin passes through the canalicular network to the bone surface [38]. Once at the bone surface, sclerostin is purported to bind LRP4, LRP5 and LRP6 on osteoblasts and inhibit canonical Wnt/beta-catenin signaling [38–40]. *SOST* KO murine models recapitulate the skeletal overgrowth condition and have extremely high levels of bone formation, without a large increase in bone resorption[41].

As sclerostin is a potent inhibitor of bone formation, monoclonal inhibiting antibodies to sclerostin (Scl-Ab) have been developed by several pharmaceutical companies, and are presently in clinical trials for the treatment of osteoporosis and have demonstrated anabolic efficacy [42, 43]. Preclinical studies have confirmed the anabolic potential, as well as examined the mechanism, in a variety of models. In a rat ovariectomy model, Scl-Ab was able to increase bone mass and strength to levels the same as, or significantly greater than, sham controls [44]. This was primarily a result of large increases in bone formation rates of ~100% to ~1000%,

depending on skeletal site. A decrease in osteoclast surface was observed, suggesting an uncoupling of resorption from formation. Moreover, detailed histologic study has revealed that Scl-Ab primarily increases bone mass by stimulation of modeling based formation [45]. Unique from anabolic PTH, where increased remodeling can be blunted by antiresorptive therapy, Scl-Ab induced bone gains are not affected by prior, or co-treatment with a bisphosphonate [46].

Global Hypothesis

Given the lack of anabolic treatment options for OI outlined above, and the anabolic potential of Scl-Ab, this thesis will investigate the following global hypothesis:

In rapidly growing and adult Brtl/+ models of OI, Scl-Ab will increase bone formation, resulting in increased bone mass and strength, without affecting the underlying alteration in material property and composition.

Chapter Overview

Chapter 2 of this thesis describes the first report of Scl-Ab in a mouse model of OI [47]. Specifically, it demonstrates the anabolic efficacy of Scl-Ab using a short-term 2 week treatment protocol in an 8 week old Brtl/+ mouse model. Significant gains in bone formation were observed by dynamic histomorphometry, as well as increased serum osteocalcin. Surprisingly, whole bone mass and strength were also improved despite the short-term treatment regimen.

Chapter 3 investigates the treatment of an adult 6mo old Brtl/+ model of OI with a 5 week Scl-Ab treatment regimen [48]. Scl-Ab significantly increased femoral trabecular bone mass, increased cortical bone formation rate and cortical bone mass, leading to improved bone strength. Unexpectedly, reductions in bone brittleness were also observed with Scl-Ab.

As OI is primarily a pediatric disease, and the 8 week old animals studied in Chapter 2 were not rapidly growing, we pursued studies in a younger Brtl/+ mouse. In Chapter 4, 3 week old Brt/+ mice were treated with Scl-Ab for 5 weeks, at an identical dose as used in Chapter 3. During the experiment, body mass doubled, confirming a high growth rate, but treatment had no effect on bone length or body mass. In rapidly growing Brtl/+ mice, Scl-Ab again increased bone formation, leading to greater cortical bone mass and strength. Interestingly, bone brittleness was only increased in WT, but not Brtl/+, rapidly growing mice.

Chapters 3 and 4 represent a set of parallel experiments at two animal ages with identical outcomes. These chapters are best read together as there is additional value gained from contrasting the data. For example, there are different effects of Scl-Ab in Brtl/+ femoral trabecular bone depending on animal age. In addition, an unexpected reduction in bone brittleness with Scl-Ab therapy was only observed in adult 6 mo Brtl/+, but not rapidly growing animals. Finally, a detailed regional dynamic histomorphometry analysis was carried out and revealed that while Scl-Ab was anabolic at both animal ages, the manner in which it increased bone formation on surfaces around the cortex was different in rapidly growing vs adult animals.

Chapter 5 describes an investigation into the material properties (nanoindentation) and composition (raman spectroscopy) of bone formed under the influence of Scl-Ab. While the previous chapters demonstrate that Scl-Ab can increase bone formation and whole bone strength, it is not clear whether the treatment has an effect on material composition. Fluorescent labels were used to control for tissue age in all analysis, and both raman spectroscopy and nanoindentation outcomes were analyzed at multiple tissue ages. Data suggest that there differences in material composition (carbonate to phosphate and mineral to matrix ratios) as a result of Scl-Ab, but no changes were observed in elastic modulus. Moreover, the response was

similar between WT and Brtl/+. Not to be lost in this study is the interesting interaction between tissue age and animal age.

In conclusion, these data collectively suggest that Scl-Ab can stimulate bone formation in rapidly growing and adult Brtl/+ model of Type IV OI. Increased bone formation led to increased bone mass and improved long bone strength. These initial data suggest that Scl-Ab may be beneficial for OI patients, with the potential to stimulate bone formation and reduce fracture risk.

References

1. Forlino A, Cabral WA, Barnes AM, Marini JC (2011) New perspectives on osteogenesis imperfecta. Nat Rev Endocrinol 7:540–557. doi: 10.1038/nrendo.2011.81

2. Christiansen HE, Schwarze U, Pyott SM, et al. (2010) Homozygosity for a missense mutation in SERPINH1, which encodes the collagen chaperone protein HSP47, results in severe recessive osteogenesis imperfecta. Am J Hum Genet 86:389–398. doi: 10.1016/j.ajhg.2010.01.034

3. Cabral WA, Chang W, Barnes AM, et al. (2007) Prolyl 3-hydroxylase 1 deficiency causes a recessive metabolic bone disorder resembling lethal/severe osteogenesis imperfecta. Nat Genet 39:359–365. doi: 10.1038/ng1968

4. Morello R, Bertin TK, Chen Y, et al. (2006) CRTAP Is Required for Prolyl 3- Hydroxylation and Mutations Cause Recessive Osteogenesis Imperfecta. Cell 127:291–304. doi: 10.1016/j.cell.2006.08.039

5. Marini JC, Forlino A, Cabral WA, et al. (2007) Consortium for osteogenesis imperfecta mutations in the helical domain of type I collagen: regions rich in lethal mutations align with collagen binding sites for integrins and proteoglycans. Hum Mutat 28:209–221. doi: 10.1002/humu.20429

6. Barsh GS, David KE, Byers PH (1982) Type I osteogenesis imperfecta: a nonfunctional allele for pro alpha 1 (I) chains of type I procollagen. PNAS 79:3838–3842.

7. Martin E, Shapiro J (2007) Osteogenesis imperfecta: Epidemiology and pathophysiology. Curr Osteoporos Rep 5:91–97. doi: 10.1007/s11914-007-0023-z

8. Sillence DO, Senn A, Danks DM (1979) Genetic heterogeneity in osteogenesis imperfecta. J Med Genet 16:101–116. doi: 10.1136/jmg.16.2.101

9. Bodian DL, Chan T-F, Poon A, et al. (2009) Mutation and polymorphism spectrum in osteogenesis imperfecta type II: implications for genotype–phenotype relationships. Hum Mol Genet 18:463–471. doi: 10.1093/hmg/ddn374

10. Baron R, Gertner JM, Lang R, Vignery A (1983) Increased bone turnover with decreased bone formation by osteoblasts in children with osteogenesis imperfecta tarda. Pediatr Res 17:204–207.

11. Rauch F, Travers R, Parfitt A., Glorieux F. (2000) Static and dynamic bone histomorphometry in children with osteogenesis imperfecta. Bone 26:581–589. doi: 10.1016/S8756-3282(00)00269-6

12. Paterson CR, McAllion S, Stellman JL (1984) Osteogenesis imperfecta after the menopause. N Engl J Med 310:1694–1696. doi: 10.1056/NEJM198406283102602

13. Grafe I, Yang T, Alexander S, et al. (2014) Excessive transforming growth factor-β signaling is a common mechanism in osteogenesis imperfecta. Nat Med 20:670–675. doi: 10.1038/nm.3544

14. Forlino A, Porter FD, Lee EJ, et al. (1999) Use of the Cre/lox Recombination System to Develop a Non-lethal Knock-in Murine Model for Osteogenesis Imperfecta with an α1(I) G349C Substitution. Journal of Biological Chemistry 274:37923 –37931. doi: 10.1074/jbc.274.53.37923

15. Kozloff KM, Carden A, Bergwitz C, et al. (2004) Brittle IV Mouse Model for Osteogenesis Imperfecta IV Demonstrates Postpubertal Adaptations to Improve Whole Bone Strength. Journal of Bone and Mineral Research 19:614–622. doi: 10.1359/JBMR.040111

16. Cabral W, Fratzl-Selman N, Roschger P, et al. (2011) Cellular Dysregulation of Gene Expression May Contribute to Matrix Hypermineralization in Osteogenesis Imperfecta. J Bone Miner Res 26 (Suppl 1):

17. Uveges TE, Collin-Osdoby P, Cabral WA, et al. (2008) Cellular mechanism of decreased bone in Brtl mouse model of OI: imbalance of decreased osteoblast function and increased osteoclasts and their precursors. J Bone Miner Res 23:1983–1994. doi: 10.1359/jbmr.080804

18. Collin-Osdoby P, Rothe L, Kwong M, et al. (2011) Increased Osteoclast Formation and Bone Resorption in the Brtl Osteogenesis Imperfecta Mouse Occur through Marrow Mesenchymal Stromal Cell and Abnormal Matrix Dependent Mechanisms. J Bone Miner Res 26 (Suppl 1):

19. Forlino A, Kuznetsova NV, Marini JC, Leikin S (2007) Selective retention and degradation of molecules with a single mutant [alpha]1(I) chain in the Brtl IV mouse model of OI. Matrix Biology 26:604–614. doi: 16/j.matbio.2007.06.005

20. Sakkers R, Kok D, Engelbert R, et al. (2004) Skeletal effects and functional outcome with olpadronate in children with osteogenesis imperfecta: a 2-year randomised placebo-controlled study. The Lancet 363:1427–1431. doi: 10.1016/S0140-6736(04)16101-1

21. Letocha AD, Cintas HL, Troendle JF, et al. (2005) Controlled trial of pamidronate in children with types III and IV osteogenesis imperfecta confirms vertebral gains but not short-term functional improvement. J Bone Miner Res 20:977–986. doi: 10.1359/JBMR.050109

22. Gatti D, Antoniazzi F, Prizzi R, et al. (2005) Intravenous neridronate in children with osteogenesis imperfecta: a randomized controlled study. J Bone Miner Res 20:758–763. doi: 10.1359/JBMR.041232

23. Rauch F, Munns CF, Land C, et al. (2009) Risedronate in the treatment of mild pediatric osteogenesis imperfecta: a randomized placebo-controlled study. J Bone Miner Res 24:1282–1289. doi: 10.1359/jbmr.090213

24. Ward LM, Rauch F, Whyte MP, et al. (2011) Alendronate for the treatment of pediatric osteogenesis imperfecta: a randomized placebo-controlled study. J Clin Endocrinol Metab 96:355–364. doi: 10.1210/jc.2010-0636

25. Evans KD, Lau ST, Oberbauer AM, Martin RB (2003) Alendronate affects long bone length and growth plate morphology in the oim mouse model for Osteogenesis Imperfecta. Bone 32:268–274. doi: 16/S8756-3282(02)00974-2

26. Marini JC (2006) Should children with osteogenesis imperfecta be treated with bisphosphonates? Nat Clin Pract Endocrinol Metab 2:14–15. doi: 10.1038/ncpendmet0075

27. Whyte MP, McAlister WH, Novack DV, et al. (2008) Bisphosphonate-Induced Osteopetrosis: Novel Bone Modeling Defects, Metaphyseal Osteopenia, and Osteosclerosis Fractures After Drug Exposure Ceases. Journal of Bone and Mineral Research 23:1698–1707. doi: 10.1359/jbmr.080511

28. Uveges TE, Kozloff KM, Ty JM, et al. (2009) Alendronate Treatment of the Brtl Osteogenesis Imperfecta Mouse Improves Femoral Geometry and Load Response Before Fracture but Decreases Predicted Material Properties and Has Detrimental Effects on Osteoblasts and Bone Formation. Journal of Bone and Mineral Research 24:849–859. doi: 10.1359/jbmr.081238

29. Marini JC, Hopkins E, Glorieux FH, et al. (2003) Positive linear growth and bone responses to growth hormone treatment in children with types III and IV osteogenesis imperfecta: high predictive value of the carboxyterminal propeptide of type I procollagen. J Bone Miner Res 18:237–243. doi: 10.1359/jbmr.2003.18.2.237

30. Vahle JL, Sato M, Long GG, et al. (2002) Skeletal Changes in Rats Given Daily Subcutaneous Injections of Recombinant Human Parathyroid Hormone (1-34) for 2 Years and Relevance to Human Safety. Toxicologic Pathology 30:312 –321. doi: 10.1080/01926230252929882

31. Adami S, Gatti D, Colapietro F, et al. (2003) Intravenous neridronate in adults with osteogenesis imperfecta. J Bone Miner Res 18:126–130. doi: 10.1359/jbmr.2003.18.1.126

32. Chevrel G, Schott A-M, Fontanges E, et al. (2006) Effects of oral alendronate on BMD in adult patients with osteogenesis imperfecta: a 3-year randomized placebo-controlled trial. J Bone Miner Res 21:300–306. doi: 10.1359/JBMR.051015

33. Shapiro JR, Thompson CB, Wu Y, et al. (2010) Bone Mineral Density and Fracture Rate in Response to Intravenous and Oral Bisphosphonates in Adult Osteogenesis Imperfecta. Calcif Tissue Int 87:120–129. doi: 10.1007/s00223-010-9383-y

34. Bradbury LA, Barlow S, Geoghegan F, et al. (2011) Risedronate in adults with osteogenesis imperfecta type I: increased bone mineral density and decreased bone turnover, but high fracture rate persists. Osteoporos Int. doi: 10.1007/s00198-011-1658-2

35. Orwoll ES, Shapiro J, Veith S, et al. (2014) Evaluation of teriparatide treatment in adults with osteogenesis imperfecta. J Clin Invest 124:491–498. doi: 10.1172/JCI71101

36. Brunkow ME, Gardner JC, Van Ness J, et al. (2001) Bone dysplasia sclerosteosis results from loss of the SOST gene product, a novel cystine knot-containing protein. Am J Hum Genet 68:577–589.

37. Balemans W, Ebeling M, Patel N, et al. (2001) Increased bone density in sclerosteosis is due to the deficiency of a novel secreted protein (SOST). Hum Mol Genet 10:537–543.

38. Poole KES, van Bezooijen RL, Loveridge N, et al. (2005) Sclerostin is a delayed secreted product of osteocytes that inhibits bone formation. FASEB J 19:1842–1844. doi: 10.1096/fj.05-4221fje

39. Li X, Zhang Y, Kang H, et al. (2005) Sclerostin Binds to LRP5/6 and Antagonizes Canonical Wnt Signaling. Journal of Biological Chemistry 280:19883–19887. doi: 10.1074/jbc.M413274200

40. Leupin O, Piters E, Halleux C, et al. (2011) Bone overgrowth-associated mutations in the LRP4 gene impair sclerostin facilitator function. J Biol Chem 286:19489–19500. doi: 10.1074/jbc.M110.190330

41. Li X, Ominsky MS, Niu Q-T, et al. (2008) Targeted Deletion of the Sclerostin Gene in Mice Results in Increased Bone Formation and Bone Strength. Journal of Bone and Mineral Research 23:860–869. doi: 10.1359/jbmr.080216

42. McClung MR, Grauer A, Boonen S, et al. (2014) Romosozumab in Postmenopausal Women with Low Bone Mineral Density. New England Journal of Medicine 370:412–420. doi: 10.1056/NEJMoa1305224

43. McColm J, Hu L, Womack T, et al. (2014) Single- and Multiple-Dose Randomized Studies of Blosozumab, a Monoclonal Antibody Against Sclerostin, in Healthy Postmenopausal Women. J Bone Miner Res 29:935–943. doi: 10.1002/jbmr.2092

44. Li X, Ominsky MS, Warmington KS, et al. (2009) Sclerostin antibody treatment increases bone formation, bone mass, and bone strength in a rat model of postmenopausal osteoporosis. J Bone Miner Res 24:578–588. doi: 10.1359/jbmr.081206

45. Ominsky MS, Niu Q-T, Li C, et al. (2014) Tissue-level mechanisms responsible for the increase in bone formation and bone volume by sclerostin antibody. J Bone Miner Res 29:1424–1430.

46. Li X, Ominsky MS, Warmington KS, et al. (2011) Increased Bone Formation and Bone Mass Induced by Sclerostin Antibody Is Not Affected by Pretreatment or Cotreatment with Alendronate in Osteopenic, Ovariectomized Rats. Endocrinology 152:3312–3322. doi: 10.1210/en.2011-0252

47. Sinder BP, Eddy MM, Ominsky MS, et al. (2013) Sclerostin antibody improves skeletal parameters in a Brtl/+ mouse model of osteogenesis imperfecta. J Bone Miner Res 28:73–80. doi: 10.1002/jbmr.1717

48. Sinder BP, White LE, Salemi JD, et al. (2014) Adult Brtl/+ mouse model of osteogenesis imperfecta demonstrates anabolic response to sclerostin antibody treatment with increased bone mass and strength. Osteoporos Int 1–11. doi: 10.1007/s00198-014-2737-y

CHAPTER 2

Short Term Sclerostin Antibody Treatment Improves Skeletal Parameters in a Brtl/+ Mouse Model of Osteogenesis Imperfecta

Introduction

Osteogenesis imperfecta (OI), or "brittle bone disease", is a heritable disorder caused predominantly by mutations in type I collagen or in proteins that promote the folding or post-translational modification of collagen. Patients with OI have increased bone fragility and are susceptible to fracture from minimal force, skeletal deformities and growth deficiency. OI fragility symptoms are generally most prominent in children; the disorder ranges in severity from mild forms with slightly elevated fracture risk to perinatal lethality [1].

Current treatment options for OI focus on anti-resorptive bisphosphonates (BP) which have been shown effective at increasing vertebral areal bone mineral density and height in clinical trials. However, BP effects in long bones are less evident and most pediatric OI trials observe little or no functional benefit [2–6]. Moreover, while BP therapy has been generally well tolerated in pediatric OI patients, there are concerns about long term retention of BPs in the skeleton and use in a growing population [7].

Sclerostin antibody (Scl-Ab) is a novel anabolic bone therapeutic presently in clinical trials for treatment of osteoporosis [8]. Sclerostin is secreted primarily by osteocytes and negatively regulates bone formation by binding to the LRP4/5/6 complex, inhibiting anabolic canonical wnt signaling in osteoblasts [9–11]. As a result, treatment with a neutralizing Scl-Ab

reduces sclerostin inhibition of canonical wnt signaling and is highly anabolic in pre-clinical models and in a phase 1 clinical trial of men and postmenopausal women [8, 12, 13]. Whether Scl-Ab therapy is capable of stimulating osteoblast activity in cells harboring a typical OI-causing mutation has yet to be demonstrated.

The Brtl/+ mouse is a knock-in model for moderately severe Type IV OI with a G349C point mutation on *col1a1* that recreates an identical defect found in an OI patient [14]. The Brtl/+ mouse recapitulates multiple features of the observed clinical phenotype, including smaller size, reduced BMD, more severe phenotype at young ages, increased bone brittleness and increased bone turnover [15, 16], making it an appropriate model for testing the anabolic efficacy of Scl-Ab in OI. The purpose of this study was to determine whether a short-term intervention with Scl-Ab in the Brtl/+ model of OI would be effective at stimulating an anabolic skeletal response and improving long bone strength.

Materials and Methods

Animals

Wildtype (WT) and Brtl/+ mice are maintained on a mixed background of Sv129/CD-1/C57BL/6S, and all Brtl/+ animals were the product of breeding male Brtl/+ with female WT. 8 week old male WT and Brtl/+ mice were randomly assigned to SclAb (Scl-AbVI, Amgen, Thousand Oaks, CA) treatment or vehicle injection (PBS) with n=7/group. Sclerostin antibody was injected subcutaneously at 25mg/kg, two times per week, for two weeks. Calcein (30mg/kg) was injected at the start of experiment, after 1 week, and 1 day prior to sacrifice by intraperitoneal injection to facilitate dynamic histomorphometry and nanoindentation placement. Body weights were recorded with each injection. Blood samples were collected at sacrifice by

intracardiac puncture, serum separated by centrifuge, and stored at -80˚C until analyzed by ELISA.

Left femurs were collected for microCT and mechanical testing, and right femurs for dynamic histomorphometry and nanoindentation tests. Both were stored at -20˚C in lactated ringers solution (LRS) soaked gauze until testing or further specimen preparation. All protocols and procedures involving animals were approved by the University of Michigan's Committee on Use and Care of Animals.

Serum Markers

To measure osteoblast activity, serum osteocalcin (OCN) was quantified with a commercially available ELISA kit (BT-470, BTI, Stoughton, MA). To quantify osteoclast number, serum TRACP5b was measured with a commercially available solid phase immunofixed enzyme activity assay (MouseTRAP, IDS, Fountain Hills, AZ). Both serum tests were performed in duplicate.

Micro Computed Tomography (µCT)

Left femora were scanned in water using cone beam computed tomography (eXplore Locus SP, GE Healthcare Pre-Clinical Imaging, London, ON, Canada). Scan parameters included a 0.5 degree increment angle, 4 frames averaged, an 80kVp and 80µA x-ray source with a 0.508mm Al filter to reduce beam hardening artifacts, and a beam flattener around the specimen holder [17]. All images were reconstructed and calibrated at an 18µm isotropic voxel size to a manufacturer supplied phantom of air, water and hydroxyapatite. Regions of interest (ROI) were located for both cortical and trabecular parameters. A diaphyseal cortical ROI

spanning 15% of total femur length was located midway between the distal growth plate and third trochanter. Cortical bone was isolated with a fixed threshold of 2000 Hounsfield Units for all experimental groups. Parameters including cortical thickness, cross sectional area, tissue mineral density (TMD), anterior-posterior bending moment of inertia, endosteal perimeter, and periosteal perimeter were quantified with commercially available software (MicroView v2.2 Advanced Bone Analysis Application, GE Healthcare Pre-Clinical Imaging, London, ON, Canada). A trabecular ROI 10% of total femur length was located immediately proximal to the distal femoral growth plate and defined along the inner cortical surface with a splining algorithm. Due to the different morphology induced by Scl-Ab treatment, a fixed threshold could not be utilized without bias. Trabecular metaphyseal bone was isolated with a more conservative autothresholding algorithm for each specimen based on the bimodal distribution between marrow and bone [18]. Parameters including bone volume fraction (BV/TV), trabecular thickness (TbTh), and trabecular number (TbN) were quantified using standard stereology algorithms (MicroView v2.2). A 3D sphere fitting algorithim was also used to confirm the stereology data for TbTh [19].

Mechanical Testing (Whole Bone) – Four-Point Bending

Following μCT scanning, left femora were loaded to failure in four-point bending using a servohydraulic testing machine (MTS 858 MiniBionix, Eden Prarie, MN). All specimens were kept hydrated in LRS-soaked gauze until mechanical testing. In the same mid-diaphyseal region analyzed by μCT, the mid-diaphysis was loaded in four point bending with the posterior surface oriented under tension. The distance between the wide, upper supports was 6.26mm, and span between the narrow, lower supports 2.085mm. The vertical displacement rate of the four-point

bending apparatus in the anterior-posterior direction was 0.5mm/sec. Force was recorded by a 50lb load cell (Sensotec) and vertical displacement by an external linear variable differential transducer (LVDT, Lucas Schavitts, Hampton, VA), both at 2000Hz. A custom MATLAB script was used to calculate stiffness, yield load, yield displacement, ultimate load, failure displacement, post-yield displacement, and energy to failure. Combining anterior-posterior bending moment of inertia data from μCT with mechanical stiffness from four point bending, the estimated elastic modulus was calculated using standard beam theory as previously described [15].

Mechanical Testing (Tissue Level) – Fluorescent Guided Nanoindentation

Right femora were dehydrated, encased in epoxy (Kold Mount, Vernon-Benshoff, Albany, NY), and cut transversely at the mid-diaphysis with a low-speed saw (IsoMet, Beuhler, Lake Bluff, IL). The distal section of tissue was polished using progressive grades of silicon carbide abrasive paper (1200, 2400, and 4000 grit) under water irrigation for two minutes at each grade. To further decrease surface roughness the encased specimens were polished on a felt pad for 5 minutes with a ¼ μm diamond suspension (Streurs Inc., Cleveland, OH). Specimens were then ultrasonically cleansed in a water bath for 10 minutes to remove surface debris, and glued to magnetic specimen plates for nanoindentation testing. The final root mean square (RMS) roughness of the specimens' surface was 10.0 ± 3.7 nm, as assessed with Scanning Probe Microscopy of a 5x5 μm^2 region of the posterior mid cortex.

A custom 950 TI TriboIndenter (Hysitron, Minneapolis, MN) instrumented with a fluorescent light-source and FITC filter allowed for simultaneous visualization of calcein labeling in specimens and accurate positioning of indents to locations matched for tissue age and

treatment status with 0.5μm spatial resolution. Four regions of interest were mechanically tested in the posterior aspect of the femoral cross section: the mid-cortex (defined as midway between the first calcein label on the periosteal and endosteal surfaces, if any), along the first calcein label on 15 day old bone, along the second calcein label on 8 day old bone, and along the third and outer calcein label along 1 day old bone. Indentation consisted of loading a diamond Berkovich indenter tip into samples at 300μN/s, hold at a maximal load of 3,000 μN for 10 s, and unload at 300μN/s. The indentation modulus E was calculated from the load-displacement curves using the standard Oliver-Pharr method [20]. Eight indents, 10 μm apart, were made along each calcein label and the mid cortex, with values averaged for each site and mouse.

Dynamic Histomorphometry

Using the same specimens tested by nanoindentation, dynamic histomorphometry was performed at the mid-diaphysis on the first and third labels according to standard nomenclature [21]. Briefly, fluorescent images were acquired using a Zeiss Axiovert 200M inverted microscope equipped with Apotome imaging system to minimize out-of-plane light, negating the need for several micron thin sections. Fluorescent images were taken with a 10x objective of calcein (excitation 485/20nm, emission: 540/25nm) labels in bone. The 10x images of the cortex were merged into a single image (Photoshop, Adobe), and these merged images were analyzed using commercially available software (Bioquant Osteo v7.20.10, Nashville, TN). Bone surface (BS), mineral apposition rate (MAR), mineralizing surface to bone surface (MS/BS), and bone formation rate (BFR) were quantified.

Statistics

A multivariate ANOVA with LSD post-hoc was used to make all comparisons with the exception of nanoindentation data. For nanoindentation data along calcein labels, a repeated measures ANOVA was used with genotype and treatment status as between-subjects factors and tissue age as the within-subjects factor with simple contrasts to mid-cortical reference values. In all cases, $p<0.05$ was considered significant. All data is presented as mean$\pm$S.D.

Results

Body Weight and Bone Length Remain Unchanged with Short-Term Sclerostin Antibody Treatment

Consistent with the reduced body size with OI, body weight was significantly lower in male Brtl/+ (25.4±1.8g) compared to male WT mice (30.4±2.8g) at 8 weeks of age. Twice weekly dosing of these mice with 25 mg/kg Scl-Ab for 2 weeks did not significantly change body weight gains (data not shown). Scl-Ab treatment also had no effect on femoral length in WT mice (15.9±0.6mm vs 16.0±0.5mm Veh) or the shorter Brtl/+ mice (15.2±0.4mm vs 15.5±0.4mm Veh) after 2 weeks.

Serum Markers Show Brtl/+ Anabolic Response to Scl-Ab

Untreated Brtl/+ animals showed marginally elevated serum osteocalcin ($p=0.060$) and serum TRACP5b ($p=0.083$) relative to WT (Fig 2.1), consistent with reported increases in Brtl/+ bone turnover [16]. Scl-Ab therapy significantly increased serum osteocalcin in both WT and Brtl/+ (Fig 2.1), demonstrating a rapid systemic anabolic response to therapy. Scl-Ab yielded trends toward reduced levels of serum TRACP5 in both WT ($p=0.10$) and Brtl/+ ($p=0.082$),

consistent with published reports observing reduced serum markers of bone resorption in rats and humans [8, 12].

Scl-Ab Differentially Increases Cortical Bone Formation in Brtl/+ and WT

At the femoral mid-shaft, Scl-Ab treatment increased periosteal BFR/BS in Brtl/+ and WT animals by 76% and 108% respectively (Fig. 2.2). In Brtl/+, these increases were caused by a 50% increase in MS/BS, with no significant improvement in MAR. Conversely, WT improvements in BFR/BS resulted from a significant 76% increase in MAR with no significant change in MS/BS.

Scl-Ab Increases Trabecular Bone Apposition on Existing Bone Surfaces

Brtl/+ animals have lower BV/TV relative to WT caused by reduced trabecular number, but not thickness (Fig. 2.3, Fig 2.4). Scl-Ab significantly increased distal femoral metaphyseal BV/TV in WT animals with a trend in Brtl/+ ($p=0.077$). These improvements resulted from significant increases in trabecular thickness in both WT and Brtl/+, with no change in trabecular number in either genotype.

Cortical Shape and Size, Not Mineralization, are Increased with Sclerostin Antibody

At the femoral mid-diaphysis, Brtl/+ animals have a reduced cortical thickness and area relative to WT as measured by microCT (Table 2.1). Scl-Ab treatment significantly increased both cortical thickness and area in Brtl/+ and WT, primarily through increased femoral cortical periosteal perimeter. Endocortical perimeter showed no significant differences with Scl-Ab treatment in either WT or Brtl/+. In combination, these individual factors contributed to

increasing trends in the anterior-posterior bending moment of inertia with Scl-Ab treatment in both WT and Brtl/+, reflecting a structurally stronger bone. Mean cortical tissue mineralization (TMD) calculated by microCT was unaffected by Scl-Ab in either WT or Brtl/+.

Sclerostin Antibody Improves Whole Bone Mechanical Properties

Brtl/+ femora have inherently lower ultimate load and stiffness ($p=0.063$) compared to WT (Table 2.1). Two weeks of Scl-Ab treatment significantly increased ultimate load and stiffness in both WT and Brtl/+ mice. The estimated tissue elastic modulus, as calculated by standard beam theory, was not affected by Scl-Ab treatment in WT or Brtl/+, corroborating similar findings in TMD.

A hallmark feature of OI bone is increased tissue brittleness. Post-yield displacement (PYD) during four point bending is a measure of ductility, an inverse indicator of material brittleness. Phenotypically, although Brtl/+ PYD was not significantly different that WT, five out of seven WT samples had a PYD greater than the largest Brtl/+ PYD value, consistent with previous reports increased brittleness at a similar age [15]. Unexpectedly, post yield displacement was increased 324% with Scl-Ab in WT ($p<0.05$), and 58% with Scl-Ab in Brtl/+, although failing to achieve statistical significance due to high variability. These data suggest Scl-Ab reduced bone brittleness, improving bone ductility in both Brtl/+ and WT.

Nanoindentation Reveals Similar Patterns of Mineralization in Scl-Ab Treated Animals

Nanoindentation measures local micromechanical properties associated with local tissue mineralization by measuring the tissue elastic modulus. Phenotypically, in the overall statistical model, genotype was a significant predictor suggesting a greater tissue elastic modulus in Brtl/+

compared to WT. However, comparisons between genotypes at specific tissue ages were not significant. Nanoindentation revealed that Scl-Ab treatment did not change the tissue elastic modulus of bone in either WT or Brtl. This indicates that despite the sudden change in osteoblastic anabolic function with Scl-Ab treatment, no differences in tissue elastic modulus were seen in bone grown under the influence of Scl-Ab (Fig. 2.5). The tissue age at which newly formed bone achieved mature tissue elastic modulus was rapid, as only bone laid down 1 day prior to euthanasia had a significantly reduced elastic modulus relative to mid-cortical values consistent with the rapid establishment of mechanical properties which has been reported in rats [22, 23]. No difference was found between 2 week old bone and 1 week old bone relative to mid-cortical values.

Discussion

In this study, mice with a genetic knock-in that recreates a typical OI-causing mutation in type I collagen showed a positive response following short-term Scl-Ab therapy. Two weeks of Scl-Ab significantly improved bone mass at both cortical and trabecular sites, and significantly reduced long bone fragility. In the context of existing anabolic and anti-resorptive treatment options, Scl-Ab is novel and has high potential as a therapeutic for OI patients. Current anabolic treatment options have not shown uniform success when applied to OI. The anabolic bone agent teraparatide is currently approved as an osteoporosis therapy, but has been associated with osteosarcoma after long term treatment in growing rats [24], and is therefore contraindicated for use in children with open growth plates. Growth hormone has also been implemented as an anabolic therapy for OI. While effective in some patients at increasing BMD as well as improving bone histomorphometry, the benefits are selective for patients who respond

to rGH with increased linear growth. Other OI patients treated with rGH experience no positive effect, and may exacerbate their existing low bone mass phenotype by increasing osteoclast surface [25].

As a result of limited anabolic therapeutics, anti-resorptive bisphosphonates have been widely used in OI. Several controlled pediatric OI clinical trials have demonstrated that bisphosphonate treatment is effective at increasing vertebral BMD [2–6]. Functionally, intravenous bisphosphonates are effective at increasing vertebral height, an indirect indicator of bone strength that suggests increased resistance to compression [3, 4]. However, in long bones a functional benefit is less clear, even in controlled trials up to 125 patients [1–6].

While bisphosphonate therapy increases areal BMD in pediatric OI populations, recent evidence suggests potential for several undesirable effects intrinsic to the BP mechanism of action. First, BP binds strongly to the skeleton and has been detected in urinary markers 8 years after cessation of treatment, resulting in long term suppression of bone turnover [26]. Long-term BP therapy has been associated with the accumulation of microdamage in several animal models [27–31]. Brtl/+ mice have an increased propensity to form and accumulate microdamage [32] and thus BP treatment may potentially exacerbate this effect. During growth, antiresorptive therapy results in retention of calcified cartilage near the growth plates. This retention of primary spongiosa manifests radiographically as sclerotic metaphyseal banding coinciding with each BP treatment cycle, and these changes can bias measured BMD gains [33] without concomitant improvements in strength. Previous studies of BP treatment in Brtl/+ found increased trabecular number, but not thickness [33]. Notably, in the present study with Scl-Ab, gains in trabecular bone mass resulted from increased trabecular thickness, not number.

In this study, we found that unlike WT osteoblasts, Brtl/+ osteoblasts did not increase their mineral apposition rate with Scl-Ab treatment. This lack of an MAR increase in Brtl/+ may be suggestive of defective osteoblasts unable to keep pace with Scl-Ab-induced bone formation demands. In support of this, Brtl/+ mice demonstrate a mild delay in secretion of collagen in cell culture, and an enlarged ER has been observed in Brtl/+ fibroblasts, suggesting ER-stress correlated with collagen production, and possibly degradation of mutant collagen [34]. Whether this result also exists in the various OI mouse models with different mutations will be important to contrast with the data presented here. Alternatively, animal age and treatment duration of the Brtl/+ mouse model used in this study may also modulate any Scl-Ab induced MAR effect. Preliminary data from Brtl/+ mice treated for 5 weeks with Scl-Ab suggest an similar increase in MAR in both WT and Brtl/+ animals [35]. Regardless, it is important that Brtl/+ mice in this study were still able to increase bone formation rate in absence of MAR increases by increasing MS/BS at the periosteal cortical surface.

Unexpectedly, we found that Scl-Ab significantly reduced bone brittleness (increased post-yield displacement) in WT animals as measured by whole bone mechanical four-point bending. Although reductions in bone brittleness were not statistically significant in Brtl/+ animals in this study, our finding of reduced brittleness in WT has broader implications about bone quality changes associated with Scl-Ab treatment. While the differing bone geometries induced by Scl-Ab treatment raises the potential for experimental bias, the large magnitude of our observed difference in WT (324% increase in post yield displacement) remains suggestive. In contrast to the Scl-Ab data presented here, previous bisphosphonate treatment in Brtl/+ found neither significant changes nor increasing trends in PYD. Moreover, BP-treated WT showed marginal reductions in PYD reflecting no improvements in bone brittleness with

bisphosphonates despite large gains in femoral bone mass [33]. Interestingly, in the contralateral femurs of the same animals which demonstrated reductions in post yield displacement, we did not observe any difference in the elastic modulus of bone formed under the influence of Scl-Ab by fluorescence guided nanoindentation. These findings represent the first tissue level mechanical test of bone formed during Scl-Ab treatment through coupling of fluorescent imagng to nanoindentation. Further studies are required to determine post-yield behavior of bone at the tissue level, unlike those reported in this study.

In summary, we have demonstrated that two weeks of Scl-Ab therapy was capable of increasing osteoblast activity in cells harboring a classical OI-causing Gly->Cys substitution in *col1a1*. These gains lead to improved bone mass and whole bone mechanical properties without altering the timing of tissue mineralization. While bisphosphonate therapy is in widespread use for pediatric OI patients, there is pressing need for more effective anabolic therapeutics to improve patient outcomes. Scl-Ab is a unique and promising anabolic therapy which may be particularly useful for the treatment of pediatric OI. The present data suggest Scl-Ab may be beneficial for the treatment of OI patients by stimulating the osteoblasts and reducing fracture risk.

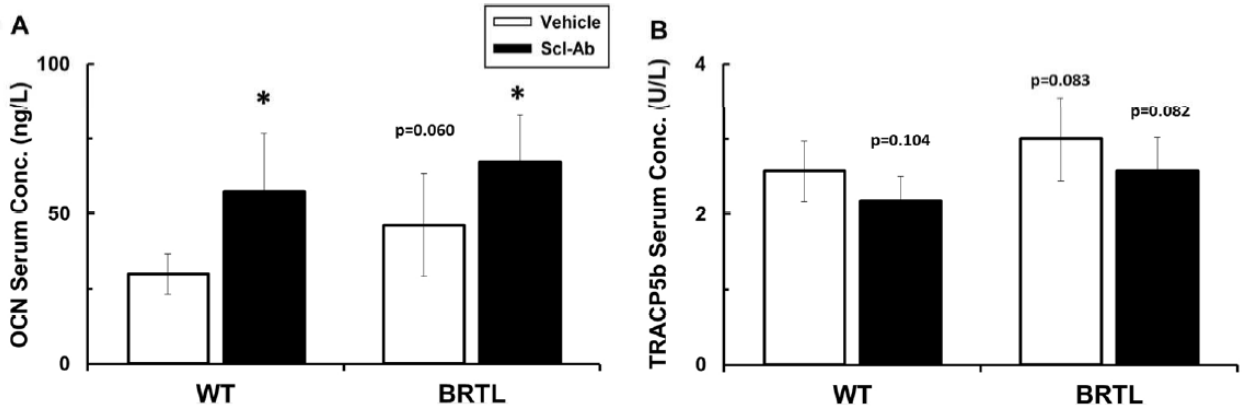

Figure 2.1: Serum TRACP5b and Osteocalcin. Serum OCN **(A)** is elevated and serum TRACP5b **(B)** is reduced with Scl-Ab therapy in both WT and Brtl/+, suggesting a decoupled effect on bone formation and bone resorption. In Vehicle treated animals, Brtl/+ trends toward higher OCN **(A)** and TRACP5b **(B)** levels suggesting increased bone turnover in Brtl/+. * $p<0.05$ Scl-Ab vs. Veh; $^{\#}p<0.05$ WT Veh vs. Brtl/+ Veh.

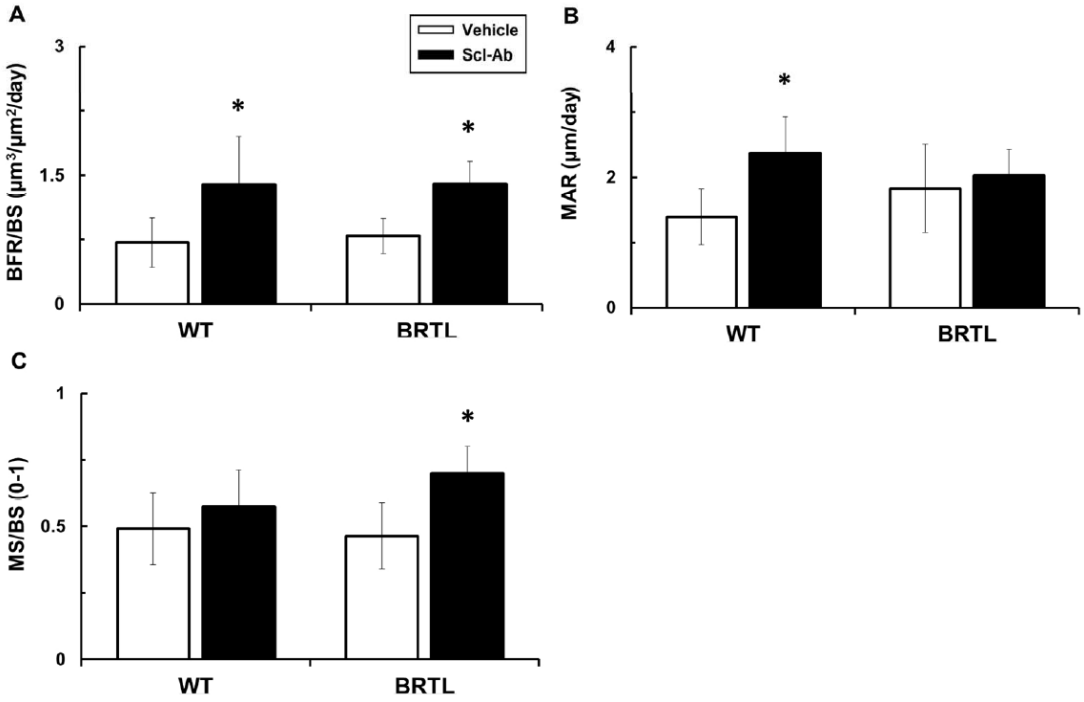

Figure 2.2: Cortical Dynamic Histomorphometry (Femur). Dynamic histomorphometry at the periosteal femoral mid-diaphysis reveals anabolic effect of Scl-Ab in WT and Brtl/+. Femoral cortical mid-diaphyseal periosteal BFR **(A)** increases with Scl-Ab are a result of increased periosteal MAR (**B**) in WT and periosteal MS/BS **(C)** in Brtl/+. Brtl/+ Veh n=6, all other groups n=7. * $p<0.05$ Scl-Ab vs. Veh; $^{\#}p<0.05$ WT Veh vs. Brtl/+ Veh.

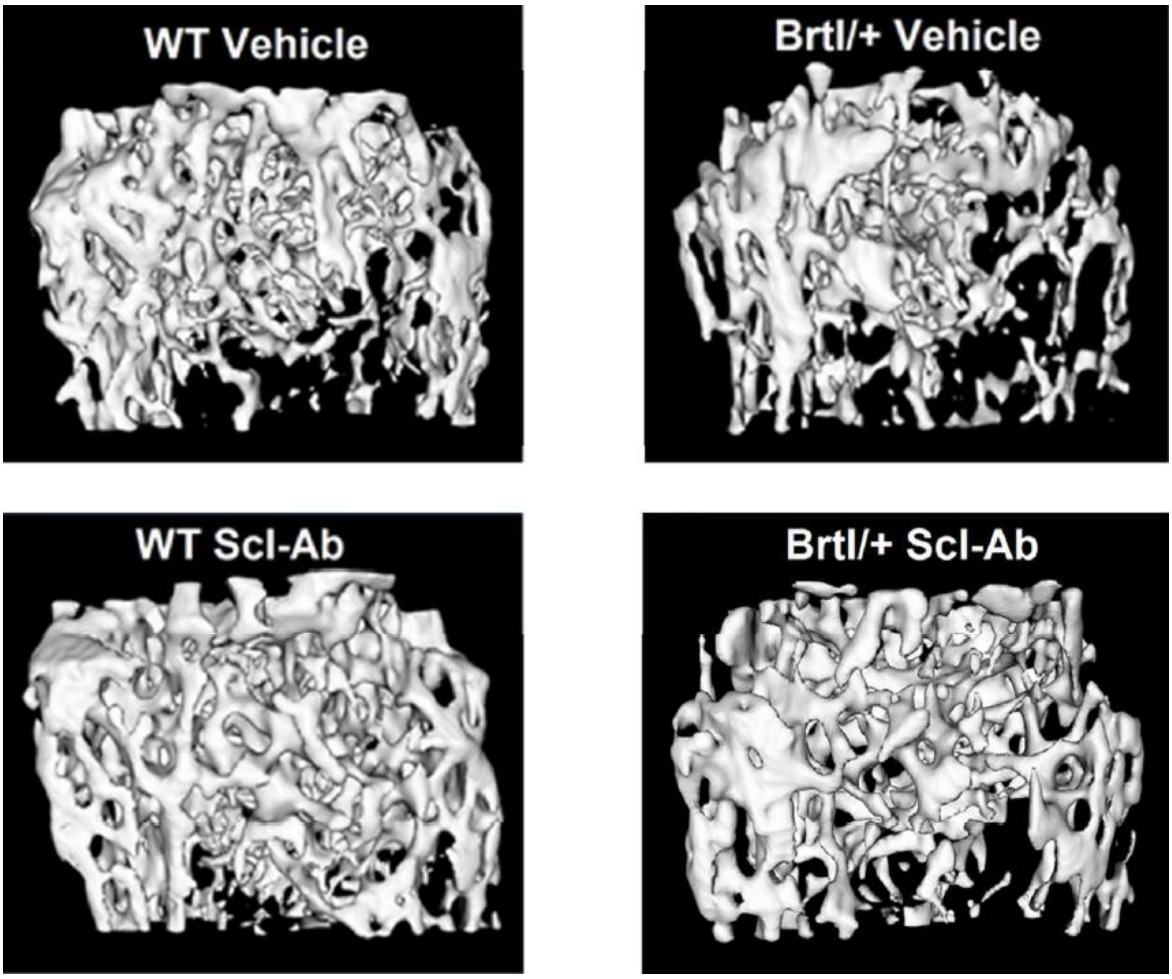

Figure 2.3: Femoral Trabecular MicroCT Representative Isosurfaces. Micro computed tomography of the distal femur metaphysis reveals anabolic changes with Scl-Ab therapy. Representative microCT images of distal metaphyseal trabecular bone reflect these changes. For each experimental group, the animal with the median BV/TV value is shown. A conservative specimen specific threshold is applied as described in the methods.

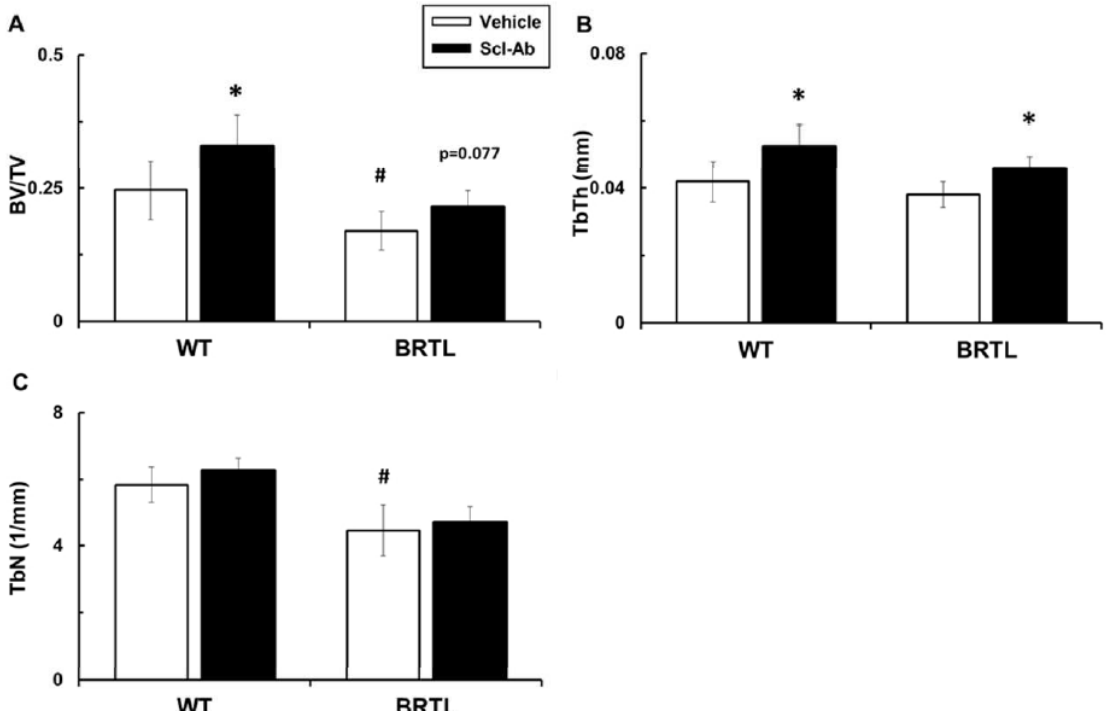

Figure 2.4: Femoral Trabecular MicroCT Data. Micro computed tomography of the distal femur metaphysis reveals anabolic changes with Scl-Ab therapy. BV/TV **(A)**, and Tb.Th (**B**) were improved by Scl-Ab with no effect on Tb.N **(C).** *$p<0.05$ Scl-Ab vs. Veh; $^{\#}p<0.05$ WT Veh vs. Brtl/+ Veh.

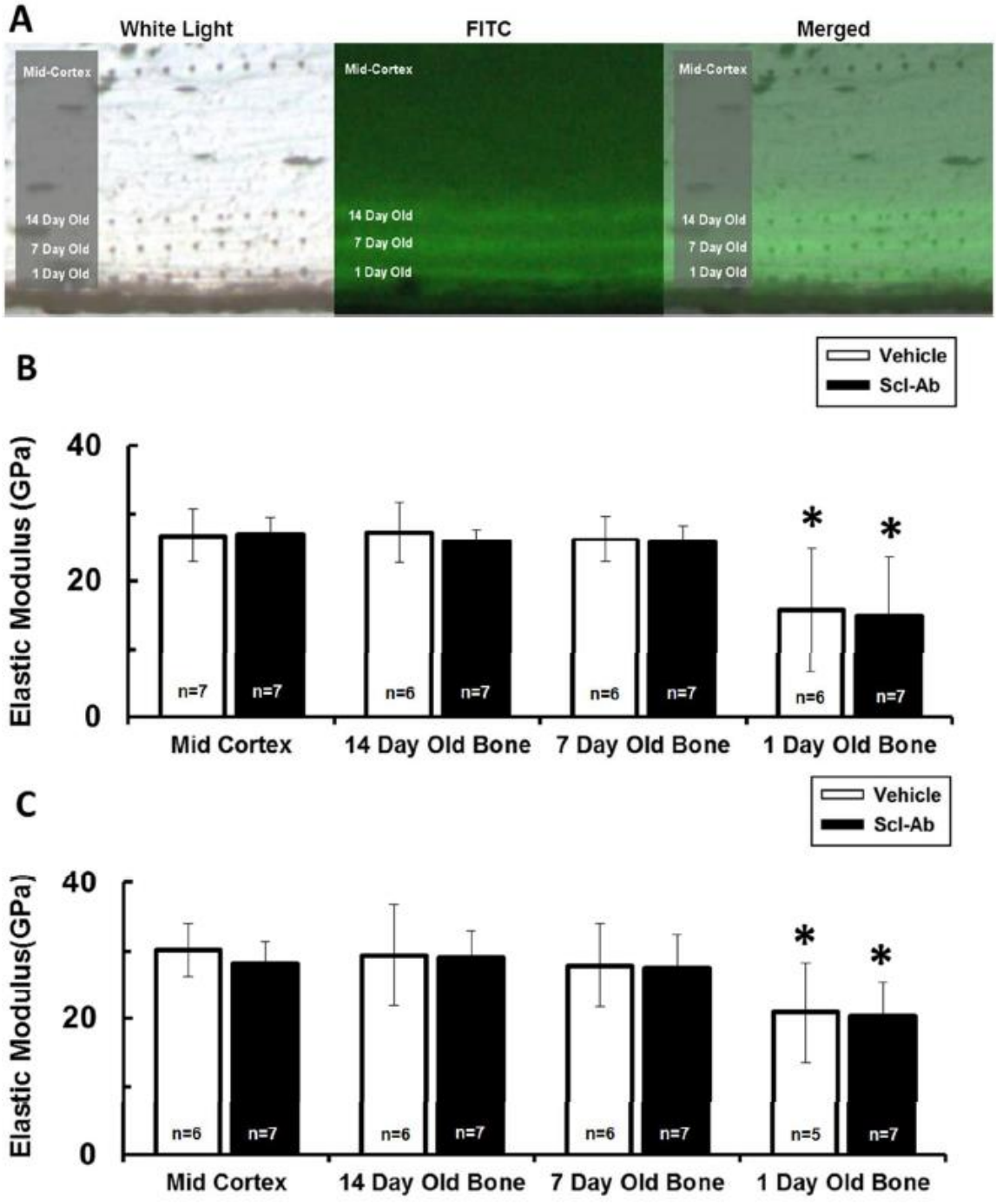

Figure 2.5 Fluorescent Guided Nanoindentation of Scl-Ab Treated Bone. Nanoindentation was performed along calcein labels to match tissue age between treated and untreated animals. White Light, FITC, and merged images showing placement of indents **(A).** Nanoindentation revealed no difference in tissue elastic modulus across treatment groups in WT **(B)** and Brtl/+ **(C)**. *notes significance relative to mid-cortical reference and denotes $p<0.05$.

Table 2.1. Cortical MicroCT and Mechanical Properties

	WT Veh	*WT Scl-Ab*	*Brtl Veh*	*Brtl Scl-Ab*
Cortical Micro CT				
Thickness (mm)	0.21 ± .01	0.24 ± .01*	0.17 ± .02$^{\#}$	0.20 ± .02*
Cross Sectional Area (mm^2)	1.01 ± .10	1.16 ± .10*	0.76 ± .10$^{\#}$	0.91 ± .10*
Endosteal Perimeter (mm)	4.51 ± .36	4.43 ± .22	4.09 ± .13$^{\#}$	4.21 ± .18
Periosteal Perimeter (mm)	5.80 ± .42	5.95 ± .32	5.15 ± .16$^{\#}$	5.48 ± .21*
Bending Moment of Inertia (mm^4)	0.21 ± .05	0.23 ± .04	0.12 ± .03$^{\#}$	0.16 ± .03$^{p=.08}$
Tissue Mineral Density (mg/cm^3)	1052 ± 43	1051 ± 50	1081 ± 39	1092 ± 41
Mechanical Four Point Bending				
Ultimate Load (N)	27.1 ± 4.5	38.7 ± 10.2*	18.2 ± 5.0$^{\#}$	26.8 ± 7.8*
Stiffness (N/mm)	237 ± 28	297 ± 66*	192 ± 35$^{p=0.063}$	256 ± 33*
Energy to Failure (J)	3.1 ± 1.6	10.6 ± 7.6*	1.0 ± .6	2.0 ± 1.1
Post Yield Displacement (mm)	0.058 ± .049	0.247 ± .143*	0.026 ± .021	0.041 ± .037
Estimated Elastic Modulus (GPa)	4.6 ± 1.2	4.8 ± .5	6.0 ± 1.2$^{\#}$	6.0 ± .7

Table 2.1. Cortical MicroCT and Mechanical 4pt Bending. Femoral mid-diaphyseal cortical microCT and mechanical four point bending data show increased cortical bone mass and strength with Scl-Ab. *$p<0.05$ Scl-Ab vs. Veh; $^{\#}p<0.05$ WT Veh vs. Brtl/+ Veh.

References

1. Forlino A, Cabral WA, Barnes AM, Marini JC (2011) New perspectives on osteogenesis imperfecta. Nat Rev Endocrinol 7:540–557. doi: 10.1038/nrendo.2011.81

2. Sakkers R, Kok D, Engelbert R, et al. (2004) Skeletal effects and functional outcome with olpadronate in children with osteogenesis imperfecta: a 2-year randomised placebo-controlled study. The Lancet 363:1427–1431. doi: 10.1016/S0140-6736(04)16101-1

3. Gatti D, Antoniazzi F, Prizzi R, et al. (2005) Intravenous neridronate in children with osteogenesis imperfecta: a randomized controlled study. J Bone Miner Res 20:758–763. doi: 10.1359/JBMR.041232

4. Letocha AD, Cintas HL, Troendle JF, et al. (2005) Controlled trial of pamidronate in children with types III and IV osteogenesis imperfecta confirms vertebral gains but not short-term functional improvement. J Bone Miner Res 20:977–986. doi: 10.1359/JBMR.050109

5. Rauch F, Munns CF, Land C, et al. (2009) Risedronate in the treatment of mild pediatric osteogenesis imperfecta: a randomized placebo-controlled study. J Bone Miner Res 24:1282–1289. doi: 10.1359/jbmr.090213

6. Ward LM, Rauch F, Whyte MP, et al. (2011) Alendronate for the treatment of pediatric osteogenesis imperfecta: a randomized placebo-controlled study. J Clin Endocrinol Metab 96:355–364. doi: 10.1210/jc.2010-0636

7. Whyte MP, McAlister WH, Novack DV, et al. (2008) Bisphosphonate-Induced Osteopetrosis: Novel Bone Modeling Defects, Metaphyseal Osteopenia, and Osteosclerosis Fractures After Drug Exposure Ceases. Journal of Bone and Mineral Research 23:1698–1707. doi: 10.1359/jbmr.080511

8. Padhi D, Jang G, Stouch B, et al. (2011) Single-dose, placebo-controlled, randomized study of AMG 785, a sclerostin monoclonal antibody. Journal of Bone and Mineral Research 26:19–26. doi: 10.1002/jbmr.173

9. Poole KES, van Bezooijen RL, Loveridge N, et al. (2005) Sclerostin is a delayed secreted product of osteocytes that inhibits bone formation. FASEB J 19:1842–1844. doi: 10.1096/fj.05-4221fje

10. Li X, Zhang Y, Kang H, et al. (2005) Sclerostin Binds to LRP5/6 and Antagonizes Canonical Wnt Signaling. Journal of Biological Chemistry 280:19883–19887. doi: 10.1074/jbc.M413274200

11. Leupin O, Piters E, Halleux C, et al. (2011) Bone overgrowth-associated mutations in the LRP4 gene impair sclerostin facilitator function. J Biol Chem 286:19489–19500. doi: 10.1074/jbc.M110.190330

12. Li X, Ominsky MS, Warmington KS, et al. (2009) Sclerostin antibody treatment increases bone formation, bone mass, and bone strength in a rat model of postmenopausal osteoporosis. J Bone Miner Res 24:578–588. doi: 10.1359/jbmr.081206

13. Ominsky MS, Vlasseros F, Jolette J, et al. (2010) Two doses of sclerostin antibody in cynomolgus monkeys increases bone formation, bone mineral density, and bone strength. Journal of Bone and Mineral Research 25:948–959. doi: 10.1002/jbmr.14

14. Forlino A, Porter FD, Lee EJ, et al. (1999) Use of the Cre/lox Recombination System to Develop a Non-lethal Knock-in Murine Model for Osteogenesis Imperfecta with an α1(I) G349C Substitution. Journal of Biological Chemistry 274:37923 –37931. doi: 10.1074/jbc.274.53.37923

15. Kozloff KM, Carden A, Bergwitz C, et al. (2004) Brittle IV Mouse Model for Osteogenesis Imperfecta IV Demonstrates Postpubertal Adaptations to Improve Whole Bone Strength. Journal of Bone and Mineral Research 19:614–622. doi: 10.1359/JBMR.040111

16. Uveges TE, Collin-Osdoby P, Cabral WA, et al. (2008) Cellular mechanism of decreased bone in Brtl mouse model of OI: imbalance of decreased osteoblast function and increased osteoclasts and their precursors. J Bone Miner Res 23:1983–1994. doi: 10.1359/jbmr.080804

17. Meganck JA, Kozloff KM, Thornton MM, et al. (2009) Beam hardening artifacts in micro-computed tomography scanning can be reduced by X-ray beam filtration and the resulting images can be used to accurately measure BMD. Bone 45:1104–1116. doi: 10.1016/j.bone.2009.07.078

18. Otsu N (1979) A threshold selection method from gray-level histograms. IEEE Transactions on Systems, Man and Cybernetics 9:62–66.

19. Hildebrand T, Rüegsegger P (1997) A new method for the model-independent assessment of thickness in three-dimensional images. Journal of Microscopy 185:67–75. doi: 10.1046/j.1365-2818.1997.1340694.x

20. Oliver WC, Pharr GM (1992) An improved technique for determining hardness and elastic modulus using load and displacement sensing indentation experiments. J Mater Res 7:1565.

21. Parfitt AM, Drezner MK, Glorieux FH, et al. (1987) Bone histomorphometry: standardization of nomenclature, symbols, and units. Report of the ASBMR Histomorphometry Nomenclature Committee. J Bone Miner Res 2:595–610. doi: 10.1002/jbmr.5650020617

22. Busa B, Miller LM, Rubin CT, et al. (2005) Rapid establishment of chemical and mechanical properties during lamellar bone formation. Calcif Tissue Int 77:386–394. doi: 10.1007/s00223-005-0148-y

23. Donnelly E, Boskey AL, Baker SP, van der Meulen MCH (2010) Effects of tissue age on bone tissue material composition and nanomechanical properties in the rat cortex. J Biomed Mater Res A 92:1048–1056. doi: 10.1002/jbm.a.32442

24. Vahle JL, Sato M, Long GG, et al. (2002) Skeletal Changes in Rats Given Daily Subcutaneous Injections of Recombinant Human Parathyroid Hormone (1-34) for 2 Years and Relevance to Human Safety. Toxicologic Pathology 30:312 –321. doi: 10.1080/01926230252929882

25. Marini JC, Hopkins E, Glorieux FH, et al. (2003) Positive linear growth and bone responses to growth hormone treatment in children with types III and IV osteogenesis imperfecta: high predictive value of the carboxyterminal propeptide of type I procollagen. J Bone Miner Res 18:237–243. doi: 10.1359/jbmr.2003.18.2.237

26. Papapoulos SE, Cremers SCLM (2007) Prolonged bisphosphonate release after treatment in children. N Engl J Med 356:1075–1076. doi: 10.1056/NEJMc062792

27. Komatsubara S, Mori S, Mashiba T, et al. (2005) Suppressed Bone Turnover by Long-Term Bisphosphonate Treatment Accumulates Microdamage but Maintains Intrinsic Material Properties in Cortical Bone of Dog Rib. Journal of Bone and Mineral Research 20:2066–2073. doi: 10.1359/jbmr.2005.20.11.2066

28. Li J, Mashiba T, Burr DB (2001) Bisphosphonate treatment suppresses not only stochastic remodeling but also the targeted repair of microdamage. Calcif Tissue Int 69:281–286.

29. Mashiba T, Hirano T, Turner CH, et al. (2000) Suppressed Bone Turnover by Bisphosphonates Increases Microdamage Accumulation and Reduces Some Biomechanical Properties in Dog Rib. Journal of Bone and Mineral Research 15:613–620. doi: 10.1359/jbmr.2000.15.4.613

30. Mashiba T, Turner CH, Hirano T, et al. (2001) Effects of suppressed bone turnover by bisphosphonates on microdamage accumulation and biomechanical properties in clinically relevant skeletal sites in beagles. Bone 28:524–531.

31. Allen MR, Reinwald S, Burr DB (2008) Alendronate Reduces Bone Toughness of Ribs without Significantly Increasing Microdamage Accumulation in Dogs Following 3 Years of Daily Treatment. Calcified Tissue International 82:354–360. doi: 10.1007/s00223-008-9131-8

32. Davis MS, Kovacic BL, Marini JC, et al. (2012) Increased susceptibility to microdamage in Brtl/+ mouse model for osteogenesis imperfecta. Bone 50:784–791. doi: 10.1016/j.bone.2011.12.007

33. Uveges TE, Kozloff KM, Ty JM, et al. (2009) Alendronate Treatment of the Brtl Osteogenesis Imperfecta Mouse Improves Femoral Geometry and Load Response Before Fracture but Decreases Predicted Material Properties and Has Detrimental Effects on Osteoblasts and Bone Formation. Journal of Bone and Mineral Research 24:849–859. doi: 10.1359/jbmr.081238

34. Forlino A, Kuznetsova NV, Marini JC, Leikin S (2007) Selective retention and degradation of molecules with a single mutant [alpha]1(I) chain in the Brtl IV mouse model of OI. Matrix Biology 26:604–614. doi: 16/j.matbio.2007.06.005

35. Reich, Adi, Cabral W, Marini, Joan (2011) Altered Transcript Pattern During Osteoblast Differntiation Associated With Improved Bone Phenotype in Homozygous Osteogenesis Imperfecta Brtl Mice. J Bone Miner Res 26 (Suppl 1):

CHAPTER 3

Adult Brtl/+ Mouse Model of Osteogenesis Imperfecta Demonstrates Anabolic Response to Sclerostin Antibody Treatment with Increased Bone Mass and Strength

Introduction

Osteogenesis imperfecta (OI) is a heritable disorder caused by mutations in type I collagen or collagen-associated proteins. Patients with OI have increased bone fragility, causing fracture susceptibility from minimal force, skeletal deformities and growth deficiency [1]. OI is a disease that most severely affects children, and fracture rate tends to decrease after puberty. Despite this relative improvement, adults remain at an increased risk for fracture compared to a normal population, and commonly have osteoporotic BMD values [2].

Treatment options to improve bone strength in adults with OI include anti-resorptive bisphosphonates (BP) which are considered the current standard of care. However, the limited clinical trials investigating BP use in adult OI have found mixed reports, with some studies citing a reduced fracture incidence with treatment, while others show no therapeutic effect despite increases in bone mass [3–6]. More effective therapies are needed for the treatment of adult OI and several preliminary reports have begun to investigate the use of anabolic teriparitide [7, 8].

Neutralizing antibodies to sclerostin are a novel anabolic osteoporosis treatment strategy presently in clinical trials for the treatment of osteoporosis, and may be useful for increasing bone mass in adult OI. Sclerostin is a negative regulator of bone formation secreted primarily by

osteocytes which inhibits anabolic canonical wnt signaling in osteoblasts by binding to the LRP4/5/6 complex [9–11]. Treatment with a neutralizing antibody to sclerostin (Scl-Ab) prevents sclerostin inhibition of canonical wnt signaling and effectively reduces sclerostin's ability to limit bone formation. Scl-Ab has been shown to be highly anabolic in pre-clinical models of osteoporosis and in phase 1 and phase 2 clinical trials of men and postmenopausal women [12–15].

The Brtl/+ mouse is a knock-in model for moderately severe Type IV OI with a G349C point mutation on c*ol1a1* that recreates an identical defect found in an OI patient [16]. The Brtl/+ mouse recapitulates multiple features of the observed clinical phenotype including short stature, reduced BMD, increased bone brittleness, and impaired remodeling [17–19]. Importantly, the Brtl/+ phenotype becomes less severe with age [17], making it an appropriate model for testing the anabolic efficacy of Scl-Ab in adult OI.

We have previously reported that short-term Scl-Ab therapy is capable of stimulating bone formation and increasing bone mass in an 8 week old Brtl/+ model of OI [20]. Importantly, no preclinical studies have analyzed the effects of any anabolic or anti-catabolic agents in an adult model of OI. The purpose of this study was to determine if Scl-Ab could increase bone formation in osteoblasts harboring a classical OI-causing mutation to improve bone mass and whole bone strength in an adult Brtl/+ model of OI.

Materials and Methods

Animals

Wildtype (WT) and Brtl/+ mice are maintained on a mixed background of Sv129/CD-1/C57BL/6S, and all Brtl/+ animals were the product of breeding male Brtl/+ with female WT. 6

month old male WT and Brtl/+ mice were randomly assigned to Scl-Ab (Scl-Ab VI, Amgen, Thousand Oaks, CA) treatment or vehicle injection (PBS) with WT Veh n=8, WT Scl-Ab n=9, Brtl/+ Veh n=8, and Brtl/+Scl-Ab =9. Sclerostin antibody was injected subcutaneously at 25mg/kg, two times per week, for five weeks, following the protocol described previously [13]. To facilitate dynamic histomorphometry, calcein (30mg/kg, i.p.) was injected at the start of the experiment, 3 weeks before sac and 1 week before sac. Alizarin (30mg/kg, i.p.) was injected 1 day prior to sacrifice. Body weights were recorded with each injection. Blood samples were collected at euthanasia by intracardiac puncture, serum separated by centrifuge, and stored at -80˚C until analyzed by ELISA.

Left femurs were collected for microCT and mechanical testing, and right femurs for dynamic histomorphometry. Both were stored at -20˚C in lactated ringers solution (LRS) soaked gauze until testing or further specimen preparation. All protocols and procedures involving animals were approved by the University of Michigan's Committee on Use and Care of Animals.

Serum Assays

To measure osteoblast activity, serum osteocalcin (OCN) was quantified with a commercially available ELISA kit (BT-470, BTI, Stoughton, MA). To quantify osteoclast number, serum TRACP5b was measured with a commercially available solid phase immunofixed enzyme activity assay (MouseTRAP, IDS, Fountain Hills, AZ). Both serum tests were performed in duplicate.

MicroCT

Left femora were scanned in water using cone beam computed tomography (eXplore Locus SP, GE Healthcare Pre-Clinical Imaging, London, ON, Canada). Scan parameters included a 0.5 degree increment angle, 4 frames averaged, an 80kVp and 80µA x-ray source with a 0.508mm Al filter to reduce beam hardening artifacts, and a beam flattener around the specimen holder [21]. All images were reconstructed and calibrated at 18µm isotropic voxel size to a manufacturer supplied phantom of air, water and hydroxyapatite. The entire femora was reoriented with the mid-diaphysis parallel to the z-axis, and bone length was measured as the distance between the most proximal and distal transverse plans containing the femur. Regions of interest (ROI) were located for both cortical and trabecular parameters. A diaphyseal cortical ROI spanning 15% of total femur length was located midway between the distal growth plate and third trochanter. Cortical bone was isolated with a fixed threshold of 2000 Hounsfield Units for all experimental groups. Parameters including cortical thickness, cross sectional area, tissue mineral density (TMD), bending moment of inertia in the anterior-posterior direction (about the medial-lateral axis), endosteal perimeter, and periosteal perimeter were quantified with commercially available software (MicroView v2.2 Advanced Bone Analysis Application, GE Healthcare Pre-Clinical Imaging, London, ON, Canada)**.** A trabecular ROI 10% of total femur length was located approximately 100 microns proximal to the central, and most proximal, portion of the distal femoral growth plate The inner cortical surface was defined with a splining algorithm. Due to the different morphology induced by Scl-Ab treatment, a fixed threshold could not be utilized without bias. Trabecular metaphyseal bone was isolated with a more conservative autothresholding algorithm for each specimen based on the bimodal distribution between marrow and bone [22]. Parameters including bone volume fraction (BV/TV), trabecular

thickness (TbTh), and trabecular number (TbN) were quantified using standard stereology algorithms (MicroView v2.2). A 3D sphere fitting algorithm was also used to confirm the stereology data for TbTh [23].

The 8th caudal vertebrae were dissected and scanned with the same protocol as the femora. Trabecular bone of the caudal vertebrae was analyzed in two ROIs, each spanning 9% of bone length and placed adjacent to the proximal and distal growth plates. The trabecular surface was defined on the inner cortical surface with a splining algorithm. Cortical bone of the 8th caudal vertebrae was analyzed in a ROI spanning 9% of bone length and placed in the middle of bone. Cortical thickness was measured along four lines originating at the center of gravity of the section, and placed 40 and 50 degrees anterior to the medial lateral plane similar to previous reports [24].

Whole Bone Mechanical Four-Point Bending

Following μCT scanning, left femora were loaded to failure in four-point bending using a servohydraulic testing machine (MTS 858 MiniBionix, Eden Prarie, MN). All specimens were kept hydrated in LRS-soaked gauze until mechanical testing. In the same mid-diaphyseal region analyzed by μCT, the mid-diaphysis was loaded in four point bending with the posterior surface oriented under tension. The distance between the wide, upper supports was 6.26mm, and span between the narrow, lower supports 2.085mm. The vertical displacement rate of the four-point bending apparatus in the anterior-posterior direction was 0.5mm/sec. Force was recorded by a 50lb load cell (Sensotec) and vertical displacement by an external linear variable differential transducer (LVDT, Lucas Schavitts, Hampton, VA), both at 2000Hz. A custom MATLAB script was used to calculate all parameters measured from the force-displacement data. Elastic energy

was defined as the area under the load-displacement curve prior to the yield point, and plastic energy was defined as the area under the load-displacement curve from the yield point until failure. The yield point was defined as a 10% reduction in secant stiffness relative to the initial tangent stiffness. Combining bending moment of inertia data from μCT with mechanical stiffness from four point bending, the estimated elastic modulus was calculated using standard beam theory as previously described [17].

Dynamic Histomorphometry

Right femora were encased in epoxy (Kold Mount, Vernon-Benshoff, Albany, NY), and cut transversely with a low-speed saw (IsoMet, Beuhler, Lake Bluff, IL). The distal section of tissue was polished using progressive grades of silicon carbide abrasive paper (1200, 2400, and 4000 grit) to a plane immediately distal to the third trochanter.

Fluorescent images were acquired using a Zeiss Axiovert 200M inverted microscope equipped with a structured illumination (Apotome) imaging system. This focuses the image on a specific plane, minimizes out-of-plane light, and negates the need for several micron thin sections. Multiple fluorescent images were taken with a 10x objective of the calcein (excitation: 485/20nm, emission: 540/25nm) and alizarin (excitation: 557/55nm, emission: 615nm) labels around the entire cortex. The 10x images of the cortex were merged into a single image (Photoshop, Adobe), and these merged images were analyzed using commercially available software (Bioquant Osteo v7.20.10, Nashville, TN). Bone surface (BS), mineral apposition rate (MAR), mineralizing surface to bone surface (MS/BS), and bone formation rate (BFR) were quantified on the calcein label given 3 weeks before sacrifice and the alizarin label given 1 day before sac on the periosteal surface and analyzed according to ASBMR standards [25].

In order to quantify the level of cortical drift in these mice and contrast the therapeutic response to prior studies analyzing rapidly growing 3 week old Brtl/+ mice treated with Scl-Ab [26], dynamic histomorphometry outcomes were also assessed in anatomic regions around the cortex with a method similar to Bivi et. al [27]. The fluorescent images were oriented anatomically by using the contralateral microCT femoral 3D images as a reference. The centroid of the fluorescent image was identified in ImageJ, and 110 degree angles from the centroid were used to define the anterior and posterior regions (Fig 3.5). MAR, MS/BS, and cortical thickness were quantified in each of these anterior and posterior subregions.

In any regions where there was no dual label, MAR was treated as a missing value. For the purpose of calculating BFR/BS, a value of 0.1μm/day was assigned to MAR where missing values were present. This value was determined from both looking at the biological limit observed in our specimens as well as values established in the literature [27]. BFR/BS was also analyzed when treated as a missing value. One animal (WT Veh) had a missing fluorescent label, most likely due to injection error, and was excluded from this analysis. Two additional animals (both WT Scl-Ab) displayed all fluorescent labels, but a portion of the endosteal surface had errors in image acquisition which could not be corrected. Both of these animals were excluded from analysis on the endosteal surface only. Final group sizes are shown in the relevant figures and tables.

Statistics

A two-factor multivariate ANOVA was performed for all data (IBM SPSS Statistics v21.0.0.0), the invididual factors as genotype (WT or Brtl/+) and treatment (Veh or Scl-Ab). The interaction term between genotype and treatment is also presented. Tukey's HSD post-hoc

test was used to make comparisons except when unequal variances were observed. Dunnett's T3 post-hoc test was used for variables which displayed unequal variances. In all cases, $p<0.05$ was considered significant. Values between $p=0.05$ and $p=0.10$ are reported in all instances, and are referred to as "trends" in the text. All data are presented as mean±S.D.

Results

Body Mass and Bone Length Not Changed by Scl-Ab

At the beginning of the experiment, WT animals (38.4±4.1g) were significantly heavier than Brtl/+ (34.9±4.7g) when pooling data from Veh and Scl-Ab groups for each genotype. Throughout the 5 weeks of experiment, WT Veh and Brtl/+ Veh did not have any significant changes in body mass. Scl-Ab did not induce a change in body mass during the 5 weeks of treatment (not shown).

Brtl/+ Veh femurs were shorter than WT Veh as assessed by endpoint microCT (Table 3.1). Scl-Ab had no effect on femoral length.

Scl-Ab Increased Serum Osteocalcin and Reduced Serum TRACP5b

Scl-Ab significantly increased serum osteocalcin (OCN) levels in both WT (+49%) and Brtl/+ (+47%) indicative of increased bone formation and an anabolic response to therapy (Fig 3.1). Serum OCN levels were not different between Veh treated WT and Brtl/+ mice.

Serum TRACP5b, a marker of osteoclast number, was significantly decreased in WT (-78%). Despite a numerical decrease in Brtl/+ (-66%) with Scl-Ab treatment, it was not statistically significant ($p=0.064$) (Fig 3.1). The interaction term between genotype and treatment was not significant, suggesting that Scl-Ab did not have a differential effect on Serum

TRACP5b between WT and Brtl/+. Similar to OCN data, there were no phenotypic differences observed between WT Veh and Brtl/+ Veh in serum TRACP5b.

Scl-Ab Increases Femoral Trabecular Thickness and Trabecular Number

Phenotypically, Brtl/+ Veh animals had reduced femoral trabecular BV/TV (Fig 3.2, Fig 3.3) compared to WT Veh (-93%). These differences were the result of significant reductions in trabecular number (-67%), but not trabecular thickness.

In WT and Brtl/+, five weeks of Scl-Ab therapy significantly increased bone volume fraction (WT +117%; Brtl +119%) and trabecular BMD. The significant gains in femoral trabecular bone mass with therapy were a result of significant increases in both trabecular thickness (WT +38%; Brtl +29%) and trabecular number (WT +70%; Brtl +55%).

Despite these significant gains in the femur, we observed no effect of Scl-Ab on trabecular bone of the 8th caudal vertebrae by microCT (Fig 3.4)

Scl-Ab Increases Brtl/+ Bone Formation on Endosteal and Periosteal Femora Surfaces

On the total periosteal surface of the diaphyseal femur, treatment of Brtl/+ with Scl-Ab significantly increased BFR/BS (+205%) as a result of large increases in MAR (+132%) and smaller gains in MS/BS (+38%) (Fig 3.5, Fig 3.6). In WT animals, Scl-Ab significantly increased MAR (+114%) which led to an increase in BFR/BS (+169%). Scl-Ab did not significantly increase MS/BS in WT on this surface even though 7 of 9 WT Scl-Ab animals had a MS/BS greater than the largest WT Veh value on the periosteal surface. The interaction term was not significant, suggesting Scl-Ab did not behave differently for periosteal MS/BS between genotypes On the total endosteal surface of both genotypes, Scl-Ab significantly increased

MS/BS (WT +181%; Brtl +155%) and MAR (WT +126%; Brtl +180%) to a similar extent. These gains led to large increases in endosteal BFR/BS in both genotypes with Scl-Ab treatment (WT +650%; Brtl +683%). No differences were found between WT Veh and Brtl Veh on either surface, but overall Brtl/+ had greater endosteal MS/BS levels.

Regional analysis in the anterior and posterior regions of the cortex revealed a weak posterior shifting cortical drift pattern in both WT Veh and Brtl/+ Veh with more bone formation observed on the posterior periosteal surface compared to the anterior periosteal surface (Fig 3.5, Table 3.2). No complimentary cortical drift pattern was observed on the endosteal surface, where bone formation was very low in both genotypes.

Analyzing the effect of Scl-Ab on the anterior and posterior sub-regions revealed a similar effect on the periosteal surface in each compartment, with BFR/BS gains primarily driven by increases in MAR (Table 3.2). On the endosteal anterior and posterior surfaces, Scl-Ab increased MAR as well as MS/BS in Brtl/+, leading to increased BFR/BS.

Analyzing BFR/BS data as a missing value when no MAR was present led to an identical statistical conclusion on the periosteal and endosteal surfaces (data not shown). Two small statistical differences are apparent in the regional data on the low-forming endosteal posterior surface. Specifically, when BFR/BS is treated as a missing value, WT Veh vs WT Scl-Ab becomes significant on the endosteal posterior surface, and is no longer significant ($p=0.068$) for Brtl/+ Veh vs Brtl/+ Scl-Ab.

Scl-Ab Increases Brtl/+ Femoral Cortical Bone Mass

Five weeks of Scl-Ab led to large increases in cortical cross-sectional area (WT +36%; Brtl +21%) and cortical thickness (WT +42%; Brtl +22%) in both genotypes (Table 3.1) as

measured by microCT of the left femora. Consistent with the stronger endosteal vs periosteal response observed by dynamic histomorphometry, Scl-Ab significantly decreased marrow area in both genotypes (WT -11%; Brtl -19%), although total area and bending moment of inertia were unchanged. A two-factor ANOVA revealed that overall Scl-Ab significantly increased the Bending Moment of Inertia and TMD, although the Scl-Ab effects were not significant within each genotype for these outcomes.

No geometric phenotypic differences were observed between WT Veh and Brtl/+ Veh in the femoral cortex at this time point. However, overall genotype effects from a two-factor ANOVA revealed that relative to WT, Brtl/+ had significantly reduced Marrow Area, significantly reduced Total Area, and significantly increased TMD.

Consistent with a lack of effect in caudal vertebral trabecular bone, there was no effect of Scl-Ab on cortical thickness in either WT or Brtl/+ 8^{th} caudal vertebrae (Fig 3.4).

Brtl/+ Whole Bone Mechanical Properties Improved by Scl-Ab

Significant gains in whole bone mass with Scl-Ab led to significant improvements in whole bone mechanical properties as measured by mechanical four-point bending of the femoral mid-diaphysis (Fig 3.7, Table 3.1). Specifically, five weeks of Scl-Ab caused large increases in Yield Load (WT +79%; Brtl +77%), Ultimate Load (WT +129%; Brtl +127%) and Bending Stiffness (WT +70%; Brtl +38%) in both genotypes (Table 3.1). While increases in Energy-to-Failure with Scl-Ab treatment were expected based on the effects on Ultimate Load, the magnitude of the increases were unexpected (WT +526%; Brtl +509%). These observed increases in Energy-to-Failure with Scl-Ab were primarily a result of significantly increased plastic energy (WT +1498%; Brtl +1660%) and in lesser part a result of increased elastic energy

(WT +96%; Brtl +153%). The increased plastic energy with Scl-Ab was a result of an increase in Post-Yield Displacement with therapy in both WT (+539%) and Brtl/+ (+541%) as demonstrated in the representative load-displacement curves in Figure 3.7. Yield Displacement was increased in Brtl/+ with Scl-Ab, but not WT. The estimated elastic modulus was increased with Scl-Ab in WT, but there was no effect in Brtl/+.

Similar to cortical microCT data, there was no significant whole bone mechanical property phenotype of Brtl Veh vs WT Veh at this age. However, overall genotype effects from a two-factor ANOVA revealed that relative to WT, Brtl/+ had significantly reduced Energy to Failure, and significantly increased Elastic Modulus.

Discussion

In this study, we demonstrated that five weeks of Scl-Ab therapy was able to stimulate bone formation in an adult Brtl/+ mouse model of Type IV OI, leading to increased long bone mass and improved mechanical properties. No preclinical studies to date have analyzed the effect of pharmaceutical intervention for an adult mouse model of OI. In the context of existing anabolic and anti-resorptive treatment options, Scl-Ab is a novel drug with strong therapeutic potential for adult OI patients. While current treatment options to improve bone strength in adults with OI focus on bisphosphonates (BP), the functional benefit of antiresorptive therapy is appears modest. A randomized control trial of intravenous neridronate in adults with Type IV OI found increased BMD at the spine and hip with treatment as well as reduced total fracture incidence [4]. In a randomized placebo-controlled trial of oral alendronate in patients with Type I OI, increased BMD at the spine and hip was observed with treatment, but the study was not powered to detect fracture risk [3]. Two more recent clinical trials have noted similar increases

in bone mass with BP treatment, but equivocal effects at reducing fractures in adults with OI [5, 6]. Moreover, BP efficacy may be dependent upon the type and severity of OI [5] as well as the dose. In light of these observations, strong motivation exists for the exploration of alternative therapies for the treatment of adult OI. To address this need, recent studies have begun to investigate the use of anabolic intermittent parathyroid hormone as a therapy for adult OI. An uncontrolled clinical trial indicates promising teriparatide efficacy in adult OI [7], and randomized double-blind placebo controlled trial also shows a benefit in Type I OI patients [8].

Here, we noted suggestions of age-specific differences in response to Scl-Ab treatment, emphasizing the importance of examining adult OI mice separately from young OI mice. Rapidly growing 3 week Brtl/+ mice treated for 5 weeks with Scl-Ab showed a similar gain in femoral cortical bone area (WT +31%; Brtl/+ 25%) when compared to the adult data (WT +36%; Brtl/+ +21%) (Chapter 4). Furthermore, in the present study, we observed significant gains in femoral BV/TV in both WT and Brtl/+ with 5 weeks of Scl-Ab (Fig 3.2). This contrasts with treatment of young Brtl/+ mice for an equivalent 5 weeks with Scl-Ab where we observed a more modest femoral trabecular response based on distance from the growth plate (Chapter 4). This data is suggestive of a differential trabecular response with age that may be related to differential turnover, altered sclerostin expression with growth, and perhaps the absence of confounding linear growth effects.

While we expected Scl-Ab to increase femoral BV/TV in adult WT and Brtl/+ mice in this study by increasing trabecular thickness, we did not expect to see large changes in trabecular number. Unexpectedly, we observed a large increase in trabecular number in the distal femoral metaphysis with five weeks of Scl-Ab (Fig 3.2). Decreased bone resorption could explain this finding by preserving trabeculae that might otherwise be lost to increased primary trabecular

turnover. In this study we found decreased serum TRACP5b with Scl-Ab, consistent with reports from others showing decreased bone resorption in humans [12] as well as preclinical rodent data [13]. Alternatively, the large differences in morphology induced by Scl-Ab could affect quantification of trabecular number. If Veh animals contain trabeculae that were too thin to be detectable by microCT at the applied resolution, thickening of these structures to a detectable level by Scl-Ab could result in the increased trabecular number observed. While our conservative specimen-specific thresholding method helps guard against these effects, it does not eliminate them.

Interestingly, we observed no effect of Scl-Ab on either the trabecular bone or cortical thickness of the 8th caudal vertebrae in this study. One previous study in adult female rats has observed an anabolic response with Scl-Ab in the caudal vertebrae [28]. Specifically, increases in BFR/BS and BV/TV were measured in sections by histomorphometry at this site of yellow marrow. Interestingly, other studies of anabolic PTH have found reduced effects in the caudal vertebrae relative to the distal femur or lumbar vertebrae in ovariectomized rats with doses 20% of the present study [29]. Additional studies have observed a robust response to anabolic PTH in caudal vertebrae [30] while others have suggested that an anabolic PTH response in caudal vertebrae may be supported by mechanical loading [31]. Our lack of difference in BV/TV may reflect differences in local sclerostin expression or drug delivery in the caudal vertebrae, as differences in the mouse compared to the rat, or dose of Scl-Ab.

The femoral cortical dynamic histomorphometry response to Scl-Ab was also qualitatively different between the adult mice analyzed in this study and our treatment of rapidly growing 3 wk Brtl/+ mice. In the present study, Scl-Ab was able to consistently increase MAR on the periosteal surface. On the endosteal surface, where lower levels of bone formation were

found in control animals, Scl-Ab was able to increase both MS/BS and MAR in most cases. Previously, we reported that a short-term two week Scl-Ab therapy in 8 week old Brtl/+ mice stimulated femoral periosteal BFR by increasing mineralizing surface, but not mineral apposition rate [20]. In addition, we have also treated rapidly growing 3 wk old Brtl/+ mice for 5 weeks with Scl-Ab and similarly found that Scl-Ab was able to increase bone formation by primarily increasing MS/BS, with no effect on MAR on both the endosteal and periosteal surfaces [26]. Although the cortical drift pattern we observed was weak in these 6 month old mice, the posterior periosteal surface remained a location of high bone formation (MS/BS) similar to our observation in rapidly growing 3 week old mice. The regional dynamic histomorphometry analysis allows us conclude that Scl-Ab can increase MAR in regions that have high MS/BS in adult animals, but is unable to increase MAR in these regions in rapidly growing animals. These findings may be related to different sclerostin expression levels with age, and a strong underlying cortical drift pattern in growing mice. In addition, rapidly growing 3 wk mice have a high Veh MAR (~1.25-2.5μm/day) and may be operating at near maximum output, leaving little room for further stimulation via Scl-Ab. In contrast, lower Veh MAR levels in adult 6 mo (~0.3μm/day) leave room for Scl-Ab to have a potent effect, and may explain the age-dependent effect of Scl-Ab on MAR.

Increased tissue brittleness is a hallmark feature of the OI phenotype. The Brtl/+ model demonstrates increased brittleness at young ages when mechanically tested to failure, and remains brittle through 6 months [17]. In this study, we observed that mid-diaphyseal cortical bone of the Brtl/+ femur had increased TMD, decreased energy to failure, and increased elastic modulus. Previously, we found an unexpected result that a short-term treatment with Scl-Ab significantly increased Post-Yield Displacement (indicating decreased tissue brittleness) in WT

animals, but not Brtl/+ [20]. In the present study, we found exceptionally large gains in PYD with 5 weeks of Scl-Ab treatment in both WT and Brtl/+. While we remain aware of the numerous violations of beam theory assumptions and loading differences that may result from Scl-Ab induced geometrical differences, the magnitude of the changes in PYD (WT +539%; Brtl +541%) is difficult to ignore. The cause of this difference could be related to the addition of new, more ductile bone, to a mature skeleton. Alternatively, it could reflect that bone formed under the influence of Scl-Ab may be of a different material independent of tissue age. It will be important to determine if these reductions in brittleness are persistent changes, or transient changes that disappear quickly after cessation of therapy. While the beneficial materials differences of Scl-Ab on PYD are suggestive, these data require corroboration with detailed composition and mechanical techniques. Interestingly, we observed an increase in the estimated elastic modulus with Scl-Ab in WT, but not Brtl/+. This finding was not accompanied by similar gains in tissue mineral density, suggesting that changes at a level of organization below that of overall cortical size, but larger than tissue ultrastructural characteristics may be at play. Alternatively, the robust changes in cortical thickness found with sclerostin antibody may induce additional artifact related to beam theory calculations, as has been previously described [32].

There are several limitations of this study. First, osteogenesis imperfecta is a heterogeneous disease with a wide range of phenotypes caused by many different mutations. In this study, we used a mouse model harboring a mutation found in a patient with moderately severe Type IV OI. The findings of this study in the Brtl/+ mouse may not apply to all mutations and types of OI, including recessive forms as well as those with null col1 alleles. In addition, while Scl-Ab was potently anabolic in adult Brtl/+ mice is this study, it is unclear how long these gains will persist after cessation of therapy. The Scl-Ab dose chosen for these studies was

consistent with prior pre-clinical ovariectomy studies modeling post-menopausal osteoporosis [15]. As drug pharmokinetics can vary greatly between human vs rodent, the human "equivalent" dose is not known, but we recognize that the 25mg/kg twice per week dose is likely higher than the currently proposed doses for humans.

In summary, we have demonstrated that five weeks of Scl-Ab therapy was capable of increasing bone formation in an adult model of OI with a classic Gly->Cys substitution in *col1a1*. OI is a disease that most severely affects children, and fracture rate tends to decrease after puberty. Despite this relative improvement, adults remain at an increased risk for fracture compared to a normal population, and commonly have osteoporotic BMD values. While bisphosphonate therapy is often used in adult OI patients, there is a need for more effective anabolic therapeutics to improve patient outcomes. Scl-Ab is a unique and promising anabolic therapy which may be particularly useful for the treatment of adult OI by stimulating bone formation, adding bone mass, and increasing bone strength.

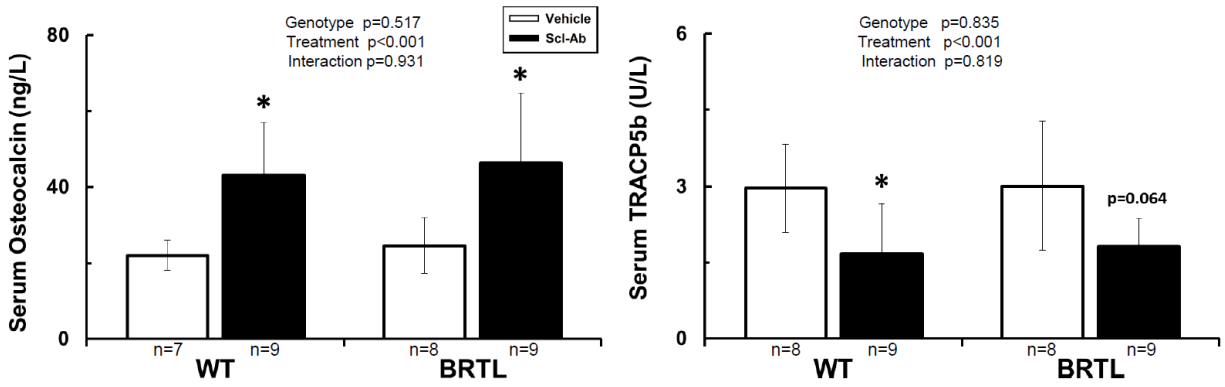

Figure 3.1: Serum TRACP5b and Osteocalcin. Serum OCN is elevated in both WT and Brtl/+ with Scl-Ab. Serum TRACP5b is reduced with Scl-Ab therapy in WT and shows a trend (p=0.064) toward reduced levels in Brtl/+, suggesting a decoupled effect on bone formation and bone resorption. * $p<0.05$ Scl-Ab vs. Veh.

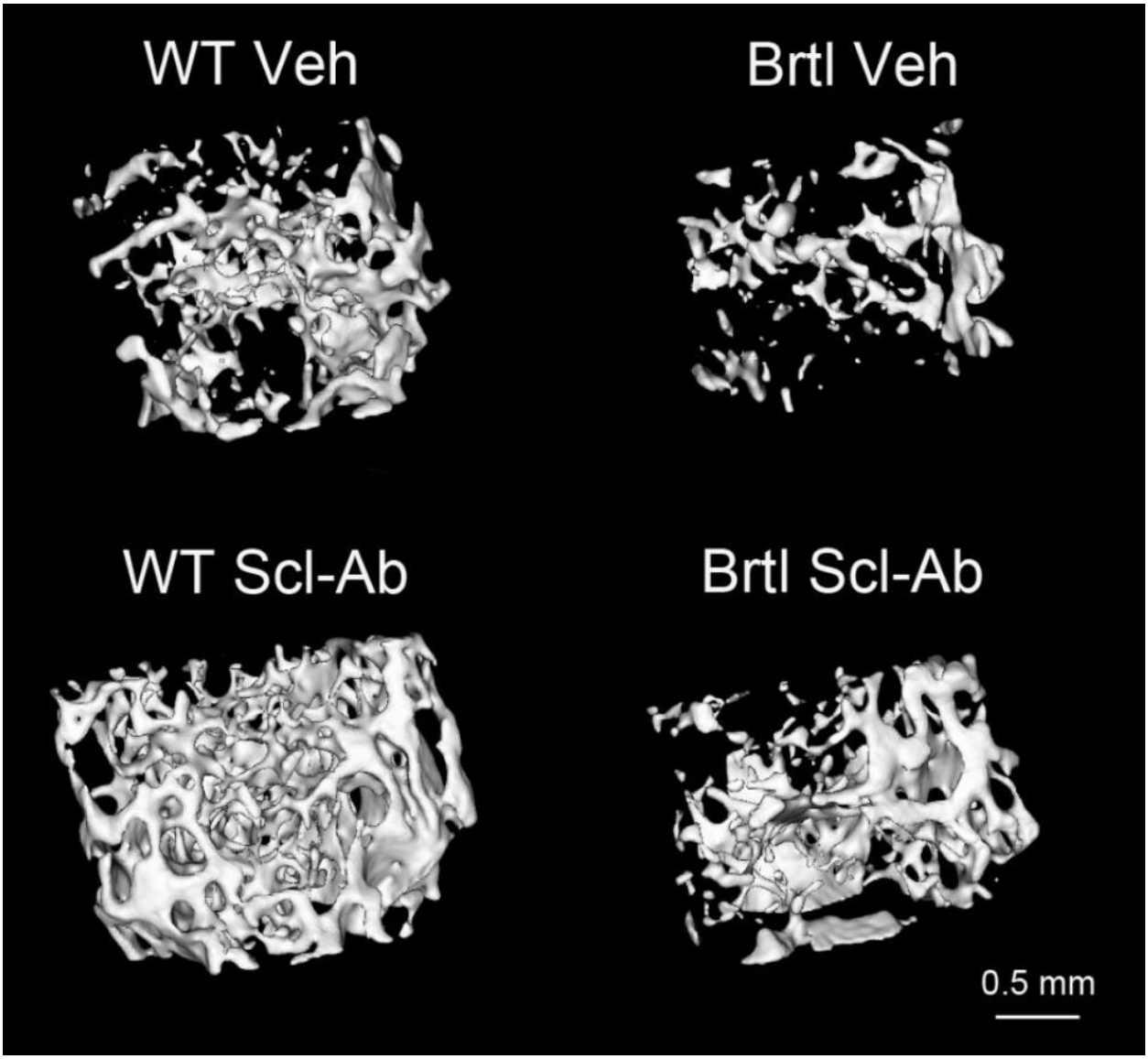

Figure 3.2: Femoral Trabecular MicroCT Representative Isosurfaces. Micro computed tomography isosurface images of the distal femur metaphysis reveals anabolic changes with Scl-Ab therapy.

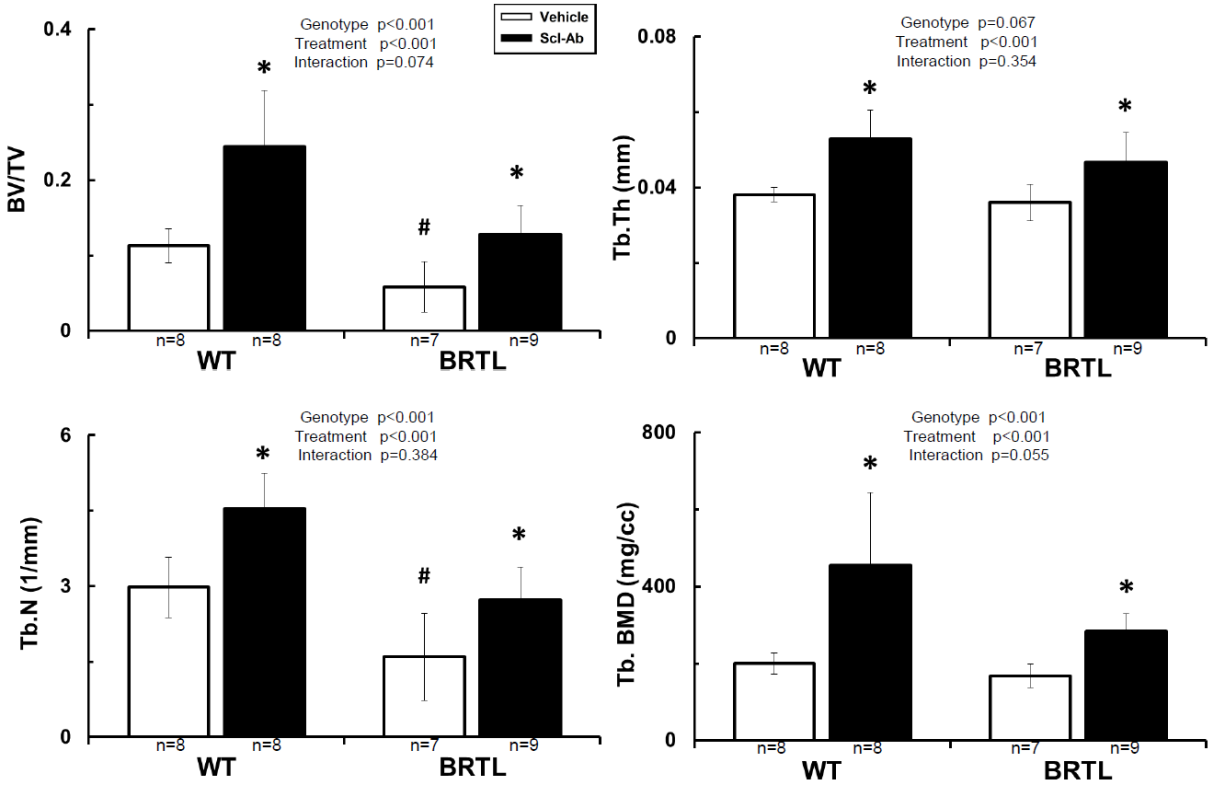

Figure 3.3: Femoral Trabecular MicroCT Data. Micro computed tomography of the distal femur metaphysis reveals anabolic changes with Scl-Ab therapy. BV/TV, Tb.Th, Tb.N, and Tb. BMD were increased with Scl-Ab in both WT and Brtl/+. A conservative specimen specific threshold is applied as described in the methods. *p<0.05 Scl-Ab vs. Veh; #p<0.05 WT Veh vs. Brtl/+ Veh.

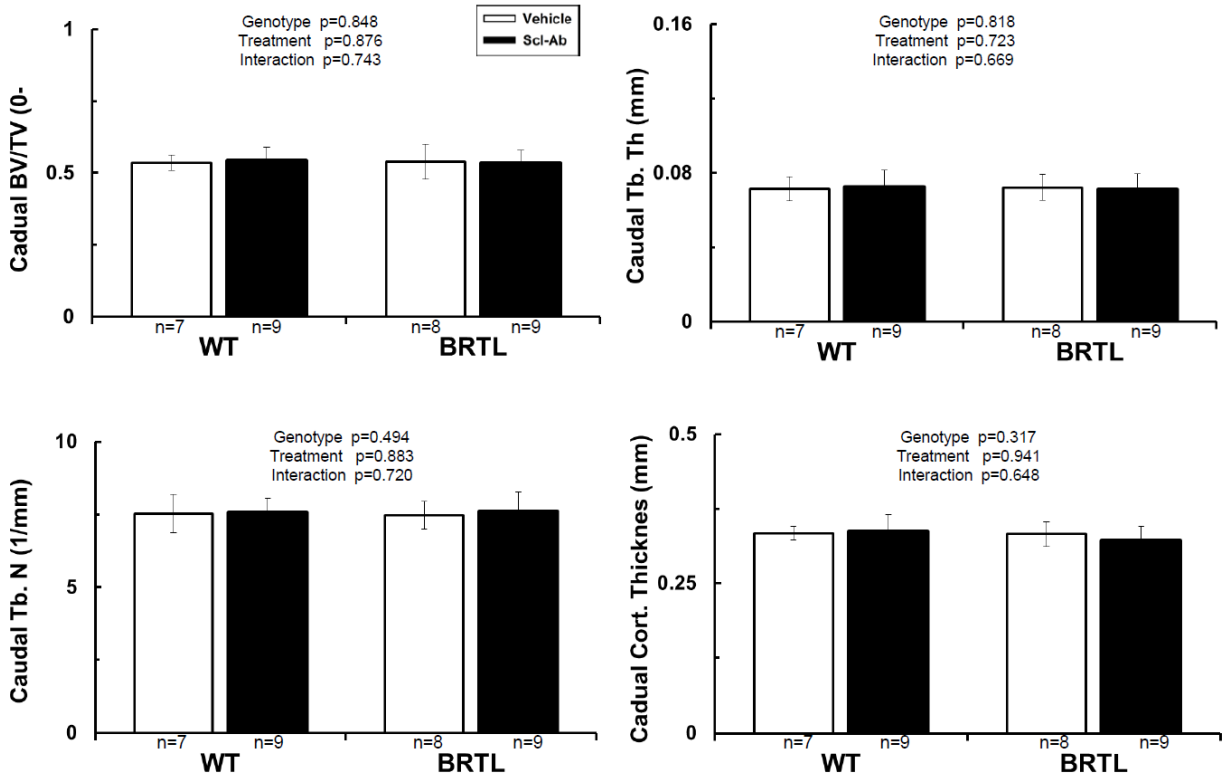

Figure 3.4: 8th Caudal Vertebrae Trabecular and Cortical MicroCT Data. MicroCT data from the 8th caudal vertebra demonstrate no effect of sclerostin antibody on trabecular or cortical bone structure in Brtl/+ or WT mice.

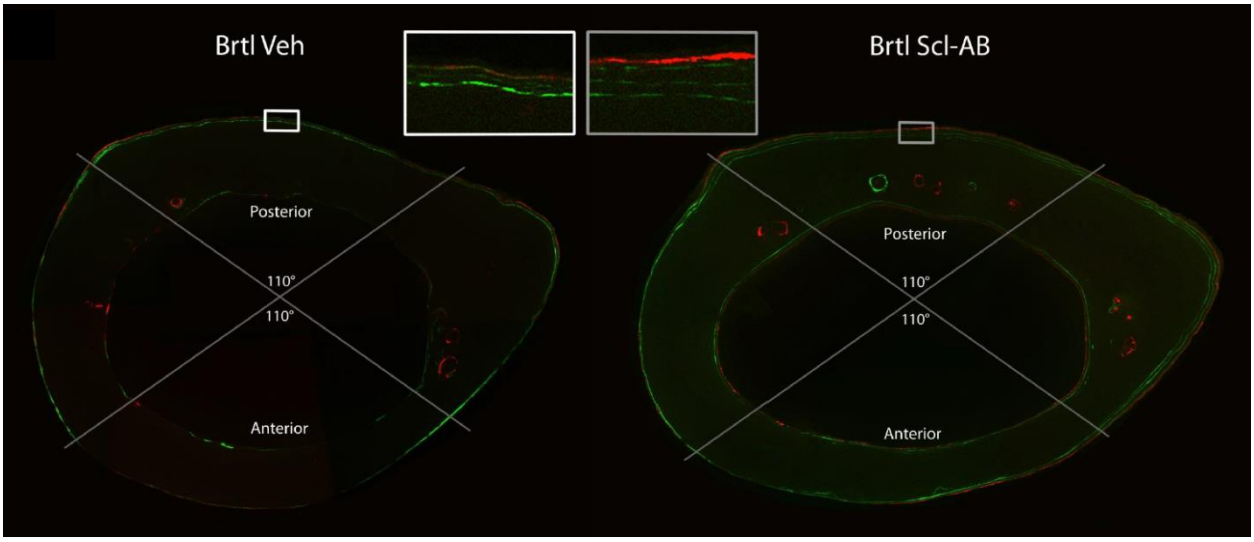

Figure 3.5: Representative Dynamic Histomorphometry and Regional Analysis Locations. Dynamic histomorphometry at the femoral mid-diaphysis reveals anabolic effect of Scl-Ab. The centroid of the bone was located, and 110deg angles drawn to define the anterior and posterior regions of bone for the purpose of regional analysis shown in Table 3.2.

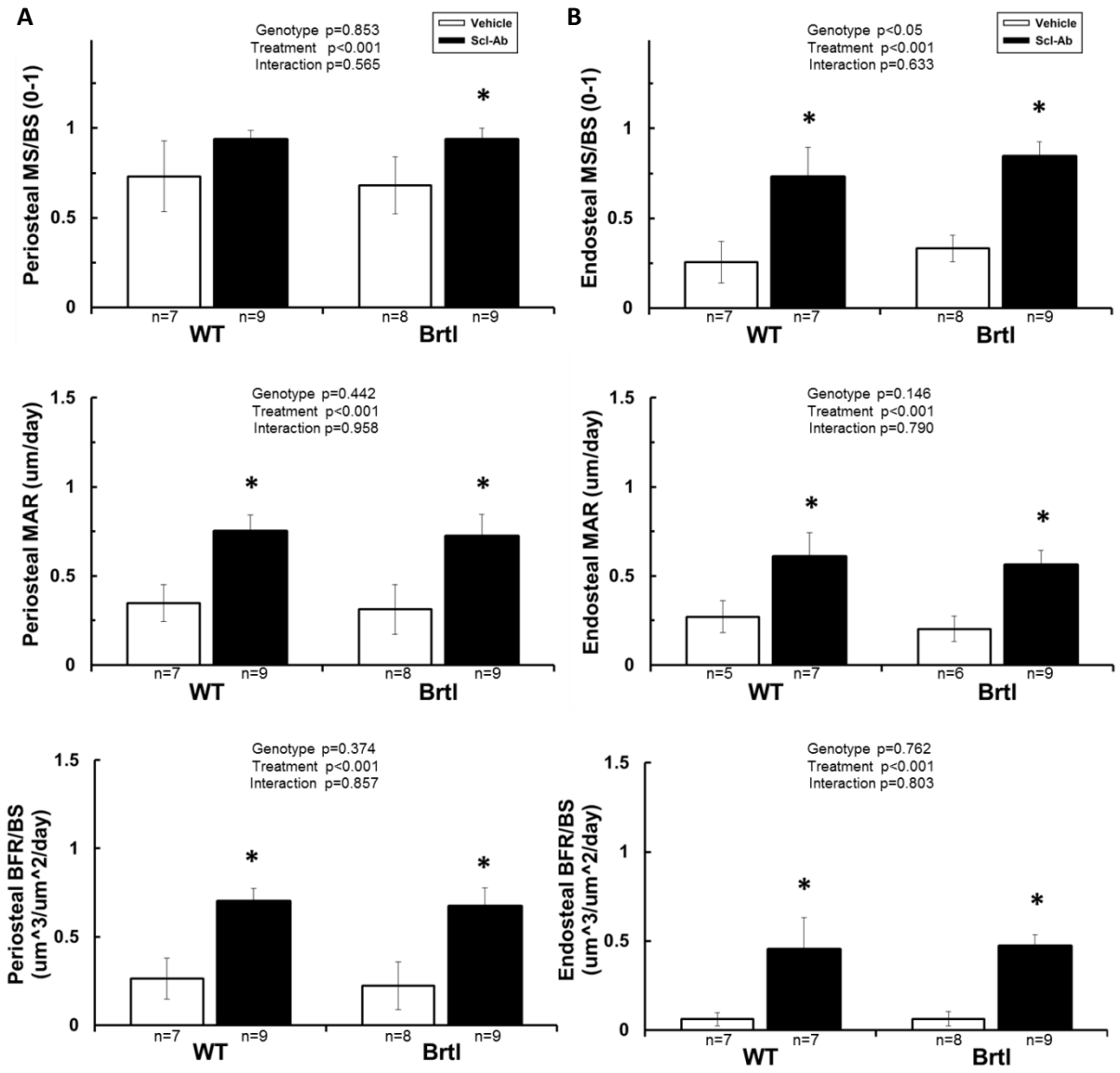

Figure 3.6: Cortical Periosteal and Endosteal Dynamic Histomorphometry (Femur). Dynamic histomorphometry at the femoral mid-diaphysis reveals anabolic effect of Scl-Ab in WT and Brtl/+. The centroid of the bone was located, and 110deg angles drawn to define the anterior and posterior regions of bone. Femoral cortical mid-diaphyseal periosteal BFR **(A)** increases with Scl-Ab are a result of increased periosteal MAR in WT and increased MAR and MS/BS in Brtl/+. Endosteal BFR **(B)** increases with Scl-Ab as a result of increased endosteal MAR and MS/BS in both WT and Brtl/+. * $p<0.05$ Scl-Ab vs. Veh.

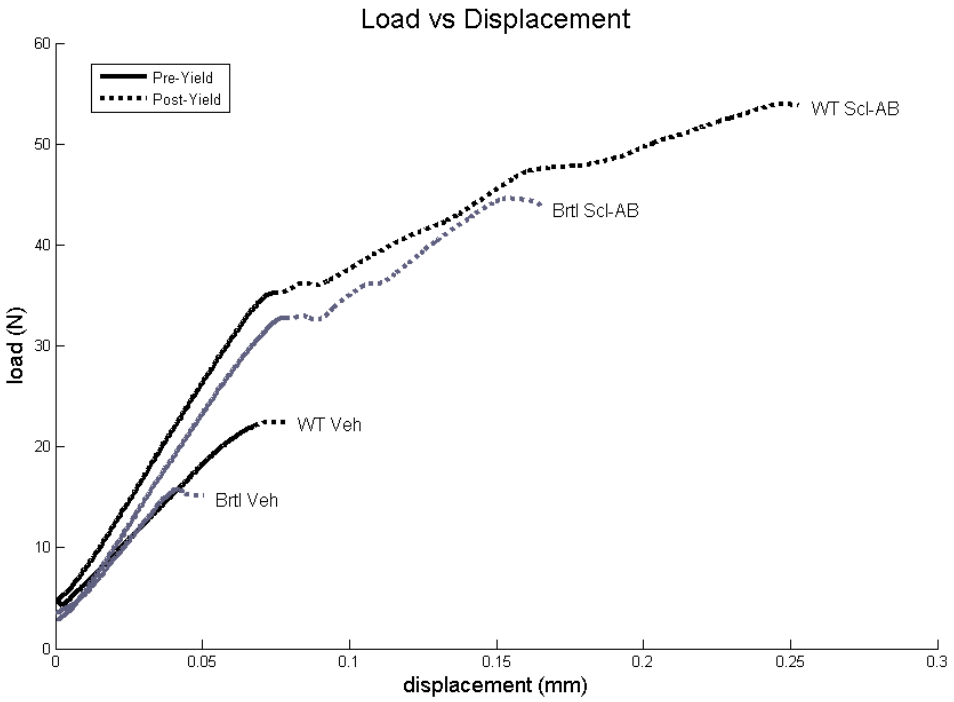

Figure 3.7: Representative Mechanical 4pt Bending Curves. Representative load-displacement plots from 4pt bending data shown in Table 3.1 summarize Scl-Ab induced strength and changes in post-yield behavior with treatment.

Table 3.1. Cortical MicroCT and Mechanical Properties

	WT Veh	*WT Scl-Ab*	*Brtl Veh*	*Brtl Scl-Ab*	*Genotype p-value*	*Treatment p-value*	*Interaction p-value*
	n=8	*n=8*	*n=7*	*n=9*			
Cortical Micro CT							
Total Femur Length (mm)	16.71 ± .40	16.58 ± .28	15.51 ± 0.78$^{\#}$	15.91 ± .48	<0.001	0.454	0.150
Thickness (mm)	0.201 ± .016	0.286 ± .028*	0.226 ± .028	0.277 ± .029*	0.412	<0.001	0.068
Cross Sectional Area (mm^2)	0.97 ± .07	1.33 ± .14*	1.00 ± .19	1.21 ± .16*	0.413	<0.001	0.162
Marrow Area (mm^2)	1.42 ± .16	1.15 ± .10*	1.16 ± .26	1.02 ± .11*	<0.01	<0.01	0.254
Total Area (mm^2)	2.39 ± .17	2.48 ± .16	2.16 ± .41	2.24 ± .22	<0.05	0.386	0.959
Bending Moment of Inertia (mm^4)	0.19 ± .03	0.25 ± .04	0.17 ± .07	0.22 ± .06	0.185	<0.01	0.742
Tissue Mineral Density (mg/cm^3)	1122 ± 40	1152 ± 33	1159 ± 38	1183 ± 32	<0.05	<0.05	0.806
Mechanical Four Point Bending							
Yield Load (N)	19.9 ± 4.6	35.6 ± 7.5*	18.2 ± 6.7	32.2 ± 7.2*	0.286	<0.001	0.720
Ultimate Load (N)	22.4 ± 3.5	51.5 ± 13.6*	19.4 ± 5.8	44.3 ± 4.9*	0.082	<0.001	0.458
Stiffness (N/mm)	274 ± 39	467 ± 75*	311 ± 90	429 ± 66*	0.945	<0.001	0.139
Energy to Failure (mJ)	1.1 ± 0.3	6.9 ± 3.5*	0.7 ± 0.3	4.2 ± 2.2*	<0.05	<0.001	0.138
Elastic Energy (mJ)	0.77 ± .32	1.51 ± 0.53*	0.53 ± .30	1.35 ± .55*	0.229	<0.001	0.807
Plastic Energy (mJ)	0.33 ± .32	5.43 ± 3.26*	0.16 ± .33	2.90 ± 2.30*	0.073	<0.001	0.117
Post Yield Displacement (mm)	0.019 ± .018	0.124 ± .07*	0.013 ± .024	0.083 ± .058*	0.183	<0.001	0.329
Yield Displacement (mm)	0.066 ± .015	0.076 ± .012	0.052 ± .015	0.077 ± .017*	0.207	<0.01	0.161
Estimated Elastic Modulus (GPa)	5.41 ± .78	7.07 ± 1.1*	7.30 ± 2.34	7.70 ± 1.98	0.042	0.091	0.293

Table 3.1: Cortical MicroCT and Mechanical 4pt Bending. Femoral mid-diaphyseal cortical microCT and mechanical four point bending data reveal increased cortical bone mass and strength with Scl-Ab. *p<0.05 Scl-Ab vs. Veh; $^{\#}$p<0.05 WT Veh vs. Brtl/+ Veh.

Table 3.2. Dynamic Histomorphometry on Femoral Cortical Subregions

	WT Veh	*WT Scl-Ab*	*Brtl/+ Veh*	*Brtl/+ Scl-Ab*	*Genotype p-value*	*Treatment p-value*	*Interaction p-value*
Anterior							
Cortical Thickness (μm)	192 ± 13	251 ± 27*	200 ± 17	232 ± 25*	0.485	<0.001	0.096
Periosteal MS/BS	0.69 ± .33	0.91 ± .10	0.57 ± .32	0.89 ± .16	0.425	<0.01	0.524
Periosteal MAR	0.16 ± .11	0.59 ± .14*	0.20 ± .09	0.52 ± .17*	0.710	<0.001	0.247
Periosteal BFR/BS	0.13 ± .12	0.53 ± .12*	0.11 ± .09	0.46 ± .15*	0.305	<0.001	0.517
Endosteal MS/BS	0.28 ± .16	0.79 ± .16*	0.36 ± .17	0.87 ± .10*	0.135	<0.001	0.939
Endosteal MAR	0.16 ± .01	0.53 ± .08*	0.14 ± .02	0.47 ± .12*	0.425	<0.001	0.717
Endosteal BFR/BS	0.04 ± .03	0.42 ± .13*	0.04 ± .02	0.41 ± .11*	0.837	<0.001	0.721
Posterior							
Cortical Thickness (μm)	216 ± 25	294 ± 46*	235 ± 40	309 ± 52*	0.262	<0.001	0.878
Periosteal MS/BS	0.92 ± .09	0.99 ± .02	0.83 ± .17	0.98 ± .02	0.133	<0.01	0.189
Periosteal MAR	0.44 ± .24	0.93 ± .16*	0.35 ± .23	0.90 ± .16*	0.422	<0.001	0.644
Periosteal BFR/BS	0.41 ± .21	0.91 ± .15*	0.31 ± .25	0.89 ± .17*	0.373	<0.001	0.604
Endosteal MS/BS	0.24 ± .10	0.67 ± .22*	0.33 ± .12	0.79 ± .16*	0.084	<0.001	0.825
Endosteal MAR	0.22 ± .07	0.80 ± .34	0.29 ± .07	0.61 ± .14*	0.601	<0.01	0.303
Endosteal BFR/BS	0.04 ± .03	0.38 ± .37	0.05 ± .05	0.47 ± .10*	0.420	<0.001	0.590

Table 3.2: Regional Dynamic Histomorphometry. Regional anterior-posterior femoral cortical dynamic histomorphometry analysis. Dual label was not present on all surfaces preventing MAR measurement in all samples.
Anterior Periosteal MAR: WT Veh n=7, WT Scl-Ab n=9, Brtl/+ Veh n=7, Brtl/+ Scl-Ab n=9.
Anterior Periosteal MS/BS, BFR/BS: WT Veh n=7, WT Scl-Ab n=9, Brtl/+ Veh n=8, Brtl/+ Scl-Ab n=9.
Anterior Endosteal MAR: WT Veh n=2, WT Scl-Ab n=7, Brtl/+ Veh n=2, Brtl/+ Scl-Ab n=9.

(Table 3.2 cont…)
Anterior Endosteal MS/BS, BFR/BS: WT Veh n=7, WT Scl-Ab n=7, Brtl/+ Veh n=8, Brtl/+ Scl-Ab n=9.
Posterior Periosteal MAR. MS/BS, BFR/BS: WT Veh n=7, WT Scl-Ab n=9, Brtl/+ Veh n=8, Brtl/+ Scl-Ab n=9.
Posterior Endosteal MAR: WT Veh n=2, WT Scl-Ab n=4, Brtl/+ Veh n=2, Brtl/+ Scl-Ab n=9.
Posterior Endosteal MS/BS, BFR/BS: WT Veh n=7, WT Scl-Ab n=7, Brtl/+ Veh n=8, Brtl/+ Scl-Ab n=9.
*$p<0.05$ Scl-Ab vs. Veh, no phenotypic differences were observed.

References

1. Forlino A, Cabral WA, Barnes AM, Marini JC (2011) New perspectives on osteogenesis imperfecta. Nat Rev Endocrinol 7:540–557. doi: 10.1038/nrendo.2011.81

2. Paterson CR, McAllion S, Stellman JL (1984) Osteogenesis imperfecta after the menopause. N Engl J Med 310:1694–1696. doi: 10.1056/NEJM198406283102602

3. Chevrel G, Schott A-M, Fontanges E, et al. (2006) Effects of oral alendronate on BMD in adult patients with osteogenesis imperfecta: a 3-year randomized placebo-controlled trial. J Bone Miner Res 21:300–306. doi: 10.1359/JBMR.051015

4. Adami S, Gatti D, Colapietro F, et al. (2003) Intravenous neridronate in adults with osteogenesis imperfecta. J Bone Miner Res 18:126–130. doi: 10.1359/jbmr.2003.18.1.126

5. Shapiro JR, Thompson CB, Wu Y, et al. (2010) Bone Mineral Density and Fracture Rate in Response to Intravenous and Oral Bisphosphonates in Adult Osteogenesis Imperfecta. Calcif Tissue Int 87:120–129. doi: 10.1007/s00223-010-9383-y

6. Bradbury LA, Barlow S, Geoghegan F, et al. (2012) Risedronate in adults with osteogenesis imperfecta type I: increased bone mineral density and decreased bone turnover, but high fracture rate persists. Osteoporos Int 23:285–294. doi: 10.1007/s00198-011-1658-2

7. Gatti D, Rossini M, Viapiana O, et al. (2013) Teriparatide Treatment in Adult Patients with Osteogenesis Imperfecta Type I. Calcif Tissue Int 93:448–452. doi: 10.1007/s00223-013-9770-2

8. Orwoll ES, Shapiro J, Veith S, et al. (2014) Evaluation of teriparatide treatment in adults with osteogenesis imperfecta. J Clin Invest 124:491–498. doi: 10.1172/JCI71101

9. Poole KES, van Bezooijen RL, Loveridge N, et al. (2005) Sclerostin is a delayed secreted product of osteocytes that inhibits bone formation. FASEB J 19:1842–1844. doi: 10.1096/fj.05-4221fje

10. Li X, Zhang Y, Kang H, et al. (2005) Sclerostin Binds to LRP5/6 and Antagonizes Canonical Wnt Signaling. Journal of Biological Chemistry 280:19883–19887. doi: 10.1074/jbc.M413274200

11. Leupin O, Piters E, Halleux C, et al. (2011) Bone overgrowth-associated mutations in the LRP4 gene impair sclerostin facilitator function. J Biol Chem 286:19489–19500. doi: 10.1074/jbc.M110.190330

12. Padhi D, Jang G, Stouch B, et al. (2011) Single-dose, placebo-controlled, randomized study of AMG 785, a sclerostin monoclonal antibody. Journal of Bone and Mineral Research 26:19–26. doi: 10.1002/jbmr.173

13. Li X, Ominsky MS, Warmington KS, et al. (2009) Sclerostin antibody treatment increases bone formation, bone mass, and bone strength in a rat model of postmenopausal osteoporosis. J Bone Miner Res 24:578–588. doi: 10.1359/jbmr.081206

14. Ominsky MS, Vlasseros F, Jolette J, et al. (2010) Two doses of sclerostin antibody in cynomolgus monkeys increases bone formation, bone mineral density, and bone strength. Journal of Bone and Mineral Research 25:948–959. doi: 10.1002/jbmr.14

15. McClung MR, Grauer A, Boonen S, et al. (2014) Romosozumab in Postmenopausal Women with Low Bone Mineral Density. New England Journal of Medicine 370:412–420. doi: 10.1056/NEJMoa1305224

16. Forlino A, Porter FD, Lee EJ, et al. (1999) Use of the Cre/lox Recombination System to Develop a Non-lethal Knock-in Murine Model for Osteogenesis Imperfecta with an α1(I) G349C Substitution. Journal of Biological Chemistry 274:37923 –37931. doi: 10.1074/jbc.274.53.37923

17. Kozloff KM, Carden A, Bergwitz C, et al. (2004) Brittle IV Mouse Model for Osteogenesis Imperfecta IV Demonstrates Postpubertal Adaptations to Improve Whole Bone Strength. Journal of Bone and Mineral Research 19:614–622. doi: 10.1359/JBMR.040111

18. Uveges TE, Collin-Osdoby P, Cabral WA, et al. (2008) Cellular mechanism of decreased bone in Brtl mouse model of OI: imbalance of decreased osteoblast function and increased osteoclasts and their precursors. J Bone Miner Res 23:1983–1994. doi: 10.1359/jbmr.080804

19. Uveges TE, Kozloff KM, Ty JM, et al. (2009) Alendronate Treatment of the Brtl Osteogenesis Imperfecta Mouse Improves Femoral Geometry and Load Response Before Fracture but Decreases Predicted Material Properties and Has Detrimental Effects on Osteoblasts and Bone Formation. Journal of Bone and Mineral Research 24:849–859. doi: 10.1359/jbmr.081238

20. Sinder BP, Eddy MM, Ominsky MS, et al. (2013) Sclerostin antibody improves skeletal parameters in a Brtl/+ mouse model of osteogenesis imperfecta. Journal of Bone and Mineral Research 28:73–80. doi: 10.1002/jbmr.1717

21. Meganck JA, Kozloff KM, Thornton MM, et al. (2009) Beam hardening artifacts in micro-computed tomography scanning can be reduced by X-ray beam filtration and the resulting images can be used to accurately measure BMD. Bone 45:1104–1116. doi: 10.1016/j.bone.2009.07.078

22. Otsu N (1979) A threshold selection method from gray-level histograms. IEEE Transactions on Systems, Man and Cybernetics 9:62–66.

23. Hildebrand T, Rüegsegger P (1997) A new method for the model-independent assessment of thickness in three-dimensional images. Journal of Microscopy 185:67–75. doi: 10.1046/j.1365-2818.1997.1340694.x

24. Reeves GM, McCreadie BR, Chen S, et al. (2007) Quantitative trait loci modulate vertebral morphology and mechanical properties in a population of 18-month-old genetically heterogeneous mice. Bone 40:433–443. doi: 10.1016/j.bone.2006.08.018

25. Parfitt AM, Drezner MK, Glorieux FH, et al. (1987) Bone histomorphometry: standardization of nomenclature, symbols, and units. Report of the ASBMR Histomorphometry Nomenclature Committee. J Bone Miner Res 2:595–610. doi: 10.1002/jbmr.5650020617

26. Sinder B, Salemi J, Caird M, et al. (2013) Sclerostin Antibody Increases Cortical Bone Thickness in a Rapidly Growing Brtl/+ Model of OI by Inducing Bone Formation on Quiescent or Resorbing Surfaces. J Bone Miner Res 28 (Suppl 1):

27. Bivi N, Condon KW, Allen MR, et al. (2012) Cell autonomous requirement of connexin 43 for osteocyte survival: consequences for endocortical resorption and periosteal bone formation. J Bone Miner Res 27:374–389. doi: 10.1002/jbmr.548

28. Tian X, Setterberg RB, Li X, et al. (2010) Treatment with a sclerostin antibody increases cancellous bone formation and bone mass regardless of marrow composition in adult female rats. Bone 47:529–533. doi: 10.1016/j.bone.2010.05.032

29. Kishi T, Hagino H, Kishimoto H, Nagashima H (1998) Bone Responses at Various Skeletal Sites to Human Parathyroid Hormone in Ovariectomized Rats: Effects of Long-term Administration, Withdrawal, and Readministration. Bone 22:515–522. doi: 10.1016/S8756-3282(98)00045-3

30. Li M, Liang H, Shen Y, Wronski TJ (1999) Parathyroid hormone stimulates cancellous bone formation at skeletal sites regardless of marrow composition in ovariectomized rats. Bone 24:95–100.

31. Chow JW, Fox S, Jagger CJ, Chambers TJ (1998) Role for parathyroid hormone in mechanical responsiveness of rat bone. Am J Physiol 274:E146–154.

32. Vanlenthe G, Voide R, Boyd S, Muller R (2008) Tissue modulus calculated from beam theory is biased by bone size and geometry: Implications for the use of three-point bending tests to determine bone tissue modulus. Bone 43:717–723. doi: 10.1016/j.bone.2008.06.008

CHAPTER 4

Rapidly Growing Brtl/+ Mouse Model of Osteogenesis Imperfecta Improves Bone Mass and Strength with Sclerostin Antibody Treatment

Introduction

Osteogenesis imperfecta (OI) is a heritable collagen-related dysplasia that results in bone fragility [1]. This condition presents with a wide range of clinical severity, depending upon the type of OI and specific mutation. While OI persists throughout life, the symptoms and fracture risk are greatest during childhood [2].

Numerous therapies have been tried to reduce fracture risk in pediatric OI. The most widely used treatment are anti-resorptive bisphosphonates. Multiple clinical trials with pediatric OI and bisphosphonates have demonstrated their efficacy at increasing vertebral BMD and surrogate measures of vertebral strength; however, the effect on long bone fracture risk appears equivocal [3–8]. Treatment of pediatric OI with growth hormone (rGH) has shown encouraging results for an anabolic therapy, but was not consistently effective among all patients [9]. In positive responders, bone histology and mass were improved, and long bone fracture rates decreased, along with increased linear growth in some mildly and moderately severe pediatric OI patients [9, 10]. Intermittent PTH is not used in children before growth plate fusion because of a reported osteosarcoma risk in rats, and as a result is not available as a treatment for pediatric OI [11].

Neutralizing antibodies to sclerostin are a candidate anabolic therapy for children with OI. Sclerostin is a potent inhibitor of bone formation which is secreted primarily by osteocytes [12]. Broadly, sclerostin functions by inhibiting canonical Wnt signaling through its binding to the Wnt signaling co-receptors LRP5 and LRP6 present on cells of the osteoblast lineage [13]. Neutralizing antibodies have been developed which functionally reduce sclerostin activity and thereby prevent sclerostin inhibition of bone formation. An anabolic response to sclerostin antibodies has been demonstrated in numerous pre-clinical studies [14–17] as well as phase I and phase II trials of osteoporosis [18, 19].

The Brtl/+ mouse is heterozygous for a G349C mutation on *col1a1* found in an OI patient, and is a model for moderately severe Type IV OI [20]. Brtl/+ recapitulates many of the phenotypic features of pediatric OI including small size, impaired remodeling, reduced trabecular and cortical bone mass, altered bone matrix structure, and impaired fracture mechanics [20–23]. As such, Brtl/+ has been used to explore multiple clinically relevant questions including fracture repair [24], bisphosphonate treatment [25], and cell therapies [26].

Treatment of the rapidly growing skeleton of children with OI is the most clinically relevant time point. Previously, we reported that a short-term, 2 week treatment of Brtl/+ with Scl-Ab successfully induced an anabolic response in 8 week old Brtl/+ mice [27]. While this proof-of-concept study demonstrated anabolic efficacy, it was not a direct correlate to the pediatric clinical condition, as mice only gained 2-5% body mass over the 2 weeks of treatment. In contrast, 3 wk old Brtl/+ mice in the present study more than doubled their body mass over the 5 wk treatment duration, highlighting the large difference between these two ages. To directly address whether Scl-Ab can elicit an anabolic response in an OI model during periods of rapid bone growth and body mass accrual, we treated rapidly growing 3 week old WT and Brtl/+ mice

for 5 weeks with Scl-Ab and hypothesized that therapy would lead to increased bone mass and strength by stimulating bone formation.

Materials and Methods

Animals

Wildtype (WT) and Brtl/+ [20] mice are maintained on a mixed background of Sv129/CD-1/C57BL/6S, and all Brtl/+ animals were the product of breeding male heterozygous Brtl/+ with female WT. 3 week old male WT and Brtl/+ mice were randomly assigned to Scl-Ab (Scl-Ab VI, Amgen, Thousand Oaks, CA) treatment or vehicle injection (PBS) with n=8-9/group. Sclerostin antibody was injected subcutaneously at 25mg/kg, two times per week, for five weeks. Calcein (30mg/kg, i.p. injection) was injected at the start of experiment (3 wks animal age), after 2 weeks of treatment (5 wks animal age), and after 4 weeks of treatment (7 wks animals age). A final alizarin label (30mg/kg, i.p. injection) was given 1 day before euthanasia (7wks + 6 days of animal age). The multiple fluorescent labels were used to visualize the growth pattern during the entire course of therapy. Body weights were recorded with each injection. Blood samples were collected at sacrifice by intracardiac puncture, serum separated by centrifuge, and stored at -80˚C until analyzed by ELISA.

Left femurs were collected for microCT and mechanical testing, and right femurs for dynamic histomorphometry. Both were stored at -20˚C in lactated ringers solution (LRS) soaked gauze until testing or further specimen preparation. All protocols and procedures involving animals were approved by the University of Michigan's Committee on Use and Care of Animals.

Bone Length and Growth

Left femur and tibia lengths were measured longitudinally using whole body radiographs taken at the beginning and end of experiments on Scl-Ab or Veh treated animals. At 3 weeks of age, animals were briefly anesthetized with isoflurane, and microradiographs were taken in the coronal plane at 3x magnification (Faxitron MX-20, Faxitron X-Ray LLC, Lincolnshire, IL). Limbs were immobilized with tape during imaging to minimize motion and keep the leg bones flat. At 8 weeks of age, the radiograph protocol was repeated immediately after sacrifice. A lead ruler was used for calibration of the field of view, and bone lengths were measured with calipers.

Serum Assays

To measure osteoblast activity, serum osteocalcin (OCN) was quantified with a commercially available ELISA kit (BT-470, BTI, Stoughton, MA). As a measure of osteoclast number, serum TRACP5b was measured with a commercially available solid phase immunofixed enzyme activity assay (MouseTRAP, IDS, Fountain Hills, AZ). Both serum tests were performed in duplicate.

MicroCT

Left femora were scanned in water using cone beam computed tomography (eXplore Locus SP, GE Healthcare Pre-Clinical Imaging, London, ON, Canada). Scan parameters included a 0.5 degree increment angle, 4 frames averaged, an 80kVp and 80µA x-ray source with a 0.508mm Al filter to reduce beam hardening artifacts, and a beam flattener around the specimen holder [28]. All images were reconstructed and calibrated at an 18µm isotropic voxel size to a manufacturer-supplied phantom of air, water and hydroxyapatite. Regions of interest (ROI) were located for both cortical and trabecular parameters. A diaphyseal cortical ROI

spanning 15% of total femur length was located midway between the distal growth plate and third trochanter. Cortical bone was isolated with a fixed threshold of 2000 Hounsfield Units for all experimental groups. Parameters including cortical thickness, cross sectional area, marrow area, total area, anterior-posterior bending moment of inertia and tissue mineral density (TMD) were quantified with commercially available software (MicroView v2.2 Advanced Bone Analysis Application, GE Healthcare Pre-Clinical Imaging, London, ON, Canada). A trabecular ROI 10% of total femur length was located immediately proximal to the distal femoral growth plate and defined along the inner cortical surface with a splining algorithm. Due to the different morphology induced by Scl-Ab treatment, a fixed threshold could not be utilized without bias. Trabecular metaphyseal bone was isolated with a more conservative autothresholding algorithm for each specimen based on the bimodal distribution between marrow and bone [29]. Parameters including bone volume fraction (BV/TV), trabecular thickness (Tb.Th), and trabecular number (Tb.N), and trabecular bone mineral density (Tb.BMD) were quantified using standard stereology algorithms (MicroView v2.2).

A qualitative difference in femoral trabecular bone morphology was noticed as a function of distance from the growth plate. To quantify this, the 10% of bone length region of interest was sub-divided into the 5% of bone length region that was more distal (closer to the growth plate), and the 5% region that was more proximal. The same threshold determined for the entire 10% of bone length ROI was used for each of the 5% of bone length subdivided regions. In this way, the relative contribution of each sub-region could be assessed.

Whole Bone Mechanical Four-Point Bending

Following μCT scanning, left femora were loaded to failure in four-point bending using a servohydraulic testing machine (MTS 858 MiniBionix, Eden Prairie, MN). All specimens were kept hydrated in LRS-soaked gauze until mechanical testing. In the same mid-diaphyseal region analyzed by μCT, the femur was loaded in four point bending with the posterior surface oriented under tension. The distance between the wide, upper supports was 6.26mm, and span between the narrow, lower supports 2.085mm. The vertical displacement rate of the four-point bending apparatus in the anterior-posterior direction was 0.5mm/sec. Force was recorded by a 50 lb load cell (Sensotec) and vertical displacement by an external linear variable differential transducer (LVDT, Lucas Schavitts, Hampton, VA), both at 2000Hz. A custom MATLAB script was used to analyze the raw force-displacement data and calculate all four-point bending parameters. Combining anterior-posterior bending moment of inertia data from μCT with mechanical stiffness from four point bending, the estimated elastic modulus was calculated using standard beam theory as previously described [21].

Dynamic Histomorphometry

Right femora were encased in epoxy (Kold Mount, Vernon-Benshoff, Albany, NY), and cut transversely with a low-speed saw (IsoMet, Beuhler, Lake Bluff, IL). The distal section of tissue was polished using progressive grades of silicon carbide abrasive paper (1200, 2400, and 4000 grit) to a plane immediately distal to the third trochanter. Specimens were further polished on a felt pad for 5 minutes with a ¼ μm diamond suspension (Struers Inc., Cleveland, OH).

Fluorescent images were acquired using a Zeiss Axiovert 200M inverted microscope equipped with Apotome imaging system to minimize out-of-plane light, negating the need for several micron thin sections. Multiple fluorescent images were taken with a 10x objective of the

calcein and alizarin labels around the entire cortex. The 10x images of the cortex were merged into a single image (Photoshop, Adobe), and these merged images were analyzed using commercially available software (Bioquant Osteo v7.20.10, Nashville, TN). Bone surface (BS), mineral apposition rate (MAR), mineralizing surface / bone surface (MS/BS), and bone formation rate / bone surface (BFR/BS) were quantified on both the periosteal and endosteal surfaces. The final two labels, given 1 week and 1 day before sacrifice, were analyzed according to ASBMR standards [30].

In order to examine the effect of Scl-Ab superimposed over a strong posterior shifting cortical drift pattern, dynamic histomorphometry outcomes were also assessed in anatomic regions around the cortex with a method similar to Bivi et. al [31]. The fluorescent images were oriented anatomically by using the contralateral microCT femoral 3D images as a reference. The centroid of the fluorescent image was identified in ImageJ, and 110 degree angles from the centroid were used to define the anterior and posterior regions (Fig 4.5). MAR, MS/BS, and cortical thickness were quantified in each of these anterior and posterior subregions.

In any regions where there was no dual label, MAR was treated as a missing value. For the purpose of calculating BFR/BS, a value of 0.3μm/day was assigned to MAR where missing values were present. This value was determined from both looking at the biological limit observed in our specimens as well as values established in the literature [32].

Statistics

A Kruskal-Wallis ANOVA and non-parametric Mann-U Whitney post-hoc tests were performed and $p<0.05$ was considered significant. Values between $p=0.05$ and $p=0.10$ are reported in all instances. Comparisons between WT Veh and Brtl/+ Scl-Ab were made for the

cortical microCT and mechanical four-point bending outcomes to assess the ability of Scl-Ab to restore the Brtl/+ phenotype to WT control levels. Data is presented as mean±S.D.

Results

Scl-Ab Does Not Change Body Mass or Linear Growth Rates in Rapidly Growing Mice

Three week old mice are rapidly growing (Fig 4.1) Throughout the five weeks of treatment, from 3 to 8 weeks of age, body mass was increased significantly by an average of 87% in WT Veh and 121% in Brtl/+ Veh. Consistent with previously reported phenotypic differences, Brtl/+ mice weigh less than WT (Fig. 4.1). Brtl/+ Veh weighed 30% less than WT Veh (11.0±2.3g vs. 15.8 ± 2.0g) at 3 weeks of age, and 22% less than WT Veh (23.9±3.8g vs. 29.2±3.0g) at 8 weeks of age. Both genotypes gained a similar amount of weight on an absolute basis (WT Veh 13.4±2.9g; Brtl/+ Veh 12.9±2.9g) over the 5 weeks of treatment. Scl-Ab did not change the rate of body mass accrual throughout the treatment as weight gain was similar between Veh and Scl-Ab groups in both WT and Brtl/+. As a result, body weight was similar at the end of experiment in both WT (WT Veh 29.2±3.0g vs. WT Scl-Ab 27.8±1.3g) and Brtl/+ (Brtl/+ Veh 23.9±3.8g vs. Brtl/+ Scl-Ab 24.1±2.5g) with therapy.

Reduced stature is a characteristic phenotype of OI patients. To determine if Scl-Ab affected linear growth rate in animals that are rapidly growing, bone length was measured on X-rays taken at the beginning and end of treatment. (Table 4.1). In the left tibia and femur, no difference in linear bone growth during treatment or overall endpoint bone length was observed with Scl-Ab in either WT or Brtl/+. Consistent with previously reported phenotypic differences, Brtl/+ bones were shorter than WT.

Serum Osteocalcin is Elevated in Rapidly Growing Brtl/+

Brtl/+ Veh had increased serum osteocalcin relative to WT Veh at 8 weeks of age (Fig. 4.2). Scl-Ab treatment did not significantly increase mean serum osteocalcin levels in either WT and Brtl/+. No effect on serum TRACP5b levels was observed.

Anabolic Scl-Ab Effect Depends on Distance of Trabecular Bone From Growth Plate

Scl-Ab treatment increased femoral trabecular BV/TV by 57% in WT, but a significant effect was not observed in Brtl/+ ($p=0.321$) over the entire distal femoral 10% of bone length ROI (Fig. 4.3). The Scl-Ab BV/TV gains in WT were a result of increases in both Tb.Th (+28%) and Tb.N (+22%). Interestingly, despite the lack of Scl-Ab effect on BV/TV in Brtl/+, Tb.Th was significantly increased by a small amount (+8.7%). Tb.BMD demonstrated a similar pattern as BV/TV, with a significant ($p<0.001$) 67% increase observed in WT with Scl-Ab, but only a marginal 33% increasing trend observed in Brtl/+ ($p=0.06$).

Despite this lack of effect over the entire distal femoral region, we observed a qualitative difference in the action of Scl-Ab as a function of distance from the distal femoral growth plate. To quantify this, we separated the 10% of bone length trabecular ROI into the 5% region closer to the growth plate and the 5% of bone length region farther from the growth plate (Fig 4.4).

In the region closest to the growth plate we observed a significant gain in WT BV/TV with Scl-Ab treatment, but not in Brtl/+ ($p=0.89$). The BV/TV gains in WT were a result of significant gains in Tb.Th (+49%), while Brtl only showed a modest trend towards increased Tb.Th ($p=0.097$). There were no Tb.N changes with Scl-Ab observed in either genotype in this 5% of bone length region closest to the growth plate.

In contrast, in the proximal 5% sub region further from the growth plate, Scl-Ab treatment resulted in a significant increase in BV/TV in both WT (126%) and Brtl/+ (69%) mice. In WT, BV/TV gains in this subregion were a result of significant gains in both Tb.Th (49%) and Tb.N (51%), while Brtl/+ only increased Tb.Th (29%), but not Tb.N.

Scl-Ab Increases Cortical Bone Mass in Brtl/+ and WT by Similar Amounts

Phenotypically, Brtl/+ Veh femoral bone had reduced cortical thickness (-18%), cross sectional area (-18%), and anterior-posterior bending moment of inertia (-31%) relative to WT Veh (Table 4.2). The marrow area was not significantly different in Brtl/+ Veh animals, but total area was less than observed in WT Veh.

Treatment with Scl-Ab significantly increased cortical thickness (WT +26%; Brtl/+ +24%) and cortical cross sectional area (WT +31%; Brtl/+ +25%) in both genotypes, leading to significantly increased anterior-posterior bending moment of inertia in both WT (+49%) and Brtl/+ (+30%). These increases returned the Brtl/+ cortical geometric phenotype to levels not significantly different from WT Veh. Neither marrow area nor total area were significantly altered by Scl-Ab in Brtl/+; WT yielded only a modest increasing trend ($p=0.077$) in total area with treatment. Cortical TMD was increased in WT with Scl-Ab, and an increasing trend was observed in Brtl/+.

Scl-Ab Rescues Reduced Brtl/+ Femoral Bone Strength to WT Veh Levels

Phenotypically, Brtl/+ Veh had reduced mechanical properties compared to WT Veh (Table 4.2). These included reduced strength outcomes such as Yield Load (-24%), Ultimate Load (-38%), Stiffness (-35%), and Energy to Failure (-60%). In addition, Brtl/+ Veh also failed

in a more mechanically brittle manner than WT Veh. This is evident in the decreased plastic energy (-75%), post yield displacement (-61%), and failure/yield displacement ratio (-39%).

Scl-Ab therapy significantly increased most mechanical outcomes in both WT and Brtl/+. Specifically, Scl-Ab treatment increased Yield Load (WT +47%; Brtl +39%), Ultimate Load (WT +68%; Brtl +51%) and Stiffness (WT +55%; Brtl +61%) in both genotypes, and in Brtl/+, restored these three parameters to the level of WT Veh. Energy-To-Failure was significantly increased by Scl-Ab in WT (+303%), but only trended (p=0.093) with treatment in Brtl/+ (+42%). This differential gain is caused by a genotype specific effect of Scl-Ab on bone brittleness. In WT, the large increase in Energy-to-Failure with Scl-Ab was primarily due to a substantial increase in Plastic Energy (+386%). The increased plastic energy was mostly due to increased Post Yield Displacement (+164%) in WT with Scl-Ab. In contrast, Scl-Ab did not alter Plastic energy or Post Yield Displacement in Brtl/+. Yield Displacement was not altered by Scl-Ab in either WT or Brtl/+. The estimated elastic modulus was not significantly different.

Regional Dynamic Histomorphometry Analysis Reveals Scl-Ab Action Superimposed over a Strong Cortical Drift Pattern

In both WT Veh and Brtl/+ Veh there was a strong posterior shifting cortical drift pattern (Fig 4.5). Specifically, we found high BFR/BS on the periosteal posterior and endosteal anterior bone, with over 90% of these surfaces forming bone in both genotypes. Conversely, low bone formation rates were found on the periosteal anterior and endosteal posterior surfaces in both WT and Brtl/+ (Table 4.3).

On the low bone forming posterior endosteal surface, Scl-Ab significantly increased MS/BS (WT +610%, Brtl +243%), which lead to increased BFR/BS (WT + 829%, Brtl/+

+542%). On the low bone forming periosteal anterior surface, Brtl/+ trended towards an increase in MS/BS, but this did not significantly change BFR/BS. The Scl-Ab response was highly variable in WT animals on the low forming posterior endosteal surface.

On the high bone forming surfaces, Scl-Ab had no effect on dynamic histomorphometry outcomes in either genotype. Specifically, on the periosteal posterior surface, no significant differences were observed for MS/BS, MAR, or BFR/BS in either WT or Brtl/+. On the high bone forming endosteal anterior surface, Scl-Ab resulted in an unexpected trend towards reduced MAR ($p=0.094$) during the last week of treatment, but this did lead to a change in BFR/BS. No changes in WT endosteal anterior surface were observed with Scl-Ab.

These regional changes with sclerostin antibody were sufficient to significantly increase cortical thickness in both WT and Brtl/+ on the anterior (WT +19%; Brtl/+ +23%) and posterior (WT +25%; Brtl/+ +32%) surfaces after 5 weeks of treatment. However, due to the regional nature of the underlying cortical drift pattern, Scl-Ab treatment did not result in any significant changes in overall periosteal MAR, MS/BS, or BFR/BS in either WT or Brtl/+ when summed over the entire periosteal surface (Table 4.3). The total endosteal surface showed a more robust response to therapy. In Brtl/+, treatment with Scl-Ab significantly increased total endosteal MS/BS (28%). In WT, Scl-Ab had opposing effects of significantly reducing total endosteal MAR (-24%) while increasing total endosteal MS/BS (+61%). The relatively larger gains in WT MS/BS led to an increasing trend ($p=0.094$) in total endosteal BFR/BS with treatment.

Discussion

This study demonstrated that Scl-Ab increased bone formation leading to improved bone mass and strength in a rapidly growing Brtl/+ mouse model of moderately severe Type IV OI. Impressively, treatment with Scl-Ab significantly improved long bone strength to levels not significantly different than WT and rescued the Brtl/+ phenotype of reduced bone mass. This potent effect of Scl-Ab on cortical bone mass and long bone strength starkly contrasts with the existing bisphosphonate data reported in both animal models and clinical studies. Previously, we examined the effect of alendronate treatment of the Brtl/+ mouse during growth [25]. While alendronate treatment of Brtl/+ between 2-8 weeks of age resulted in extremely large gains in femoral metaphyseal bone mass, alendronate had little effect on cortical bone mass and strength, which required a full 12 weeks of treatment to show a modest effect. The absence of a strong alendronate effect on OI cortical bone is not specific to the Brtl/+ mouse model and similar data has been observed in other OI mouse models such as *oim* [33]. This observation of a reduced or absent effect of bisphosphonate on OI cortical bone mass is also reflected in clinical data. The controlled clinical trials of bisphosphonates in pediatric OI suggest a beneficial effect on vertebral trabecular bone but an equivocal effect on long bone strength [3–7]. Therefore, a therapy which consistently increases long bone strength in pediatric OI is currently lacking. The current study suggests that Scl-Ab may provide a novel and unique therapeutic option for pediatric OI by reducing long-bone susceptibility to fracture.

The underlying cause of classical OI fragility is that a collagen structural defect produces bone of both reduced material quality as well as reduced bone mass. In this study, Scl-Ab was able to significantly improve femoral strength by increasing bone mass without altering the underlying brittle nature of the material. Specifically, Scl-Ab was able to increase cortical bone

mass in Brtl/+ by significantly increasing cortical thickness (+24%) and cortical area (+25%). Although the unchanged post-yield displacement in Brtl/+ with Scl-Ab treatment suggests that Scl-Ab did not improve the inherent brittle material behavior of Brtl/+ bone, Scl-Ab did significantly improve long bone strength by increasing cortical bone mass, making the bone less fragile. A trend towards increased cortical TMD with Scl-Ab in Brtl/+ could be suggestive of increased mineralization, but this finding did not correlate with the estimated elastic modulus as measured by four-point bending. Rather, this increase could be a result of porosity changes below the resolution of our microCT, or partial volume effects, both of which could artificially increase this index of bone mineralization.

In this study, the Brtl/+ trabecular response to Scl-Ab in the distal femur was notably less robust than in WT. Trabecular thickness increased after 5 weeks of Scl-Ab treatment in both WT and Brtl/+, confirming our previous work where Brtl/+ was treated between 8-10 weeks of age [27]. In both studies, BV/TV was not significantly increased in Brtl/+. However, the extended 5 week treatment duration of the present study allowed us to discriminate more subtle treatment effects, and further analysis revealed a significant anabolic BV/TV response in the Brtl/+ Scl-Ab group in a more proximal subregion of the femur metaphysis. The lesser gains in bone mass near the growth plate in both genotypes may be related to the shorter duration of Scl-Ab exposure to this newly formed bone. In addition, the function of sclerostin near the growth plate may be reduced and not critical to the initial patterning of trabeculae. However, this would not explain the differential Scl-Ab response we observed in Brtl/+ vs. WT. The reduced trabecular response to Scl-Ab in Brtl/+ may be a result of increased bone resorption levels in Brtl/+ animals [22] which may mask equivalent bone formation responses, although we did not observe significant serum TRACP5b differences in this study. Alternatively, there may be a

reduced anabolic response to Scl-Ab in Brtl/+ trabecular bone compared to WT which may be a result of differential sclerostin levels or impaired osteoblast function.

The reduced Brtl/+ femoral trabecular response observed in this study contrasts with the robust Scl-Ab increases in cortical bone mass in both WT and Brtl/+. Furthermore, these findings also contrast with our observations studying adult 6 month old Brtl/+ mice that were treated for 5 weeks with Scl-Ab [34]. In these adult mice, we observed significant BV/TV gains in both WT and Brtl/+ using an identical Scl-Ab treatment period and microCT methodology. Furthermore, serum results from the present study contrast with our prior reports of a strong anabolic serum response shown in short term treatment [27] and 5 weeks of Scl-Ab treatment in 6 month old Brtl/+ mice [34]. This suggests a potential age dependent response to Scl-Ab that must be considered in greater detail before undertaking the translation of Scl-Ab to pediatric OI patients.

Patients with OI often have severely reduced stature. To examine if Scl-Ab treatment altered linear growth rates during this phase of rapid growth of the Brtl/+ mouse we examined pre- and post- treatment bone lengths by X-ray. Here, we found no significant effects of treatment on long bone length after 5 weeks of therapy, consistent with prior reports of neutral effects of Scl-Ab on bone length in 7 week old mice [35]. While Scl-Ab appears promising for increasing bone mass, it does not appear to increase the short stature phenotypic of Brtl/+ OI mice. However, the lack of a bone length increase in mice does not necessarily preclude an effect in humans; *SOST* KO mice do not have longer bones [36] but patients with sclerosteosis do have increased stature [37].

We observed a mechanistic difference between increasing MAR on existing bone formation surfaces, and stimulating new bone formation on otherwise quiescent or resorbing

bone surfaces. The regional anterior/posterior dynamic histomorphometry analysis performed in this study helps to separate these two effects by analyzing the superposition of a strong underlying cortical drift pattern characteristic of young animals [38, 39] with a potent anabolic therapy. Scl-Ab activated bone formation surfaces on quiescent or low bone forming surfaces in Brtl/+ and WT mice, with minimal additional effect on increasing osteoblast activity on surfaces with already high levels of bone formation. These findings may have important clinical impact when considering where Scl-Ab may have its most potent effects during growth and development, and where its effect may be limited, perhaps due to already high levels of bone formation.

The regional dynamic histomorphometry responses to Scl-Ab treatment were not always consistent within experimental group. For example, on the anterior periosteal surface where no bone formation was observed in WT Veh controls, the bone formation response to Scl-Ab was either robust or non-existent. Specifically, Scl-Ab activated bone formation in only 3 of the 8 mice in the WT Scl-Ab group. Moreover, these three mice had MS/BS values that were greater than 0.95, highlighting the strong anabolic response in this subset of animals. The 5 out of 8 mice that did not respond had no fluorescent labeling on this surface, and an MS/BS of zero.

The changes in cortical thickness in the posterior compartment of the femoral cortex are likely due to the strong endosteal BFR/BS response to therapy (Table 4.3). However, the significant increases in anterior femoral thickness are not easily explained by regional response differences, as no significant differences in BFR/BS occurred in either genotype with Scl-Ab. It is possible that Scl-Ab treatment reduced bone resorption on the periosteal anterior surface, which would increase cortical thickness. Another possibility is that significant gains in bone formation with Scl-Ab occurred in the anterior compartment before the last week of treatment.

Finally, we were able to measure cortical thickness in all specimens (n=8-9/group) allowing for greater statistical power, but had slightly smaller group sizes for the dynamic histomorphometry outcomes due to missed injections of fluorescent label (n=7-8).

This study has several limitations. First, despite the fact that the Brtl/+ mouse was made to have a mutation identical to that found in a Type IV OI patient, it does not fully recapitulate the phenotype of humans and suffer spontaneous fractures. In addition, as OI is a disease of many mutations, the results of this study may not extend to all types of OI. Before considering translation to humans, future studies need to analyze the potential effect of sclerostin inhibition on skeletal overgrowth in undesired locations apparent in human diseases of sclerostin deficiency [40]

In summary, Scl-Ab significantly increased bone formation, bone mass, and long bone strength in growing mice with a typical OI-causing mutation in type I collagen during a period of rapid bone mass accrual. These results contrast with existing bisphosphonate treatment strategies which have not demonstrated convincing improvements in long bone fragility in pre-clinical models or clinical trials. On bone surfaces where osteoblasts were highly active in rapidly growing animals in this study, Scl-Ab had a minimal additional anabolic effect. Rather, increased anabolic activity resulted from activation of quiescent or resorbing surfaces. These observations, along with regional improvements in trabecular bone mass associated with tissue age reflect the necessity of testing anabolic agents during periods of rapid growth to prepare for pediatric indications. The current data suggest that Scl-Ab may be a candidate pharmacologic for the treatment of pediatric osteogenesis imperfecta.

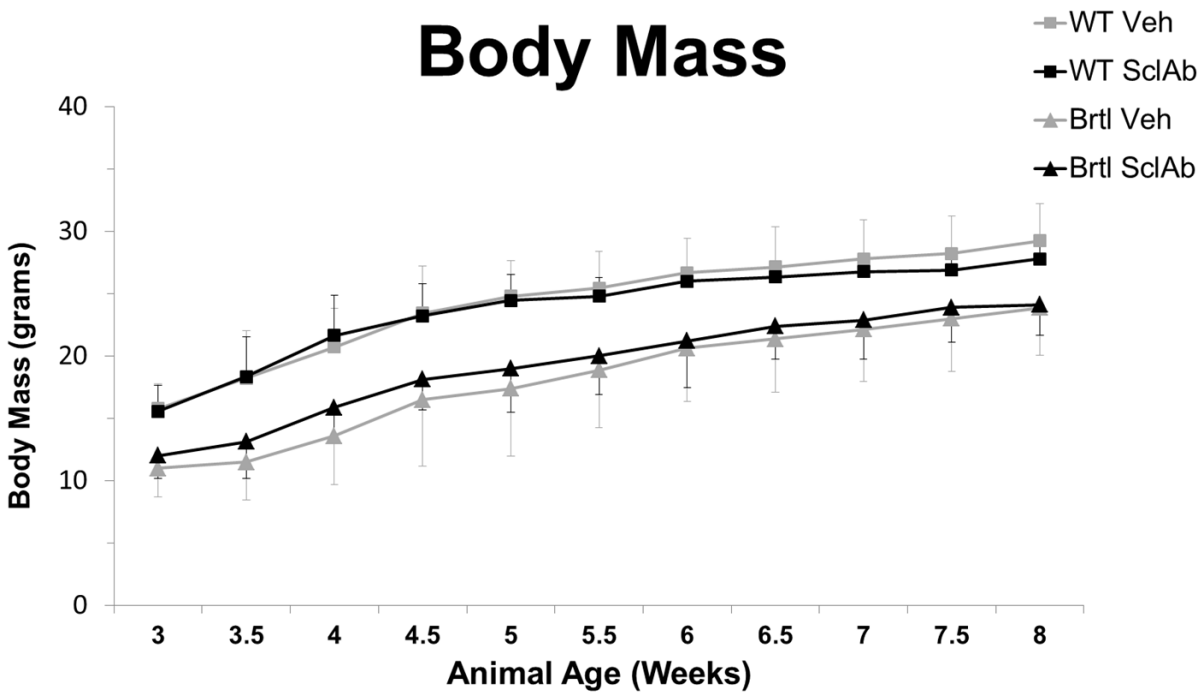

Figure 4.1. Body Mass Over from 3wks to 8wks of Age. Body mass curves throughout the course of experiment from 3 wks of age to 8 wks of age confirm that Brtl/+ animals are lighter than WT and reveal Scl-Ab does not effect body mass. Data are n=8-9/group.

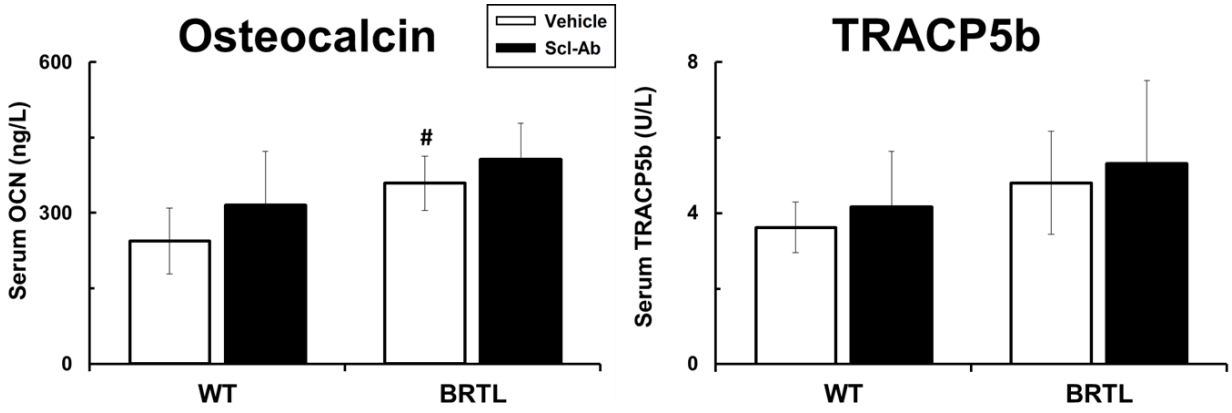

Figure 4.2. Serum TRACP5b and Osteocalcin. Serum osteocalcin is significantly greater in Brtl/+ Veh vs. WT Veh, but no significant effect of Scl-Ab on serum osteocalcin is observed in either genotype. The inability to obtain serum samples from all animals results in a slight reduction in group sizes. For OCN: WT Veh n=6, WT Scl-Ab n= 9; Brtl/+ Veh n =6, Brtl/+ Scl-Ab n=6. For TRACP5b: WT Veh n=9, WT Scl-Ab n= 9; Brtl/+ Veh n=7, Brtl/+ Scl-Ab n=7.

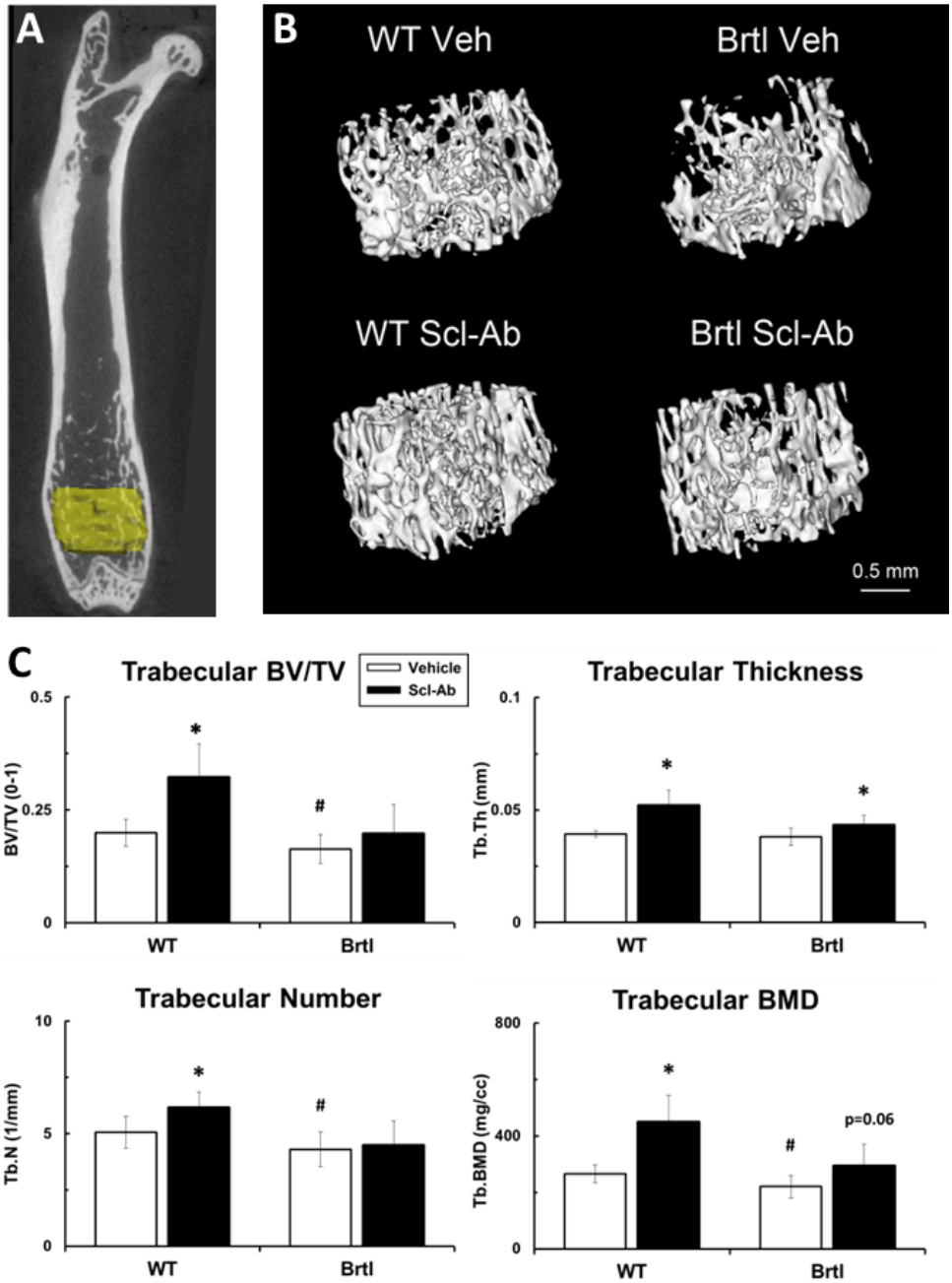

Figure 4.3. Femoral Trabecular MicroCT Isosurface and Data. Micro computed tomography of the distal femur metaphysis reveals anabolic changes with Scl-Ab therapy. The ROI (**A**) was 10% of bone length and placed immediately proximal to the growth plate. Representative median BV/TV isosurface images (**B**) reveal a qualitative reduction in Brtl/+ bone mass and the anabolic effect of Scl-Ab therapy. Quantitative analysis (**C**) reveals a reduction in Brtl/+ BV/TV as a result of decreased trabecular number. Scl-Ab significantly increased trabecular number and thickness in WT, leading to increased BV/TV. In Brtl/+, Scl-Ab increased trabecular thickness but did not alter trabecular number or BV/TV. There was a trend (p=0.06) towards increased trabecular BMD in Brtl/+ with Scl-Ab. *p<0.05 Scl-Ab vs. Veh; #p<0.05 WT Veh vs. Brtl/+ Veh. Data are n=8-9/group.

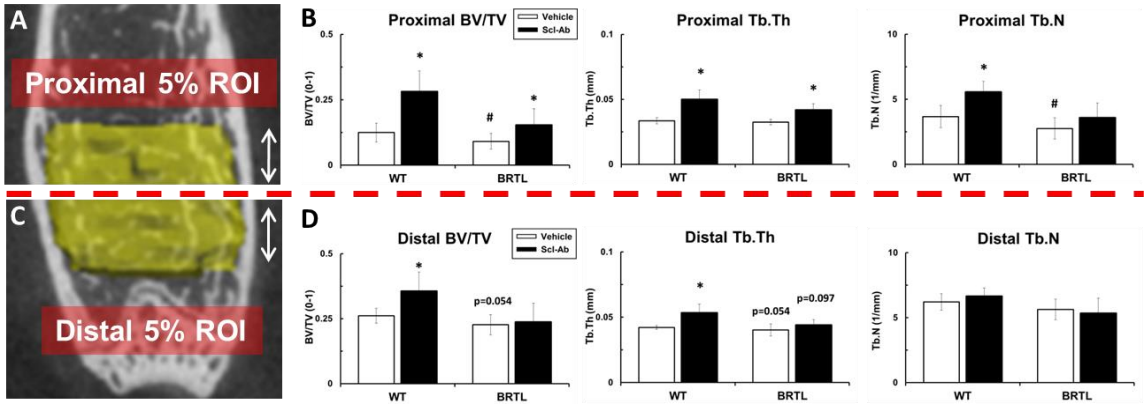

Figure 4.4. Femoral Trabecular MicroCT Proximal and Distal Sub-region Analysis. Differential response of Scl-Ab on trabecular bone mass as a function of distance from the growth plate. The trabecular 10% ROI shown in Fig 3A was separated into proximal (**A**) and distal(**C**) 5% on bone length subregions. In the proximal compartment (**B**), we found that Scl-Ab significantly improved trabecular BV/TV and thickness in both WT and Brtl/+. In the distal ROI (**D)**, there were few genotype differences and Scl-Ab increased BV/TV and trabecular thickness in WT, but had little effect on Brtl/+. *p<0.05 Scl-Ab vs. Veh; $^{\#}$p<0.05 WT Veh vs. Brtl/+ Veh. Data are n=8-9/group.

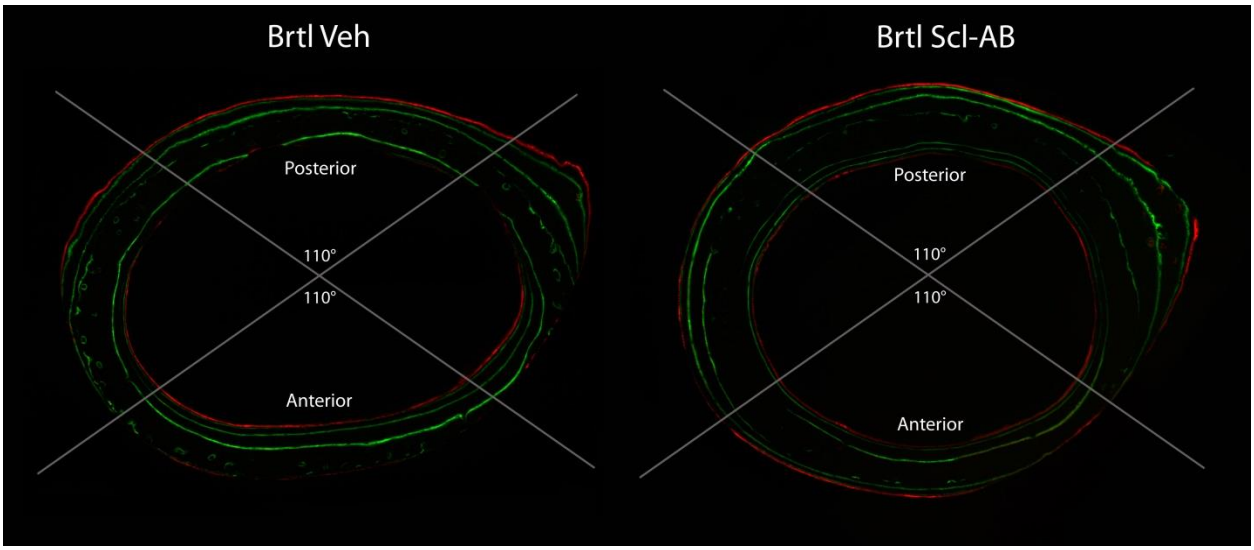

Figure 4.5. Representative Dynamic Histomorphometry and Regional Analysis Locations. Representative dynamic histomorphometry images of a Brtl/+ Veh animal showing a strong posterior shifting cortical drift pattern and the bone formation induced by Scl-Ab. In all samples, the centroid of the bone was located, and 110° angles drawn to define the anterior and posterior regions of bone. These subregions were used to define the anterior-posterior cortical drift dynamic histomorphometry response shown in Table 4.3.

Table 4.1. Linear Bone Growth as Measured by Pre and Post Treatment X-ray

	WT Veh	*WT Scl-Ab*	*Brtl Veh*	*Brtl/+ Scl-Ab*
Left Femur				
Length at 3 weeks of age (mm)	11.43 ± .43	11.34 ± .42	10.25 ± .80 #	10.49 ± .39
Length at 8 weeks of age (mm)	14.00 ± .43	14.25 ± .33	13.03 ± .90 #	13.10 ± .58
Paired percent bone growth (%)	22.5 ± 3.4	25.8 ± 4.1	27.3 ± 3.3	24.9 ± 4.1
Left Tibia				
Length at 3 weeks of age (mm)	14.72 ± .37	14.67 ± .57	13.44 ± .75 #	13.55 ± .77
Length at 8 weeks of age (mm)	17.50 ± .42	17.31 ± .45	16.29 ± .70 #	16.44 ± .42
Paired percent bone growth (%)	19.0 ± 3.1	18.1 ± 2.8	21.4 ± 4.0	21.6 ± 5.1

Table 4.1. Linear Bone Growth Rates of Femur and Tibia. Linear bone growth of the femur and tibia from 3 wks to 8 wks of age as assessed by microradiograph. *$p<0.05$ Scl-Ab vs. Veh; #$p<0.05$ WT Veh vs. Brtl/+ Veh. Data are n=8-9/group.

Table 4.2. Cortical MicroCT and Mechanical Properties

	WT Veh	*WT Scl-Ab*	*Brtl/+ Veh*	*Brtl/+ Scl-Ab*
Cortical Micro CT				
Thickness (mm)	0.20 ± .01	0.25 ± .03*	0.16 ± .02 $^{\#}$	0.20 ± .01*
Cross Sectional Area (mm^2)	0.91 ± .07	1.19 ± .22*	0.71 ± .10$^{\#}$	0.89 ± .08*
Marrow Area (mm^2)	1.30 ± .17	1.33 ± .18	1.20 ± .08	1.17 ± .15
Total Area (mm^2)	2.21 ± .22	2.53 ± .40$^{p=0.077}$	1.91 ± .16$^{\#}$	2.06 ± .21
Bending Moment of Inertia (mm^4)	0.17 ± .03	0.26 ± .09*	0.12 ± .02$^{\#}$	0.16 ± .03*
Tissue Mineral Density (mg/cm^3)	1017 ± 35	1046 ± 33*	1004 ± 48	1054 ± 47$^{p=0.059,\ +}$
Mechanical Four Point Bending				
Yield Load (N)	19.7 ± 3.2	28.8 ± 5.3*	15.0 ± 3.1$^{\#}$	20.8 ± 3.3*
Ultimate Load (N)	27.6 ± 2.4	46.4 ± 10.8*	17.0 ± 3.6$^{\#}$	25.6 ± 3.9*
Stiffness (N/mm)	198 ± 25	308 ± 71*	129 ± 30$^{\#}$	208 ± 32*
Energy to Failure (mJ)	4.6 ± 1.5	18.4 ± 12.4*	1.8 ± 1.0$^{\#}$	2.6 ± 1.0$^{p=0.093,+}$
Elastic Energy (mJ)	1.10 ± .30	1.55 ± .41*	0.95 ± .22	1.19 ± .36
Plastic Energy (mJ)	3.5 ± 1.5	16.8 ± 12.3*	0.88 ± .92$^{\#}$	1.4 ± 1.1^{+}
Yield Displacement (mm)	0.109 ± .013	0.112 ± .022	0.129 ± .027	0.116 ± .023
Post Yield Displacement (mm)	0.144 ± .058	0.380 ± .198*	0.056 ± .059$^{\#}$	0.062 ± .042^{+}
Fail/Yield Displacement Ratio	2.32 ± .51	4.65 ± 2.37*	1.42 ± .44$^{\#}$	1.59 ± .46^{+}
Estimated Elastic Modulus (GPa)	4.46 ± .73	4.79 ± 1.07	4.05 ± .48	5.16 ± 1.09

Table 4.2. Cortical MicroCT and Mechanical 4pt Bending. Data collected at femoral mid-diaphysis show increased bone mass and strength with Scl-Ab. *p<0.05 Scl-Ab vs. Veh; $^{\#}$p<0.05 WT Veh vs. Brtl/+ Veh; $^{+}$p<0.05 WT Veh vs. Brtl/+ Scl-Ab. Data are n=8-9/group.

Table 4.3. Dynamic Histomorphometry on Femoral Cortical Subregions

	WT Veh	*WT Scl-Ab*	*Brtl/+ Veh*	*Brtl/+ Scl-Ab*
Anterior				
Cortical Thickness (μm)	182 ± 17	217 ± 27*	158 ± 21$^{\#}$	194 ± 17*****
Periosteal MS/BS	0.00 ± .00	0.36 ± .51	0.43 ± .25$^{\#}$	0.73 ± .28 $^{p=0.094}$
Periosteal MAR	NA ± NA	1.31 ± .56	1.18 ± .98	1.14 ± .48
Periosteal BFR/BS	0.00 ± .00	0.48 ± .73	0.59 ± .78$^{\#}$	0.85 ± .46
Endosteal MS/BS	0.91 ± .20	0.96 ± .04	0.93 ± .09	0.86 ± .09
Endosteal MAR	2.06 ± .29	1.66 ± .61	1.36 ± .51$^{\#}$	0.96 ± .39 $^{p=0.094}$
Endosteal BFR/BS	1.76 ± .75	1.59 ± .56	1.28 ± .52	0.81 ± .40
Posterior				
Cortical Thickness (μm)	213 ± 15	267 ± 41*****	178 ± 29$^{\#}$	235 ± 19*****
Periosteal MS/BS	0.94 ± .09	0.99 ± .01	0.99 ± .01	0.98 ± .02
Periosteal MAR	1.90 ± .54	2.38 ± .77	2.11 ± .50	2.55 ± .61
Periosteal BFR/BS	1.79 ± .56	2.37 ± .78	2.10 ± .49	2.55 ± .61
Endosteal MS/BS	0.07 ± .08	0.71 ± .16*	0.32 ± .19$^{p=0.053}$	0.91 ± .18*
Endosteal MAR	1.65 ± 1.2	0.92 ± .29	0.63 ± .18	1.03 ± .45
Endosteal BFR/BS	0.08 ± .13	0.72 ± .33*	0.15 ± .15	0.96 ± .48*
Total Endosteal				
MS/BS	0.53 ± .17	0.86 ± .06*	0.69 ± .07$^{p=0.097}$	0.89 ± .07*
MAR	1.92 ± .24	1.46 ± .31*	1.20 ± .24$^{\#}$	1.13 ± .37
BFR/BS	1.13 ± .12	1.25 ± .24$^{p=0.094}$	0.83 ± .17$^{p=0.053}$	0.99 ± .30
Total Periosteal				
MS/BS	.43 ± .03	.64 ± .27	.71 ± .09$^{\#}$	.84 ± .11
MAR	2.23 ± .71	2.18 ± .43	2.34 ± .53	2.40 ± .62
BFR/BS	.97 ± .31	1.49 ± .86	1.71 ± .61$^{\#}$	1.99 ± .49

Table 4.3. Regional Dynamic Histomorphometry. Dynamic histomorphometry of femoral cortical bone. Regional anterior-posterior femoral cortical dynamic histomorphometry analyses are shown on top, with traditional data from the entire periosteal and endosteal surface at the bottom. MAR was treated as a missing value when no dual label was present. Deviations from n=6-9 group size are noted here. Periosteal Anterior MAR (WT Veh n=0, WT Scl-Ab n=3). Endosteal Posterior MAR (WT Veh n=2, Brtl/+ Veh n=5). *$p<0.05$ Scl-Ab vs. Veh; $^{\#}p<0.05$ WT Veh vs. Brtl/+ Veh.

References

1. Forlino A, Cabral WA, Barnes AM, Marini JC (2011) New perspectives on osteogenesis imperfecta. Nat Rev Endocrinol 7:540–557. doi: 10.1038/nrendo.2011.81

2. Paterson CR, McAllion S, Stellman JL (1984) Osteogenesis imperfecta after the menopause. N Engl J Med 310:1694–1696. doi: 10.1056/NEJM198406283102602

3. Sakkers R, Kok D, Engelbert R, et al. (2004) Skeletal effects and functional outcome with olpadronate in children with osteogenesis imperfecta: a 2-year randomised placebo-controlled study. The Lancet 363:1427–1431. doi: 10.1016/S0140-6736(04)16101-1

4. Gatti D, Antoniazzi F, Prizzi R, et al. (2005) Intravenous neridronate in children with osteogenesis imperfecta: a randomized controlled study. J Bone Miner Res 20:758–763. doi: 10.1359/JBMR.041232

5. Letocha AD, Cintas HL, Troendle JF, et al. (2005) Controlled trial of pamidronate in children with types III and IV osteogenesis imperfecta confirms vertebral gains but not short-term functional improvement. J Bone Miner Res 20:977–986. doi: 10.1359/JBMR.050109

6. Rauch F, Munns CF, Land C, et al. (2009) Risedronate in the treatment of mild pediatric osteogenesis imperfecta: a randomized placebo-controlled study. J Bone Miner Res 24:1282–1289. doi: 10.1359/jbmr.090213

7. Ward LM, Rauch F, Whyte MP, et al. (2011) Alendronate for the treatment of pediatric osteogenesis imperfecta: a randomized placebo-controlled study. J Clin Endocrinol Metab 96:355–364. doi: 10.1210/jc.2010-0636

8. Marini JC (2009) Bone: Use of bisphosphonates in children-proceed with caution. Nat Rev Endocrinol 5:241–243. doi: 10.1038/nrendo.2009.58

9. Marini JC, Hopkins E, Glorieux FH, et al. (2003) Positive linear growth and bone responses to growth hormone treatment in children with types III and IV osteogenesis imperfecta: high predictive value of the carboxyterminal propeptide of type I procollagen. J Bone Miner Res 18:237–243. doi: 10.1359/jbmr.2003.18.2.237

10. Antoniazzi F, Bertoldo F, Mottes M, et al. (1996) Growth hormone treatment in osteogenesis imperfecta with quantitative defect of type I collagen synthesis. J Pediatr 129:432–439.

11. Vahle JL, Sato M, Long GG, et al. (2002) Skeletal Changes in Rats Given Daily Subcutaneous Injections of Recombinant Human Parathyroid Hormone (1-34) for 2 Years and Relevance to Human Safety. Toxicologic Pathology 30:312 –321. doi: 10.1080/01926230252929882

12. Poole KES, van Bezooijen RL, Loveridge N, et al. (2005) Sclerostin is a delayed secreted product of osteocytes that inhibits bone formation. FASEB J 19:1842–1844. doi: 10.1096/fj.05-4221fje

13. Li X, Zhang Y, Kang H, et al. (2005) Sclerostin Binds to LRP5/6 and Antagonizes Canonical Wnt Signaling. Journal of Biological Chemistry 280:19883–19887. doi: 10.1074/jbc.M413274200

14. Li X, Ominsky MS, Warmington KS, et al. (2009) Sclerostin antibody treatment increases bone formation, bone mass, and bone strength in a rat model of postmenopausal osteoporosis. J Bone Miner Res 24:578–588. doi: 10.1359/jbmr.081206

15. Ominsky MS, Vlasseros F, Jolette J, et al. (2010) Two doses of sclerostin antibody in cynomolgus monkeys increases bone formation, bone mineral density, and bone strength. Journal of Bone and Mineral Research 25:948–959. doi: 10.1002/jbmr.14

16. Agholme F, Isaksson H, Li X, et al. (2011) Anti-sclerostin antibody and mechanical loading appear to influence metaphyseal bone independently in rats. Acta Orthop 82:628–632. doi: 10.3109/17453674.2011.625539

17. Li X, Ominsky MS, Warmington KS, et al. (2011) Increased Bone Formation and Bone Mass Induced by Sclerostin Antibody Is Not Affected by Pretreatment or Cotreatment with Alendronate in Osteopenic, Ovariectomized Rats. Endocrinology 152:3312–3322. doi: 10.1210/en.2011-0252

18. Padhi D, Jang G, Stouch B, et al. (2011) Single-dose, placebo-controlled, randomized study of AMG 785, a sclerostin monoclonal antibody. Journal of Bone and Mineral Research 26:19–26. doi: 10.1002/jbmr.173

19. McClung MR, Grauer A, Boonen S, et al. (2014) Romosozumab in Postmenopausal Women with Low Bone Mineral Density. New England Journal of Medicine 370:412–420. doi: 10.1056/NEJMoa1305224

20. Forlino A, Porter FD, Lee EJ, et al. (1999) Use of the Cre/lox Recombination System to Develop a Non-lethal Knock-in Murine Model for Osteogenesis Imperfecta with an α1(I) G349C Substitution. Journal of Biological Chemistry 274:37923 –37931. doi: 10.1074/jbc.274.53.37923

21. Kozloff KM, Carden A, Bergwitz C, et al. (2004) Brittle IV Mouse Model for Osteogenesis Imperfecta IV Demonstrates Postpubertal Adaptations to Improve Whole Bone Strength. Journal of Bone and Mineral Research 19:614–622. doi: 10.1359/JBMR.040111

22. Uveges TE, Collin-Osdoby P, Cabral WA, et al. (2008) Cellular mechanism of decreased bone in Brtl mouse model of OI: imbalance of decreased osteoblast function and increased osteoclasts and their precursors. J Bone Miner Res 23:1983–1994. doi: 10.1359/jbmr.080804

23. Davis MS, Kovacic BL, Marini JC, et al. (2012) Increased susceptibility to microdamage in Brtl/+ mouse model for osteogenesis imperfecta. Bone 50:784–791. doi: 10.1016/j.bone.2011.12.007

24. Meganck JA, Begun DL, McElderry JD, et al. (2013) Fracture healing with alendronate treatment in the Brtl/+ mouse model of osteogenesis imperfecta. Bone 56:204–212. doi: 10.1016/j.bone.2013.06.003

25. Uveges TE, Kozloff KM, Ty JM, et al. (2009) Alendronate Treatment of the Brtl Osteogenesis Imperfecta Mouse Improves Femoral Geometry and Load Response Before Fracture but Decreases Predicted Material Properties and Has Detrimental Effects on Osteoblasts and Bone Formation. Journal of Bone and Mineral Research 24:849–859. doi: 10.1359/jbmr.081238

26. Panaroni C, Gioia R, Lupi A, et al. (2009) In utero transplantation of adult bone marrow decreases perinatal lethality and rescues the bone phenotype in the knockin murine model for classical, dominant osteogenesis imperfecta. Blood 114:459–468. doi: 10.1182/blood-2008-12-195859

27. Sinder BP, Eddy MM, Ominsky MS, et al. (2013) Sclerostin antibody improves skeletal parameters in a Brtl/+ mouse model of osteogenesis imperfecta. J Bone Miner Res 28:73–80. doi: 10.1002/jbmr.1717

28. Meganck JA, Kozloff KM, Thornton MM, et al. (2009) Beam hardening artifacts in micro-computed tomography scanning can be reduced by X-ray beam filtration and the resulting images can be used to accurately measure BMD. Bone 45:1104–1116. doi: 10.1016/j.bone.2009.07.078

29. Otsu N (1979) A threshold selection method from gray-level histograms. IEEE Transactions on Systems, Man and Cybernetics 9:62–66.

30. Parfitt AM, Drezner MK, Glorieux FH, et al. (1987) Bone histomorphometry: standardization of nomenclature, symbols, and units. Report of the ASBMR Histomorphometry Nomenclature Committee. J Bone Miner Res 2:595–610. doi: 10.1002/jbmr.5650020617

31. Bivi N, Condon KW, Allen MR, et al. (2012) Cell autonomous requirement of connexin 43 for osteocyte survival: consequences for endocortical resorption and periosteal bone formation. J Bone Miner Res 27:374–389. doi: 10.1002/jbmr.548

32. Hauge E, Mosekilde L, Melsen F (1999) Missing observations in bone histomorphometry on osteoporosis: implications and suggestions for an approach. Bone 25:389–395. doi: 10.1016/S8756-3282(99)00194-5

33. Misof BM, Roschger P, Baldini T, et al. (2005) Differential effects of alendronate treatment on bone from growing osteogenesis imperfecta and wild-type mouse. Bone 36:150–158. doi: 10.1016/j.bone.2004.10.006

34. Sinder BP, White LE, Salemi JD, et al. (2014) Adult Brtl/+ mouse model of osteogenesis imperfecta demonstrates anabolic response to sclerostin antibody treatment with increased bone mass and strength. Osteoporos Int 1–11. doi: 10.1007/s00198-014-2737-y

35. Marenzana M, Greenslade K, Eddleston A, et al. (2011) Sclerostin antibody treatment enhances bone strength but does not prevent growth retardation in young mice treated with dexamethasone. Arthritis Rheum 63:2385–2395. doi: 10.1002/art.30385

36. Li X, Ominsky MS, Niu Q-T, et al. (2008) Targeted Deletion of the Sclerostin Gene in Mice Results in Increased Bone Formation and Bone Strength. Journal of Bone and Mineral Research 23:860–869. doi: 10.1359/jbmr.080216

37. Beighton P (1988) Sclerosteosis. J Med Genet 25:200–203.

38. Sontag W (1986) Quantitative measurements of periosteal and cortical-endosteal bone formation and resorption in the midshaft of female rat femur. Bone 7:55–62. doi: 10.1016/8756-3282(86)90152-3

39. Jepsen KJ (2009) Systems Analysis of Bone. Wiley Interdiscip Rev Syst Biol Med 1:73–88. doi: 10.1002/wsbm.15

40. Epstein S, Hamersma H, Beighton P (1979) Endocrine function in sclerosteosis. S Afr Med J 55:1105–1110.

CHAPTER 5

Tissue Level Mechanical Properties and Matrix Composition After Scl-Ab Treatment in Rapidly Growing and Adult Brtl/+ Mouse Models of OI

Introduction

The mechanical competence of bone is a product of geometry and its material properties and composition. Osteogenesis imperfecta (OI), also known as "brittle bone disease," is a genetic collagen-related disorder which causes fragile bones [1]. Increased fracture risk of OI is often a product of altered bone geometry and material.

Sclerostin antibody (Scl-Ab) is a new anabolic therapy presently in clinical trials for post-menopausal osteoporosis [2, 3]. Numerous studies in a variety of animal models have demonstrated the efficacy of Scl-Ab at stimulating bone formation and increasing bone mass [4–7]. Recently, several studies have also described Scl-Ab as effective at increasing bone formation and strength in mouse models of OI, including those described in the previous three chapters [8–11].

However, the effect of Scl-Ab treatment on tissue level material properties and composition has not been well studied in any population. Specifically, a single study described a nominal effect of Scl-Ab on back-scatter SEM and FTIR material composition outcomes in middle aged male rats and female monkeys [12]. The only study to examine the effect of Scl-Ab on tissue level mechanical properties, and in OI, is reported in Chapter 2 of this dissertation [8]. However, due to technique limitations, this analysis was performed in dehydrated samples. In

addition, these animals were not rapidly growing and this is not an ideal model for pediatric OI. While tissue level material properties of Scl-Ab treated bone were studied for the first time in Chapter 2, material composition of bone formed under the influence of Scl-Ab has not yet been studied in OI.

Therefore, the purpose of this study was to examine the material composition by Raman spectroscopy, and hydrated tissue level mechanical properties by nanoindentation, of rapidly growing 3 wk and adult 6 mo Brtl/+ mice treated with Scl-Ab [13]. Utilizing fluorescent labels given throughout the course of a 5 wk Scl-Ab treatment regimen, we were able to rigorously control for tissue age. We hypothesize that Scl-Ab will not have large effects on material property and composition, but tissue age and animal age will significantly influence these outcomes.

Materials and Methods

Animals

Wildtype (WT) and Brtl/+ [13] mice are maintained on a mixed background of Sv129/CD-1/C57BL/6S, and all Brtl/+ animals were the product of breeding male heterozygous Brtl/+ with female WT. 3 week and 6 month old male WT and Brtl/+ mice were randomly assigned to Scl-Ab (Scl-Ab VI, Amgen, Thousand Oaks, CA) treatment or vehicle injection (PBS). Sclerostin antibody was injected subcutaneously at 25 mg/kg, two times per week, for five weeks. Calcein (30mg/kg, i.p. injection) was injected at the start of experiment (3 weeks animal age, 5 weeks before euthanasia), after 2 weeks of treatment (5 weeks animal age, 3 weeks before euthanasia), and after 4 weeks of treatment (7 weeks animals age, 1 week before euthanasia). A final alizarin label (30mg/kg, i.p. injection) was given 1 day before euthanasia

(7weeks + 6 days of animal age). The multiple fluorescent labels were used to visualize the growth pattern during the entire course of therapy. Body weights were recorded with each injection. Right femurs were harvested and stored at -20˚C in lactated ringers solution (LRS) soaked gauze until testing or further specimen preparation. All protocols and procedures involving animals were approved by the University of Michigan's Committee on Use and Care of Animals.

Two distinct cohorts of animals were used for this study. Nanoindentation data was performed on the same animals described in Chapters 3 and 4, on the same femurs used for dynamic histomorphometry. These samples underwent ~2-4 freeze cycles in the course of harvesting and specimen preparation, but this was not rigorously controlled for. Nanoindentation group sizes are n=7-9/group before accounting for testing errors.

All Raman spectroscopy tests were performed on a new cohort of animals (both 3 wk and 6 mo) that were treated in an identical manner as described above. This additional cohort of animals was added to control for, and limit, the number of freeze/thaw cycles which have the potential to confound Raman spectroscopy results [14]. All Raman spectroscopy data was collected on femora that had one freeze/thaw cycle prior to imaging. All Raman Spectroscopy data was n=5-7/group.

Nanoindentation Specimen Preparation

Right femora were thawed, encased in a quick setting (~30min) epoxy (Kold Mount, Vernon-Benshoff, Albany, NY) without dehydration, and cut transversely at the mid-diaphysis with a low-speed saw (IsoMet, Beuhler, Lake Bluff, IL). The distal section of tissue was polished using progressive grades of silicon carbide abrasive paper (1200, 2400, and 4000 grit) under

water irrigation for two minutes at each grade. Each specimen was polished to a plane just distal to the third trochanter, identical to that performed by dynamic histomorphometry, and similar to a plane included in our cortical microCT and mechanical 4pt testing data reported in Chapters 3 and 4. To further decrease surface roughness for nanoindentation, the encased specimens were polished on a felt pad for 5 minutes with a ¼ µm diamond suspension (Streurs Inc., Cleveland, OH). Specimens were then ultrasonically cleansed in a water bath for 10 minutes to remove surface debris, and glued to a glass slide specimen plate for nanoindentation testing in a custom-made hydration chamber.

Nanoindentation

A custom 950 TI TriboIndenter (Hysitron, Minneapolis, MN) instrumented with a fluorescent light-source and FITC filter allowed for simultaneous visualization of calcein labeling in specimens and accurate positioning of indents to locations matched for tissue age and treatment status with 0.5 µm spatial resolution. Five (rapidly growing) or six (adult) regions of interest were mechanically tested in the posterior aspect of the femoral cross section (Fig 5.2): the mid-cortex (defined as midway between the first calcein label on the periosteal and endosteal surfaces, if any), 15 µm endosteal to ("inside") the first 5 wk old label, along the first calcein label on 5 wk old bone, along the second calcein label on 3 wk old bone, along the third calcein label on 1 wk old bone, and along the final alizarin label on 1 day old bone. As our fluorescent nanoindenter only has a FITC filter and adding a second filter is not possible, the outer alizarin label positions were identified by looking at dynamic histomorphometry images taken of these same bones (Chapters 3 and 4) and measuring the distance from the 1 wk old calcein label. The mid-cortex and 15 um endosteal to the 5 wk label positions were nearly identical locations in

rapidly growing 3 week animals. As such, nanoindentation values were only collected at one location and characterized as "15 um inside 5wk" label in all analysis. As Veh treated 6 mo old animals grow much slower than 3 wk old animals, it was not always possible to delineate the outer 1 wk and 1 day old labels in adult 6 mo mice as they appeared in the same location. Moreover, nanoindentation requires spacing between indents to not indent on the tissue deformed by a previous indent. Therefore, in these instances, data was only collected in one location, and it was treated as a tissue age of 1 wk.

Indentation consisted of a 10 μN pre-load, with a diamond Berkovich indenter tip into samples, followed by loading the sample at 300 μN/s, hold at a maximal load of 3,000 μN for 10 s, and unloading at 300μN/s. The indentation modulus E was calculated from the load-displacement curves using the standard Oliver-Pharr method [15]. Eight indents, 10 μm apart, were made along each fluorescent label and region of interest, with values averaged for each site and mouse.

Raman Spectroscopy

Raman measurements were performed with a custom microscope outfitted for Raman spectroscopy as previously described [16]. Briefly, Raman spectra were collected by directing a 785-nm stabilized diode laser (Invictus, Kaiser Optical Systems, Inc., Ann Arbor, Michigan) through a Nikon E600 microscope (Nikon Instruments Inc., Melville, New York) with a 40x/0.90 NA objective (S Fluor, Nikon Instruments, Inc., Melville, New York) operated in epi-illumination and collection. Collected light from the sample was passed through an imaging spectrograph with a 50-μm slit (Holospec f/1.8i, Kaiser Optical Systems, Inc., Ann Arbor MI) and detected with a deep depletion, back-illuminated CCD camera (DU 401-BR-DD, Andor

Technologies, South Windsor, Connecticut). Estimated spectral resolution is ~8 cm^{-1}. After data preprocessing, the estimated imaging spot size is 2.3 by 69.1 μm.

For each specimen, periosteal bone was mapped in a 9 by 4 grid from the map origin. The map origin was defined as the upper left corner of a relatively flat and uniform region of the bone. The 9 measurement rows were determined by the fluorescent labels. The 4 measurement columns spanned were equally spaced 75 μm apart starting from the origin. The 9 measurement locations, as guided by the fluorescent labels, were the midcortex, 15 μm endosteal to the 5 week old bone label, atop the 5 weeks old bone label, halfway between the labels marking 5 and 3 weeks old bone, atop the 3 weeks old bone label, halfway between the labels marking 3 weeks and 1 week old bone, atop the 1 week old bone label, halfway between the 1 week and 1 day old bone label, and atop the 1 day old bone label (Fig. 5.1, 5.2). At each location, a spectrum was collected in 120 s with ~ 45 mW laser power. Custom-built Matlab (The Mathworks, Inc., Natick, MA) software was employed for data processing. The processing routine included cosmic spike correction, dark subtraction, correction for spectrograph slit curvature, calibration for wavelength-dependent changes in the CCD's quantum efficiency, and wavenumber calibration.

Raman spectroscopic parameters were computed with locally written scripts to assess changes in the mineral and matrix components of the cortical bone. Carbonate content was analyzed by assessing the carbonate to phosphate ratio (1070 cm^{-1}/959 cm^{-1}). The mineral to matrix ratio was assessed, and defined as the intensity of the phosphate ν_1 band at 959 cm^{-1} divided by the maximum intensity of the proline and hydroxyproline bands between 850 and 880 cm^{-1} .

Statistics

Comparisons between tissue ages were made with a two-factor general linear model with repeated measures. Specifically, within each animal age, genotype (WT and Brtl/+) and treatment (Veh and Scl-Ab) were between-subjects factors, and tissue age identified as a within-subjects factor. All pairwise tissue age comparisons were performed with a conservative Bonferroni correction to a reference point of 5 weeks of tissue age A tissue age of 5 weeks was chosen as the reference, instead of mid-cortex, because this allowed us to control for tissue age across two animals ages and directly contrast findings between rapidly growing and adult animals. These data are shown in Fig 5.3, 5.5 and 5.7.

To assess the overall effect of genotype, and treatment, within a specific tissue age, a two factor multivariate model was performed with genotype (WT and Brtl/+) and treatment (Veh and Scl-Ab) as the between subjects factors that were analyzed at each tissue age. These data are shown in Fig 5.4, 5.6, and 5.8.

To assess the overall effect of animal age on material property and composition when controlling for tissue age, a three factor multivariate model was employed, with animal age (rapidly growing 3 wk and adult 6 mo), genotype (WT and Brtl/+), and treatment (Veh and Scl-Ab) as the between subjects factors that were analyzed for each outcome at all tissue ages. The data for animal age is shown in Fig. 5.10.

$p<0.05$ was considered significant in all cases. Mean ± standard deviation is shown unless otherwise noted.

Results

Treatment Effect: Scl-Ab Decreases the Carbonate to Phosphate Ratio, Increases the Mineral to Matrix Ratio, and Does not Affect the Elastic Modulus

In rapidly growing animals, Scl-Ab significantly decreased the carbonate to phosphate ratio at all tissue ages with the exception of 1 Day old bone (Fig 5.4). In adult 6 mo animals, Scl-Ab significantly reduced the carbonate to phosphate ratio only at newer tissue ages of 1 Week, 4 Days, and 1 Day (Fig 5.4). This led to a different pattern of carbonate to phosphate ratios across the fluorescent labeled region (5 Week to 1 Day) of bone in 6 mo Scl-Ab treated WT and Brtl/+ when compared to Veh controls (Fig 5.3). Specifically, newer tissue ages of 2 Weeks, 1 Week, 4 Days, and 1 Day had significantly lower carbonate to phosphate ratios than 5 week values in Scl-Ab treated specimens. Correspondingly, no differences were noted below 5 week old tissue age in Veh controls.

In 6 mo old specimens, Scl-Ab significantly increased the Mineral to Matrix ratio at Tissue ages of 4 wks, 3 wks, and 2 wks on the periosteal posterior surface of the diaphyseal femur (Fig. 5.6). In rapidly growing (3 wk) animals, Scl-Ab only increased the mineral to matrix ratio at a location 15um inside the 5week label.

The elastic modulus measured by nanoindentation was not significantly affected by Scl-Ab at any tissue age in rapidly growing (3 wk) or adult (6 mo) animals (Fig 5.8).

Genotype Effect: Brtl/+ Has Increased Mineral to Matrix and Elastic Modulus at Some Tissue and Animals Ages, and Transient Decreases in Carbonate to Phosphate

Overall phenotypic changes in the carbonate to phosphate ratio due to mouse genotype were small and few. In rapidly growing 3 wk Brtl/+ mice, significantly lower carbonate to

phosphate was observed at the newest tissue age of 1 day, and 4 week old bone relative to WT (Fig 5.4). No differences in the carbonate to phosphate ratio were observed between Brtl/+ and WT in adult 6 mo old animals at any tissue age, despite consistent but non-significant reductions in the mean.

Increases in Brtl/+ mineral to matrix ratio were observed in both rapidly growing and adult animals. Specifically, in 6 mo adult animals, increased mineral to matrix ratios were observed at tissue ages of 3 weeks, 4 weeks, 5 weeks, and 15um inside the 5week label (Fig 5.6). In rapidly growing 3 weeks animals, significantly increased mineral to matrix ratio was observed at 4 weeks of age, 15um inside the 5 week label, and at Mid-Cortex.

No changes in elastic modulus were observed in rapidly growing 3 week old animals (Fig 5.8). Brtl/+ mid-cortex values were significantly greater than WT in adult 6 mo old animals, but no changes were observed at other tissue ages (Fig 5.8).

Tissue Age Effect: Elastic Modulus and Material Composition Continue to Increase with Tissue Age in Adult Mice, But Plateau in the Rapidly Growing Mice

In rapidly growing 3 wk and adult 6 mo animals, the carbonate to phosphate ratio was not changed at tissue ages of 5weeks or less in Veh treated animals. In 6 mo old adult animals, mid-cortex and tissue 15um inside the 5week label had a significantly greater carbonate to phosphate ratio relative to 5 week values in all groups (Fig 5.3). In rapidly growing animals, mid-cortex and tissue 15um inside the 5week label were not significantly different than mid-cortical controls.

In adult 6 mo old WT and Brtl/+, increasing tissue age is associated with increasing mineral to matrix ratio, with the highest levels seen at mid-cortex (Fig 5.5). In rapidly growing

animals, the mineral to matrix ratio increased rapidly until peak values were achieved at ~3weeks of tissue age. At tissue ages greater than 3 weeks in rapidly growing animals, increasing tissue age correlated with decreased mineral to matrix ratios (Fig 5.5, 5.9). The mean slope of the mineral to matrix ratio from 3 weeks of tissue age to 5 weeks of tissue age in all rapidly growing animals is negative (-1.06/day) and significantly less than the positive slope observed in adult 6 mo animals over this same time period (0.098/day) (Fig 5.9).

The pattern of elastic modulus was similar to that observed in the mineral to matrix ratio. Specifically, in adult 6 mo animals, increasing tissue age was associated with increasing elastic modulus, and the highest levels were observed at mid-cortex (Fig 5.7). By contrast, in rapidly growing animals, the elastic modulus reached peak values at ~3weeks of tissue age, and further increases were not observed with increasing tissue age. The mean slope of the elastic modulus from 3 weeks of tissue age to 5 weeks of tissue age in rapidly growing animals is negative (-0.035GPa/Day), and significantly less than the positive slope observed in adult 6 mo animals (0.148GPa/Day) over this same time period (Fig 5.9).

The Age of the Animal at Which a Tissue was Formed, Independent of the Age of the Tissue, Influences Material Composition and Elastic Modulus

The graphs in Figure 5.10 show the estimated marginal means across all groups within an animal age. The estimated marginal means account for treatment and genotype effects, and are not the simple average of all values from a certain animals age. They serve to make clear the differences between animal age that are (sometimes) visually apparent in Figures 5.3, 5.5, and 5.7.

Adult 6 mo animals had a significantly greater carbonate to phosphate ratio at all Tissue Ages (1 Day through Mid-Cortex) when compared to rapidly growing animals (Fig 5.10).

The differences in mineral to matrix ratio between adult 6 mo animals and rapidly growing 3 week animals depend on tissue age (Fig 5.10). Between tissue ages of 4 weeks and 1 week, rapidly growing animals had a greater mineral to matrix ratio than adult 6 mo animals. At the newest, and oldest tissue ages, 6 mo animals had a greater mineral to matrix ratio. Specifically, adult 6 mo animals had a greater mineral to matrix ratio than rapidly growing 3week animals at a tissue age of 1 day, and at Mid-Cortex and 15um inside the 5 week label.

Elastic modulus in 6 mo old animals was significantly greater than rapidly growing 3 week animals at tissue ages of 3 weeks and 5 weeks, and at a location 15um inside the 5 week label (Fig 5.10).

Discussion

While we have previously demonstrated that Scl-Ab can increase bone mass and strength in a mouse model of OI, this study represents the first investigation into the effect of Scl-Ab on the material composition of OI tissue. Although overall effects of Scl-Ab was often similar between WT and Brtl/+, the data did demonstrate that Scl-Ab has an effect on material composition. However, despite these effects on composition, no significant effect on elastic modulus was observed. Collectively, this study adds to an emerging, but extremely limited, set of data describing the effect of Scl-Ab on material property and composition.

Before discussing the data in detail, two brief comments on nomenclature as it relates to interpretation of the "tissue age" data are merited. First, numerous references are made to bone of a certain tissue age; for example, "at a tissue age of 3 weeks". Tissue age, however, can be a

misleading term in this application. A more precise definition is, "A region of bone that had a fluorescent calcein label bind to it 3 weeks before the animal was euthanized". With the understanding that calcein rapidly binds to mineral, this should be interpreted as "a region of bone that just started to mineralize 3 weeks before the animal was euthanized". Mineralization lag time has been ignored. This may be convenient, and even ideal. However, one should be cognizant of this.

Second, fluorescent label that bound to a tissue 5 weeks ago may not be indicative of the fact that all tissue in a particular region has been mineralizing for 5 weeks. For example, in rapidly growing animals the "5 week old" tissue age on posterior surface is anatomically located near the middle of the cortex, and characterized by porous woven looking bone (Fig 5.2, 5.11). It is possible that some level of apposition continues in these pores after the initial woven bone is laid down, and this may even be modulated by treatment. It should be noted that tissue ages 3 weeks or newer in rapidly growing animals were always lamellar in appearance. In adult 6 month old animals, all bone throughout the five week treatment period was lamellar in nature. Finally, it is important to note that tissue ages at mid-cortex and 15um inside the 5 wk label in adult animals are almost certainly greater than in rapidly growing 3 wk mice, and should be interpreted as such.

Interestingly, the pattern of material composition and elastic modulus with tissue age is different between rapidly growing 3 wk, and adult 6 mo, animals. In both adult and rapidly growing animals we observed a rapid increase in the mineral to matrix ratio from tissue ages of 1 day through 3 weeks. However, after 3 weeks of age, the pattern diverged. Adult animals continued to increase the mineral to matrix ratio and elastic modulus from 3 weeks of tissue age through 5 weeks of tissue age (Fig 5.9). Conversely, we observed decreasing mineral to matrix

ratio and elastic modulus in rapidly growing animals from 3 weeks of tissue age to 5 weeks of tissue age. These findings may be related to the woven nature of the bone present beginning between 3 and 5 weeks of tissue age (Fig 5.2, 5.11).

While the pattern of the mineral to matrix ratio and elastic modulus across tissue age correlated with one another at different animals ages (Fig 5.9), a positive correlation between these two variables was not always observed. For example, the absolute value of the mineral to matrix ratio was greater in rapidly growing 3 wk mice than adult 6 mo animals, but rapidly growing 3 wk animals had a lower elastic modulus at some tissue ages (Fig. 5.10). Although the mineral to matrix ratio often positively correlates with the elastic modulus, numerous factors can modulate this relationship. In support of this notion, less than half of the variation in tissue level elastic modulus has been reported to be explained by tissue mineralization [17]. Some of these factors are explicitly related to alterations within the mineral component, and would not be captured by the mineral to matrix ratio which measures the relative amount of mineral. For example, a recent study showed that in regenerate bone, the orientation of apatite crystals, rather than BMD, correlated with Young's modulus [18]. It is possible that alterations apatite crystal orientation in regions of woven bone could account for differences in the correlation between elastic modulus and mineral to matrix ratio. In addition, mineral crystallinity describes a quality of the mineral not captured in the mineral to matrix ratio, and may independently modulate the relationship between mineralization and elastic modulus [19–21].

Many other factors describing material composition can modulate the elastic modulus. In addition to outcomes describing specific qualities of the mineral, additional factors relating to the organic component of bone can also affect the elastic modulus. The organic component of bone is 90% Type I collagen, but extracellular matrix proteins which comprise the remaining

10% can also have a significant effect on material properties. Among many examples, both osteocalcin and TGF-β have been shown to affect the tissue level elastic modulus, in addition to other mechanical parameters [22, 23]. In addition, collagen cross-linking is another organic factor has been shown to influence the elastic modulus of bone [24, 25]. The relationships between composition and mechanical property are complex and span interactions at multiple hierarchical levels. Moreover, the relationship between mechanical property and material composition have been shown to vary with animal age [25, 26].

In this study, the carbonate to phosphate ratio was highest at mid-cortex of adult 6 mo animals (Fig 5.3). The lack of difference at mid cortex in rapidly growing 3 week animals is likely attributable to the relatively small difference in tissue age between mid-cortex and 5 week old bone, when compared to adult 6 mo animals. Unique from mineral to matrix ratio and elastic modulus, tissue age and the presence of woven bone do not appear to affect carbonate to phosphate ratios in rapidly growing animals. Moreover, carbonate to phosphate does not vary across the fluorescently labeled 5 weeks of bone in Veh treated adult 6 mo WT and Brtl/+.

We observed that Scl-Ab reduced the carbonate to phosphate ratio in both rapidly growing and adult mice, although the effect was different within each animal age (Fig 5.4). In adult mice, reduced carbonate to phosphate was only observed at very young tissue ages of 1 week or less. Conversely, in rapidly growing mice, a reduced carbonate to phosphate ratio was observed at nearly all tissue ages. Effects of bone material composition by Scl-Ab have only recently begun to be examined, with a single report suggesting an opposite effect of reduced carbonate substitution with Scl-Ab treatment [12]. The cited study was performed in the trabecular bone of 4-5 year old cynomolgus monkeys, with different specimen preparation, and by FTIR; all factors which may be related to our differential result.

In our study, Scl-Ab transiently increased the mineral to matrix ratio at some tissue ages and animal ages. Specifically, in rapidly growing 3 week animals, Scl-Ab significantly increased the mineral to matrix ratio only at a location 15um inside the 5week old label. The isolated nature of this effect suggests it should be interpreted with caution. In contrast, in adult 6 mo animals, a transient pattern of increased mineral to matrix with Scl-Ab was observed at 2 weeks, 3 weeks and 4 weeks of tissue age with Scl-Ab. This finding correlates with data at the intracortical compartment of 4-5 year old cynomolgus monkeys [12]. In this study, the elastic modulus data did not reveal a significant effect of Scl-Ab.

The finding of small but significant increases in mineral to matrix in Brtl/+ vs WT animals (Fig 5.6) is in agreement many studies that have consistently found increased mineralization and TMD in this OI mouse model [27, 28]. Unique from these prior studies is that the data in this study controls for tissue age, and suggests that differences in mineral to matrix do not present at tissue ages <3weeks in adult mice. Similar findings were observed in rapidly growing animals and significant differences were not observed at tissue ages <4 weeks. While it may be tempting to conclude that Brtl/+ and WT mineral to matrix levels start out at identical levels, and only diverge with secondary mineralization, a quick inspection of the data reveals non-significant trends that are present in young tissue. These should not be conveniently dismissed. The elastic modulus was significantly greater at mid-cortex of adult 6 mo Brtl/+ animals, but no phenotypic differences were observed in rapidly growing animals.

Perhaps most interesting is the data which suggests that at two different animal ages, bone of an equivalent tissue age can be of a different material property and composition. For example, our data show that even when controlling for tissue age, increased carbonate to phosphate ratio is observed at all tissue ages. Thus, it is not simply tissue age which accounts for

differences in material composition in old vs young animals. Rather, the age of the animal at which a tissue was initially formed also accounts for some of its composition. Differences in the mineral to matrix ratio and elastic modulus were also observed between animal ages when controlling for tissue age. While several studies have utilized fluorescent labeling to look at the effect of tissue age within a single animal age [29, 30], this technique has not been utilized across different animal ages. However, studies have touched on such an interaction by examining numerous tissue ages [19, 26], or inferring tissue age by osteonal morphology [31].

There are several important limitations to this study. First, raman spectroscopy and nanoindentation were carried out in separate animals. While this prevented direct correlations from data taken at identical locations, similar trends observed in different animals provide independent confirmation of main effects. Second, our data is limited to cortical bone of the posterior femur in a mouse model. What happens at one skeletal site and species may not be true in another. Additionally, as nanoindentation primarily quantifies pre-yield mechanical effects, future studies should examine post-yield effects at the tissue level. Band-fitting of raman spectroscopy data is currently underway to assess changes in cross-linking. Finally, as OI is a disease of many mutations, the results from one OI type may not extend to another. Therefore, these data should be tested in other dominant and recessive OI types that feature unique mutations and phenotypes.

In conclusion, our data suggest that Scl-Ab affects material composition, decreasing the carbonate to phosphate ratio, while imparting transient increases in mineral to matrix. In addition, by controlling for tissue age across two animals ages, we have directly shown that age of an animal at which bone is formed can influence tissue composition and mechanical

properties. For the material properties and compositional parameters we analyzed in this study, the data does not suggest that there are unique concerns of Scl-Ab use in a Brtl/+ model of OI.

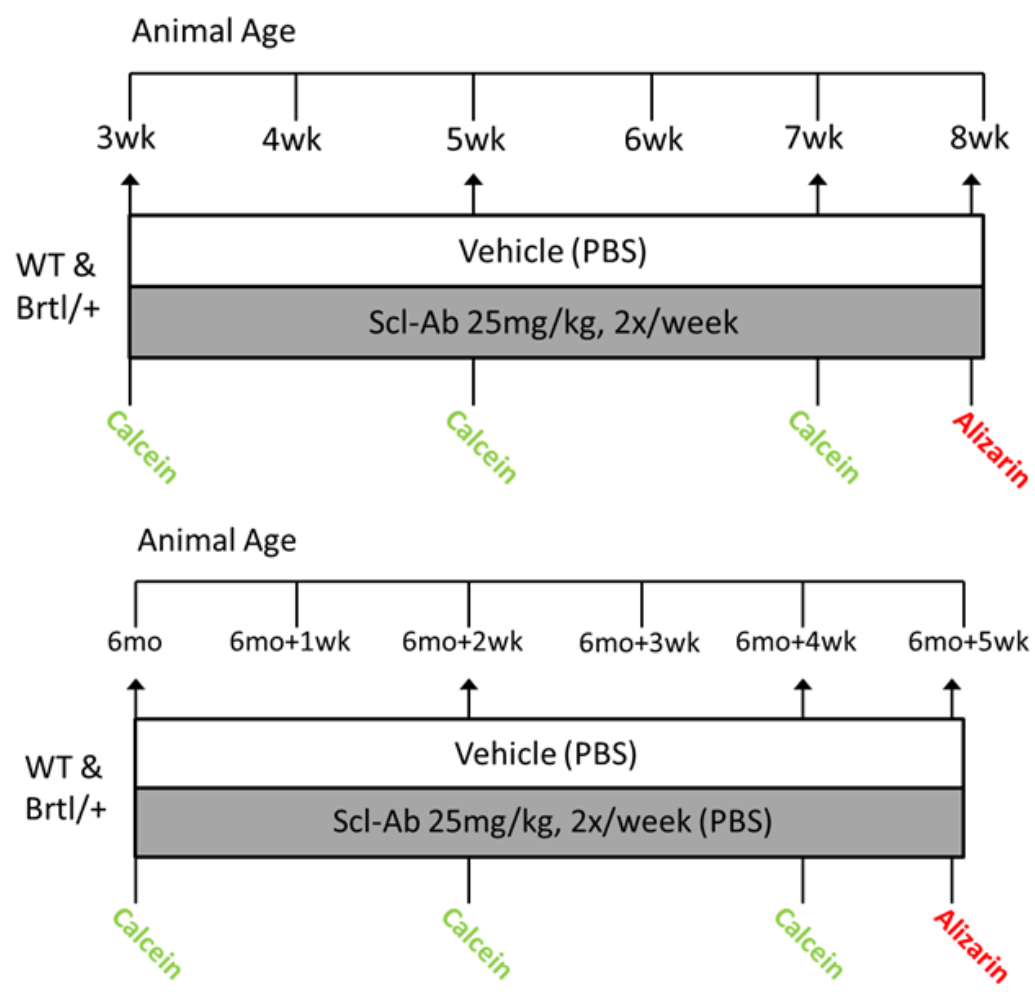

Figure 5.1: Experimental Design and Fluorescent Label Timing. Experimental design and calcein labeling scheme for these experiments is shown above, and is the same as that used in Chapters 3 and 4. The final alizarin label was given 1 Day before euthanasia.

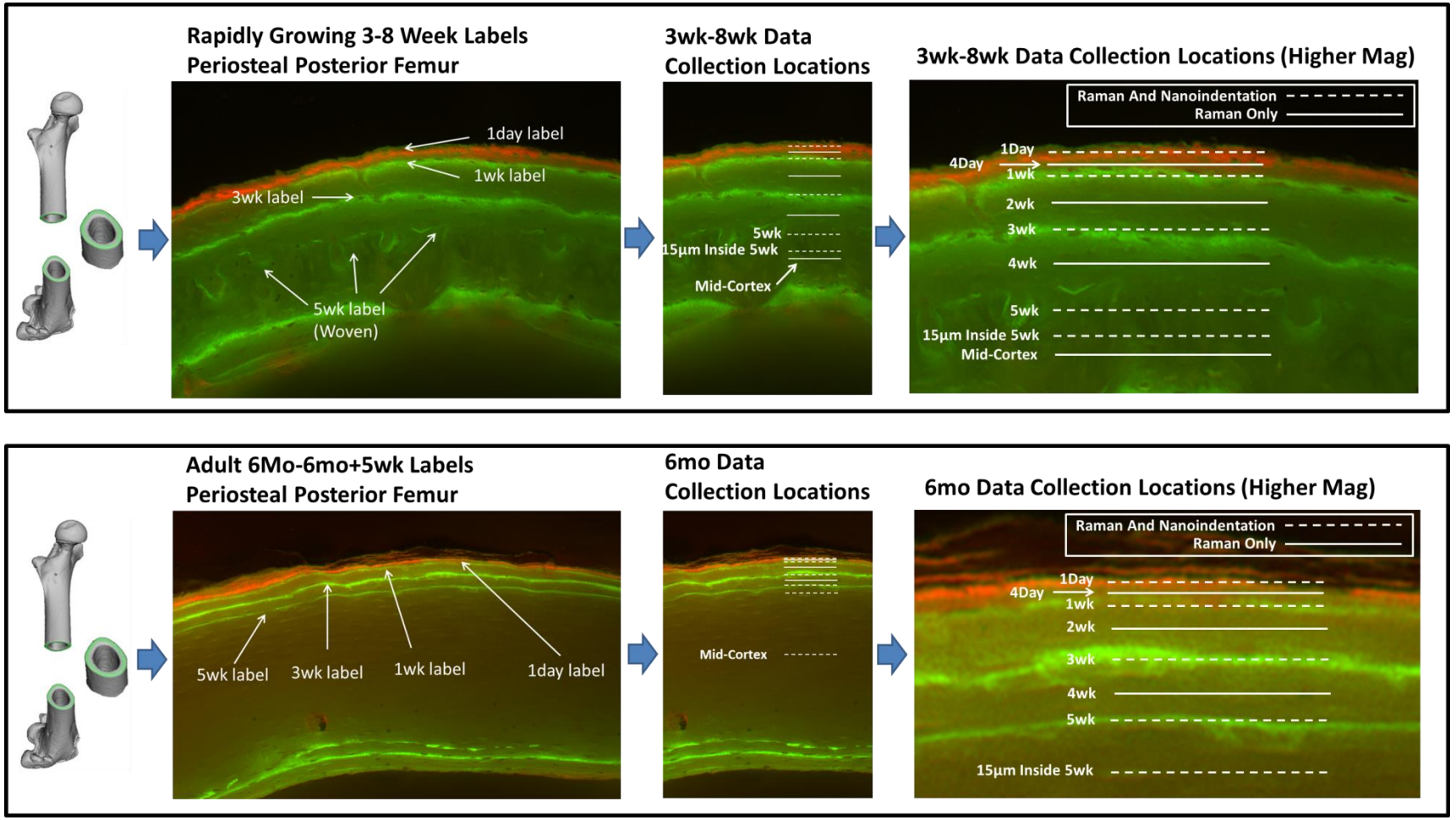

Figure 5.2: Raman Spectroscopy and Nanoindentation Data Collection Locations**.** All data collected at mid-diaphyseal femur of rapidly growing 3wk-8wk and adult 6mo-6mo+5wk animals. Calcein and alizarin labels were given as shown in Fig 5.1. Nanoindentation was not performed between labels due to resolution issues, or collected at mid-cortex in rapidly growing animals because it was nearly identical in location to the "15um inside 5wk" label location. In some adult 6mo Veh specimens, the 1wk and 1 Day labels were almost on top of each other. As indents for nanoindentation can not be placed on top of one another, in some cases, data was only collected for 1 week old tissue. The 6 month animal shown is treated with Scl-Ab and has much greater separation between labels than that typical of adult 6mo Veh mice.

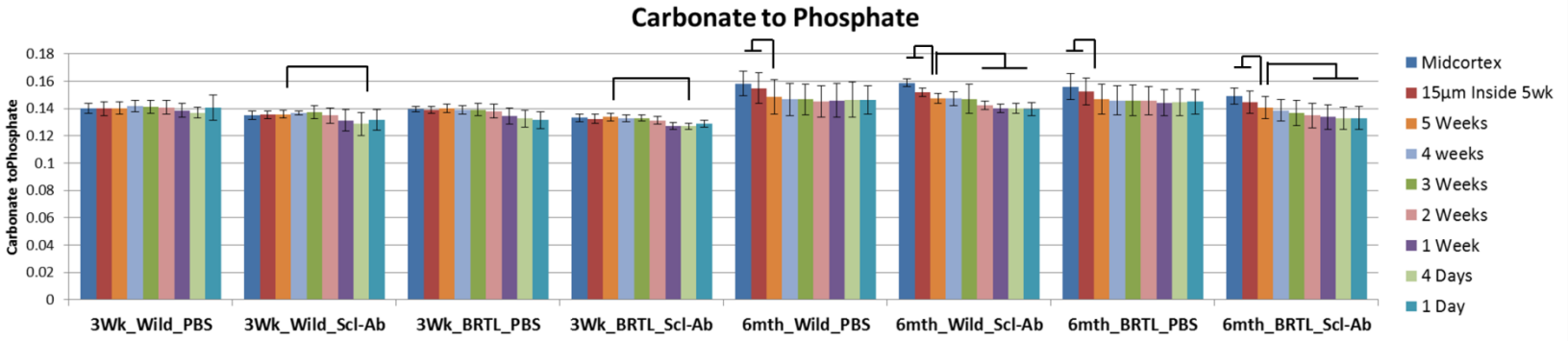

Figure 5.3: Carbonate to Phosphate Ratio. Carbonate to Phosphate ratio at nine tissue ages on the periosteal posterior surface of the mid-diaphyseal femur. All differences from a 5 week tissue age (orange bars) are shown within each experimental group. Lines indicate $p<0.05$, repeated measures pairwise comparison with Bonferonni correction. All data is mean±stdev.

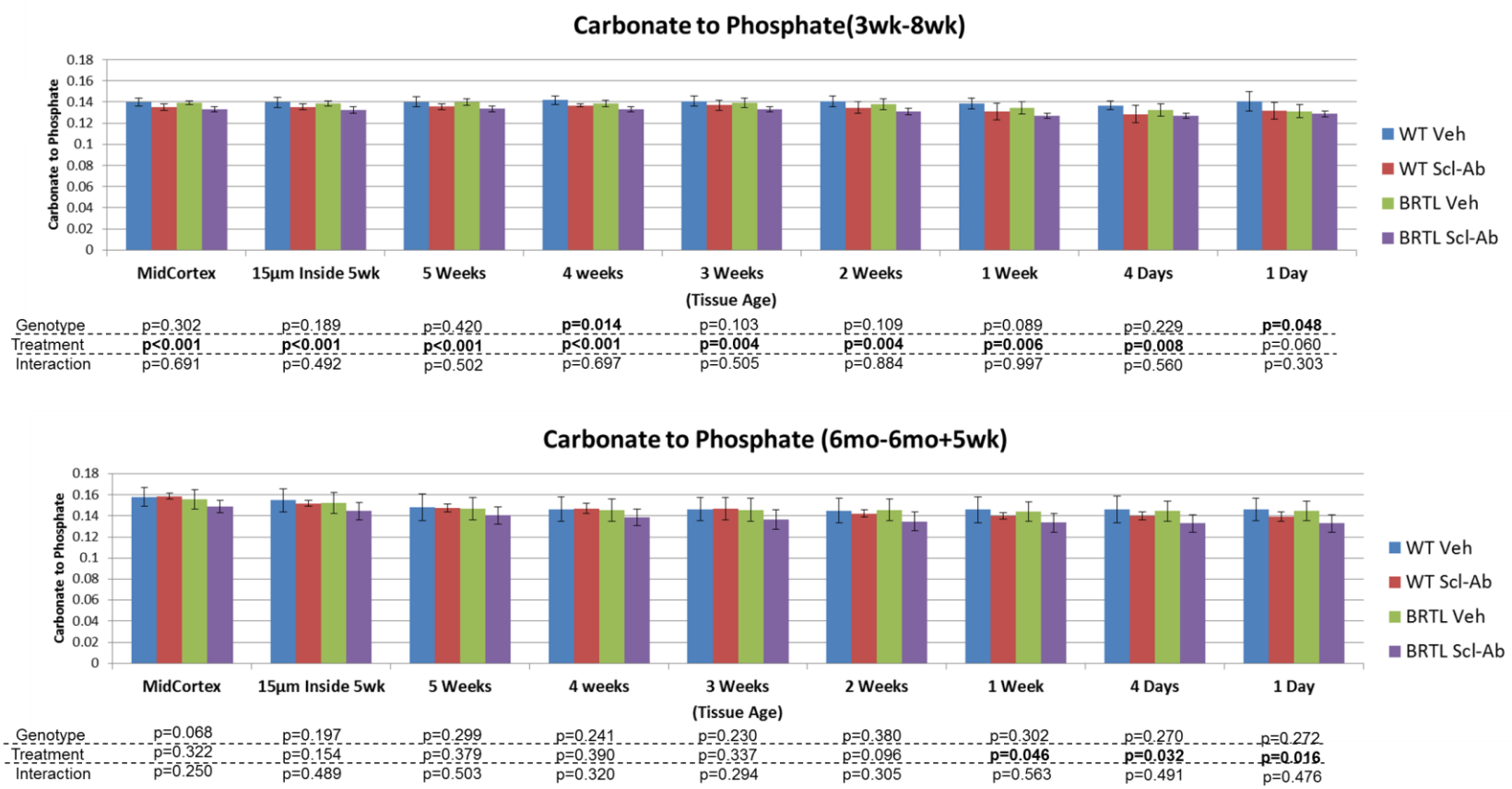

Figure 5.4: Carbonate to Phosphate Ratio (grouped by Tissue Age). Carbonate to Phosphate ratio at nine tissue ages on the periosteal posterior surface of the mid-diaphyseal femur. This is the same data shown in figure 5.3, but formatted to reveal differences of treatment and genotype within tissue age. P-values listed represent the result of a two-factor analysis and show the overall effect of genotype and treatment at each tissue age. All data is mean±stdev.

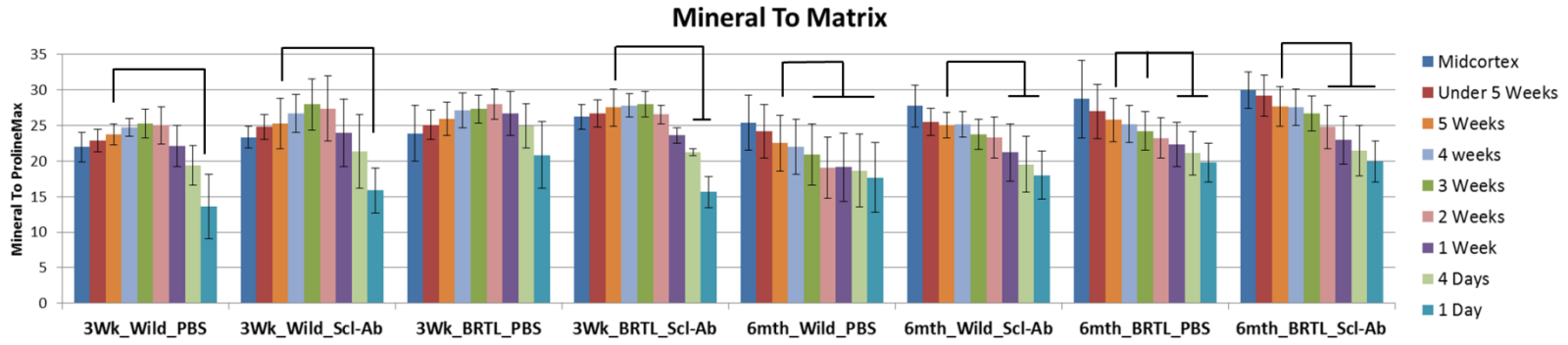

Figure 5.5: Mineral to Matrix Ratio. Mineral to Matrix ratio at nine tissue ages on the periosteal posterior surface of the mid-diaphyseal femur. All differences from a 5 week tissue age are shown within each experimental group. Bars indicate $p<0.05$, repeated measures pairwise comparison with Bonferonni correction. All data is mean±stdev.

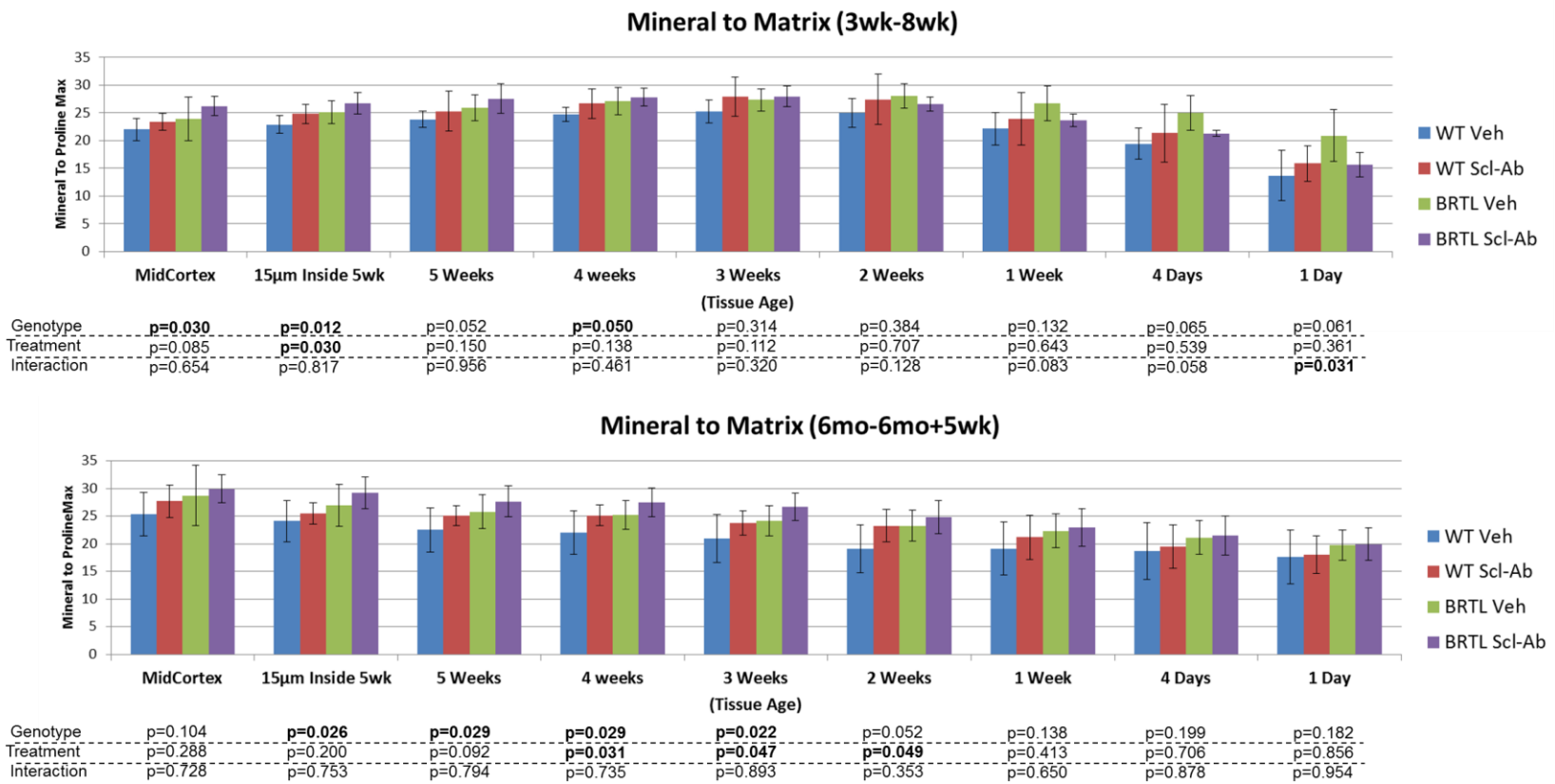

Figure 5.6: Mineral to Matrix Ratio (grouped by Tissue Age). Mineral to Matrix ratio at nine tissue ages on the periosteal posterior surface of the mid-diaphyseal femur. This is the same data shown in Figure 5.5, but formatted to reveal differences of treatment and genotype within tissue age. P-values listed represent the result of a two-factor analysis and show the overall effect of genotype and treatment at each tissue age. All data is mean±stdev.

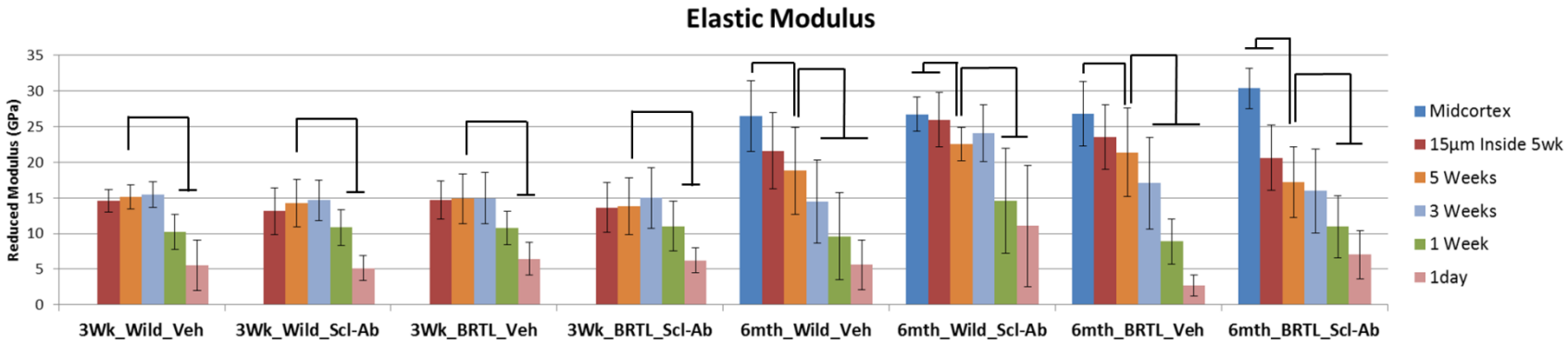

Figure 5.7: Elastic Modulus. Elastic Modulus as measured by nanoindentation at nine tissue ages on the periosteal posterior surface of the mid-diaphyseal femur. All differences from a 5 week tissue age are shown within each experimental group. Bars indicate $p<0.05$, repeated measures pairwise comparison with Bonferonni correction. All data is mean±stdev.

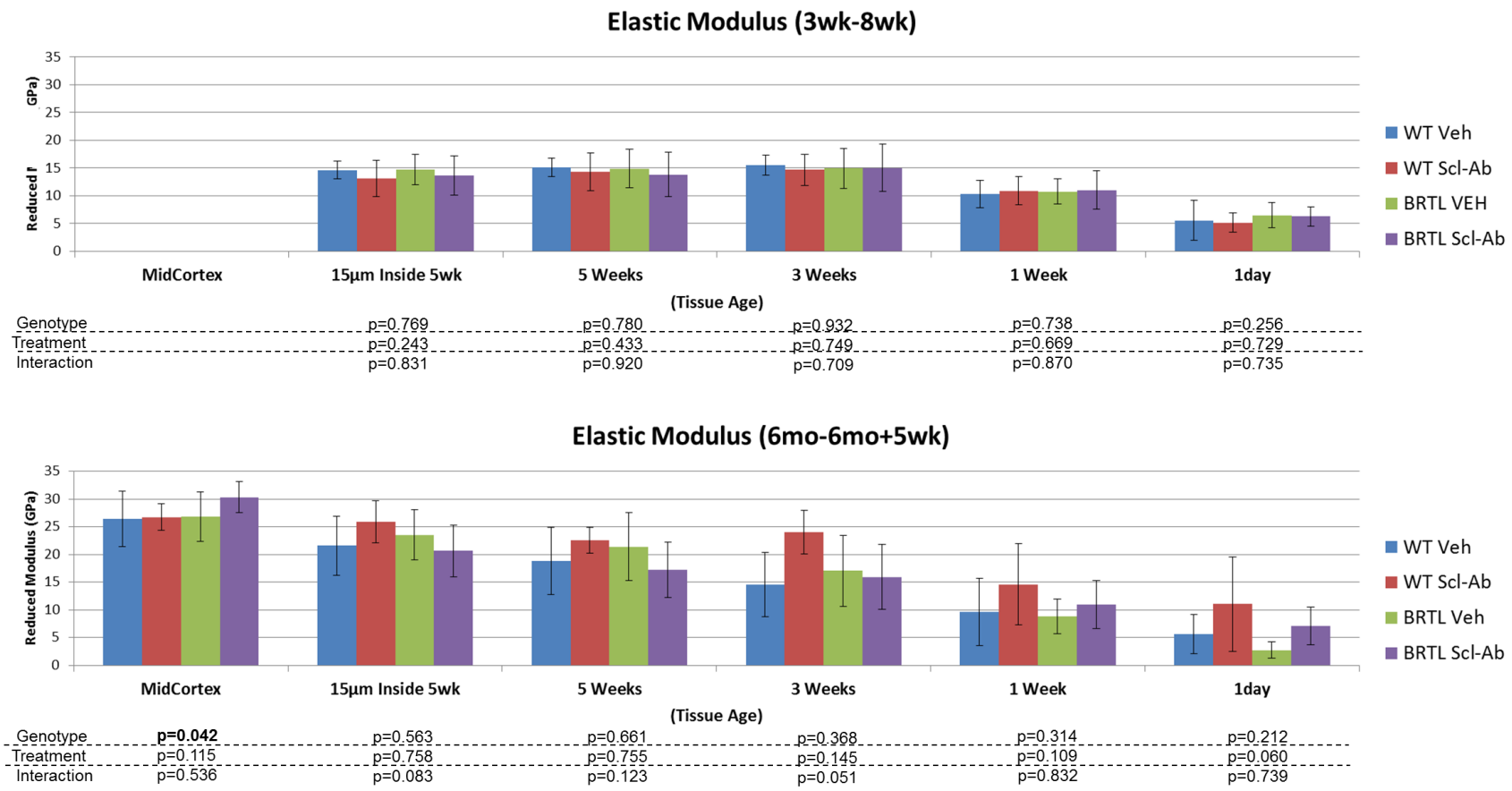

Figure 5.8: Elastic Modulus (grouped by Tissue Age). Elastic Modulus as measured by nanoindentation at five or six tissue ages on the periosteal posterior surface of the mid-diaphyseal femur. This is the same data shown in Figure 5.7, but formatted to reveal differences of treatment and genotype within tissue age. P-values listed represent the result of a two-factor analysis and show the overall effect of genotype and treatment at each tissue age. All data is mean±stdev.

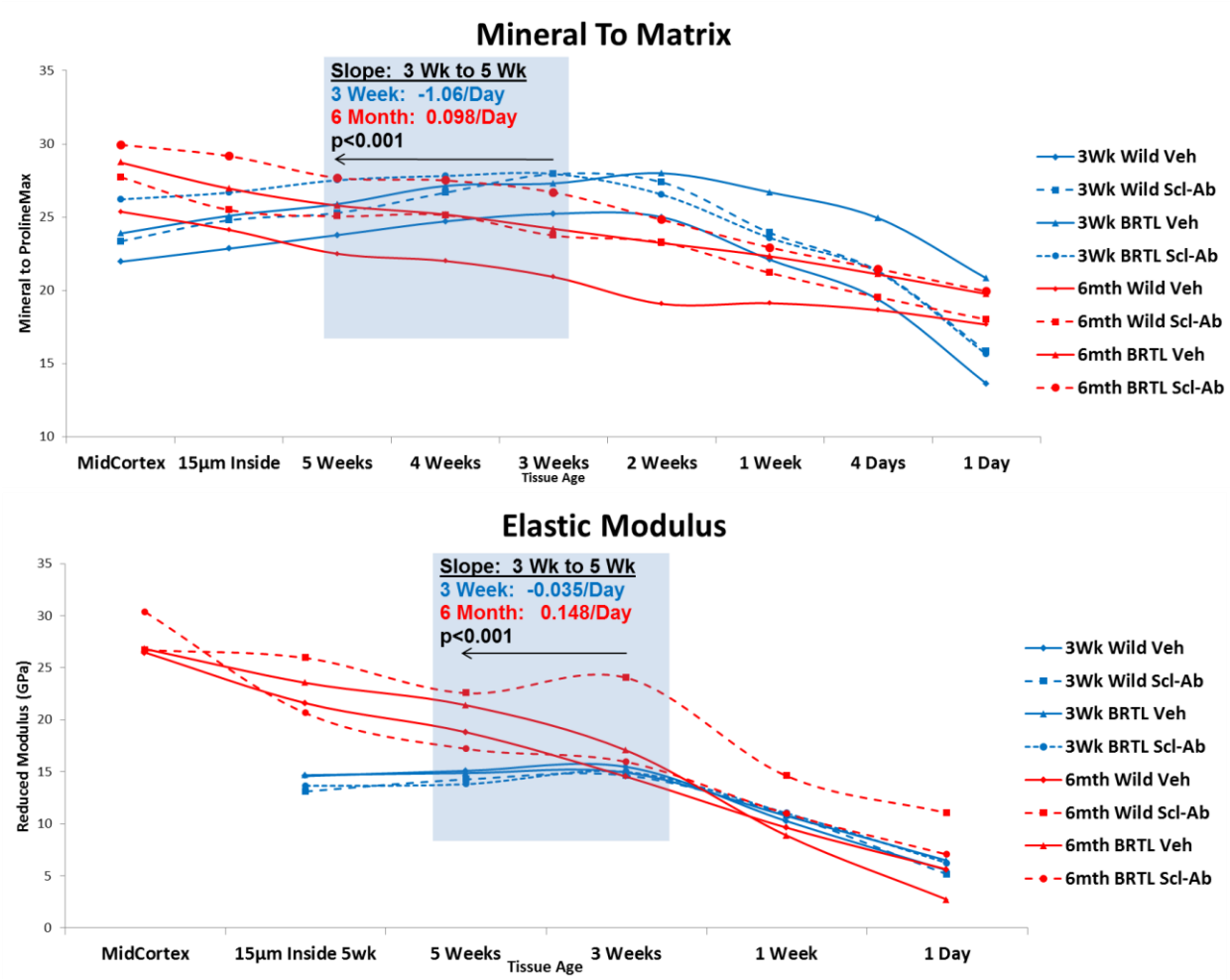

Figure 5.9: Mineral to Matrix and Elastic Modulus Slopes (Grouped by Animal Age). These plots are of the same data shown in Figures 5.3, and 5.7, but displayed on top of one another in order to aid visualization of similar patterns between the two tissue ages. For mineral to matrix, and elastic modulus, the average slope of all specimens from 3 weeks of tissue age, to 5 weeks of tissue age was quantified for rapidly growing 3 week and adult 6mo animals. The sign of the slope value describes correlation with increasing tissue age, and increasing tissue age is shown moving in the left direction on the graph – the reason for the apparent contradiction. Data shown are means, but stdev is not plotted here

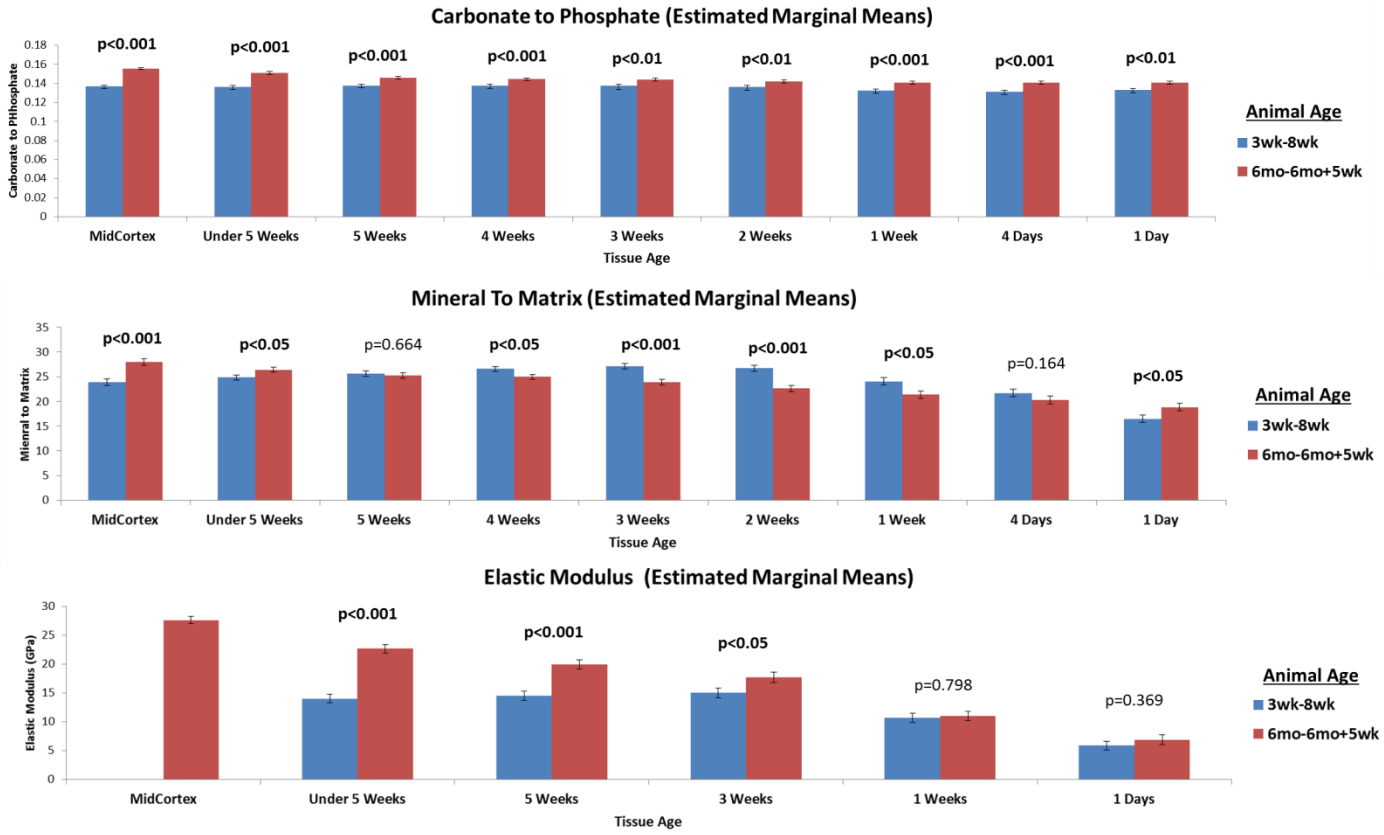

Figure 5.10: Effect of Animal Age on Material Composition and Property Independent of Tissue Age. Differences between Carbonate to Phosphate, Mineral to Matrix, and Elastic Modulus exist between animal ages, even when controlling for tissue age (i.e., tissue ages 5 weeks or less). These differences are apparent in Figures 5.3, 5.5 and 5.7, but can be hard to visualize. Here, we plot the estimated marginal means for each variable across genotype and treatment, and patterns were similar between tissue age. Significant differences from a three-factor anova (Animal Age p-values displayed on graph) suggest that material properties and composition are influenced by animal age, independent of tissue age. All data is mean±stderr.

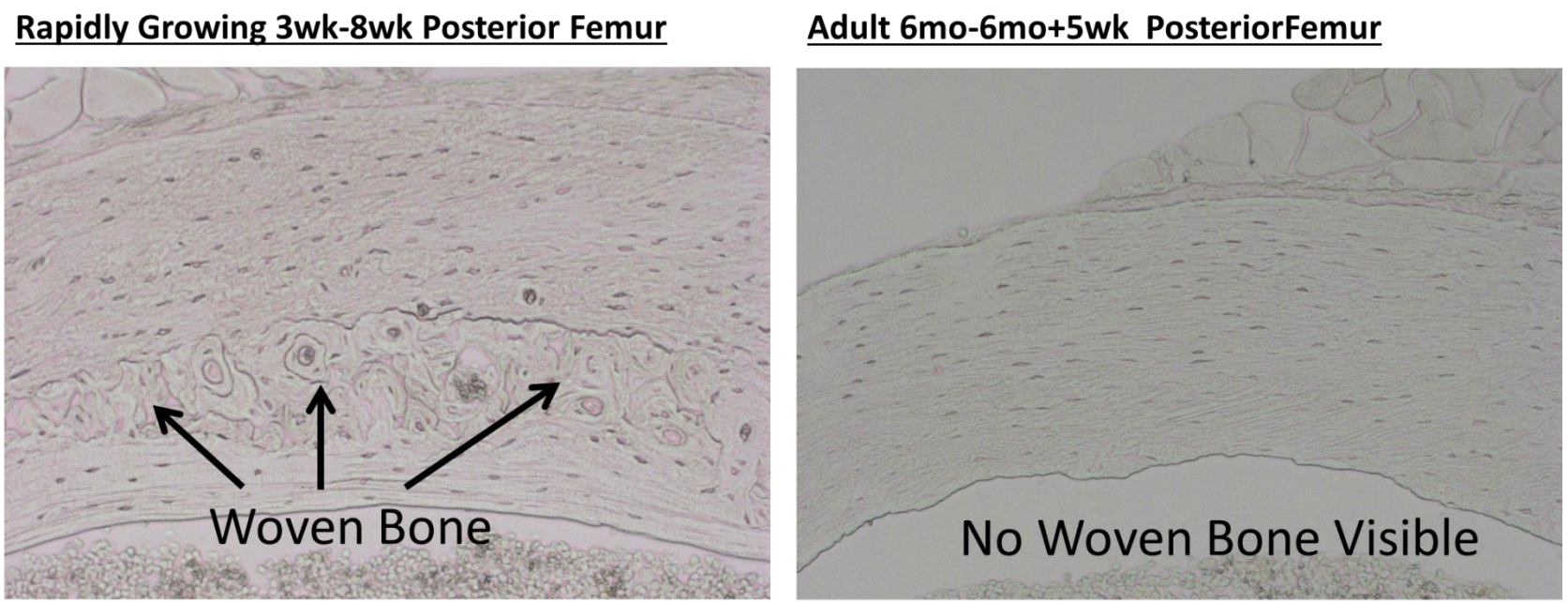

Figure 5.11: Presence of Woven Bone in Rapidly Growing vs Adult Mice. WL Images show presence of woven bone on the posterior mid-diaphyseal femur of rapidly growing animals (8wk at euthanasia) used in this study. This is also seen in the fluorescent image shown in Fig 5.2 No woven bone is visible in the adult 6mo+5wk animals.

References

1. Forlino A, Cabral WA, Barnes AM, Marini JC (2011) New perspectives on osteogenesis imperfecta. Nat Rev Endocrinol 7:540–557. doi: 10.1038/nrendo.2011.81

2. Padhi D, Jang G, Stouch B, et al. (2011) Single-dose, placebo-controlled, randomized study of AMG 785, a sclerostin monoclonal antibody. Journal of Bone and Mineral Research 26:19–26. doi: 10.1002/jbmr.173

3. McClung MR, Grauer A, Boonen S, et al. (2014) Romosozumab in Postmenopausal Women with Low Bone Mineral Density. New England Journal of Medicine 370:412–420. doi: 10.1056/NEJMoa1305224

4. Li X, Ominsky MS, Warmington KS, et al. (2009) Sclerostin antibody treatment increases bone formation, bone mass, and bone strength in a rat model of postmenopausal osteoporosis. J Bone Miner Res 24:578–588. doi: 10.1359/jbmr.081206

5. Ominsky MS, Vlasseros F, Jolette J, et al. (2010) Two doses of sclerostin antibody in cynomolgus monkeys increases bone formation, bone mineral density, and bone strength. Journal of Bone and Mineral Research 25:948–959. doi: 10.1002/jbmr.14

6. Ominsky MS, Niu Q-T, Li C, et al. (2014) Tissue-level mechanisms responsible for the increase in bone formation and bone volume by sclerostin antibody. J Bone Miner Res 29:1424–1430.

7. Li X, Ominsky MS, Warmington KS, et al. (2011) Increased Bone Formation and Bone Mass Induced by Sclerostin Antibody Is Not Affected by Pretreatment or Cotreatment with Alendronate in Osteopenic, Ovariectomized Rats. Endocrinology 152:3312–3322. doi: 10.1210/en.2011-0252

8. Sinder BP, Eddy MM, Ominsky MS, et al. (2013) Sclerostin antibody improves skeletal parameters in a Brtl/+ mouse model of osteogenesis imperfecta. J Bone Miner Res 28:73–80. doi: 10.1002/jbmr.1717

9. Sinder BP, White LE, Salemi JD, et al. (2014) Adult Brtl/+ mouse model of osteogenesis imperfecta demonstrates anabolic response to sclerostin antibody treatment with increased bone mass and strength. Osteoporos Int 1–11. doi: 10.1007/s00198-014-2737-y

10. Sinder B, White L, Caird M, et al. (2012) Sclerostin Antibody Improves Bone Mass and Mechanical Properties in Brtl/+ Model of Osteogenesis Imperfecta When Administered During Growth. J Bone Miner Res 27 (Suppl 1):

11. Jacobsen CM, Barber LA, Ayturk UM, et al. (2014) Targeting the LRP5 Pathway Improves Bone Properties in a Mouse Model of Osteogenesis Imperfecta. J Bone Miner Res. doi: 10.1002/jbmr.2198

12. Ross RD, Edwards LH, Acerbo AS, et al. (2014) Bone Matrix Quality Following Sclerostin Antibody Treatment. J Bone Miner Res n/a–n/a. doi: 10.1002/jbmr.2188

13. Forlino A, Porter FD, Lee EJ, et al. (1999) Use of the Cre/lox Recombination System to Develop a Non-lethal Knock-in Murine Model for Osteogenesis Imperfecta with an α1(I) G349C Substitution. Journal of Biological Chemistry 274:37923 –37931. doi: 10.1074/jbc.274.53.37923

14. McElderry J-DP, Kole MR, Morris MD (2011) Repeated freeze-thawing of bone tissue affects Raman bone quality measurements. J Biomed Opt 16:071407. doi: 10.1117/1.3574525

15. Oliver WC, Pharr GM (1992) An improved technique for determining hardness and elastic modulus using load and displacement sensing indentation experiments. J Mater Res 7:1565.

16. Gong B, Oest ME, Mann KA, et al. (2013) Raman spectroscopy demonstrates prolonged alteration of bone chemical composition following extremity localized irradiation. Bone 57:252–258. doi: 10.1016/j.bone.2013.08.014

17. Zebaze RMD, Jones AC, Pandy MG, et al. (2011) Differences in the degree of bone tissue mineralization account for little of the differences in tissue elastic properties. Bone 48:1246–1251. doi: 10.1016/j.bone.2011.02.023

18. Ishimoto T, Nakano T, Umakoshi Y, et al. (2013) Degree of biological apatite c-axis orientation rather than bone mineral density controls mechanical function in bone regenerated using recombinant bone morphogenetic protein-2. Journal of Bone and Mineral Research 28:1170–1179. doi: 10.1002/jbmr.1825

19. Akkus O, Polyakova-Akkus A, Adar F, Schaffler MB (2003) Aging of Microstructural Compartments in Human Compact Bone. J Bone Miner Res 18:1012–1019. doi: 10.1359/jbmr.2003.18.6.1012

20. Yerramshetty JS, Akkus O (2008) The associations between mineral crystallinity and the mechanical properties of human cortical bone. Bone 42:476–482. doi: 10.1016/j.bone.2007.12.001

21. Bala Y, Depalle B, Farlay D, et al. (2012) Bone micromechanical properties are compromised during long-term alendronate therapy independently of mineralization. J Bone Miner Res 27:825–834. doi: 10.1002/jbmr.1501

22. Balooch G, Balooch M, Nalla RK, et al. (2005) TGF-β regulates the mechanical properties and composition of bone matrix. PNAS 102:18813–18818. doi: 10.1073/pnas.0507417102

23. Thurner PJ, Chen CG, Ionova-Martin S, et al. (2010) Osteopontin deficiency increases bone fragility but preserves bone mass. Bone 46:1564–1573. doi: 10.1016/j.bone.2010.02.014

24. Wang X, Shen X, Li X, Mauli Agrawal C (2002) Age-related changes in the collagen network and toughness of. Bone 31:1–7. doi: 10.1016/S8756-3282(01)00697-4

25. Raghavan M, Sahar ND, Kohn DH, Morris MD (2012) Age-specific profiles of tissue-level composition and mechanical properties in murine cortical bone. Bone 50:942–953. doi: 10.1016/j.bone.2011.12.026

26. Miller LM, Little W, Schirmer A, et al. (2007) Accretion of Bone Quantity and Quality in the Developing Mouse Skeleton. J Bone Miner Res 22:1037–1045. doi: 10.1359/jbmr.070402

27. Kozloff KM, Carden A, Bergwitz C, et al. (2004) Brittle IV Mouse Model for Osteogenesis Imperfecta IV Demonstrates Postpubertal Adaptations to Improve Whole Bone Strength. Journal of Bone and Mineral Research 19:614–622. doi: 10.1359/JBMR.040111

28. Uveges TE, Kozloff KM, Ty JM, et al. (2009) Alendronate Treatment of the Brtl Osteogenesis Imperfecta Mouse Improves Femoral Geometry and Load Response Before Fracture but Decreases Predicted Material Properties and Has Detrimental Effects on Osteoblasts and Bone Formation. Journal of Bone and Mineral Research 24:849–859. doi: 10.1359/jbmr.081238

29. Busa B, Miller LM, Rubin CT, et al. (2005) Rapid establishment of chemical and mechanical properties during lamellar bone formation. Calcif Tissue Int 77:386–394. doi: 10.1007/s00223-005-0148-y

30. Donnelly E, Boskey AL, Baker SP, van der Meulen MCH (2010) Effects of tissue age on bone tissue material composition and nanomechanical properties in the rat cortex. J Biomed Mater Res A 92:1048–1056. doi: 10.1002/jbm.a.32442

31. Burket J, Gourion-Arsiquaud S, Havill LM, et al. (2011) Microstructure and nanomechanical properties in osteons relate to tissue and animal age. J Biomech 44:277–284. doi: 10.1016/j.jbiomech.2010.10.018

CHAPTER 6

Discussion and Conclusion

Much of the data has already been discussed at length in the respective discussion sections for each chapter. This will not be repeated here. However, some discussion points that outline technical considerations, integrate broader concepts, and offer future perspective, are included below.

Interpretation of Dynamic Histomorphometry Data

Chapters 3 and 4 of this thesis included the presentation of regional dynamic histomorphometry data. Traditionally, cortical dynamic histomorphometry data is presented as the average value over the entire periosteal or endocortical surface. Discussed below, are the reasons and conditions to consider deviating from this standard.

There is a fundamental difference between amplifying sites of existing bone formation, and stimulating bone formation at sites that would otherwise be quiescent or resorbing. When bone formation is stimulated at an unnatural location by an intervention, combining this data with regions that would normally have bone formation can bias the result.

Mineral Apposition Rate, or MAR, quantifies the average distance between fluorescent labels (e.g. calcein) given when a mouse was alive. The generally accepted interpretation of MAR is that it indicates osteoblast activity. As specifically put by a recent consortium of experts

in skeletal biology and histomorphometry assembled by the American Society for Bone and Mineral Research, "… apposition rate represents in some sense the activity of a team of osteoblasts." [1] The common interpretation is that if MAR increases, osteoblast activity increased; and if MAR decreases, this indicates that osteoblast activity decreased.

However, when new bone formation is stimulated in areas that were otherwise quiescent or resorptive, the relationship between MAR and osteoblast activity can become misleading. Consider the example shown in Fig 6.1. If we assume that MAR is normally 1 on the periosteal surface of the top half of the bone, and no labeling is present on the bottom half of the bone, the average MAR is 1. Now, let us assume that an anabolic intervention was taken that amplified bone formation on the existing top half of the bone (from 1 to 1.5), and stimulated bone formation to occur (from nothing to 0.5) on the bottom half. The average MAR in this case would also be 1! (the average of 1.5 on the top half, and 0.5 on the bottom) Thus, even though the anabolic intervention increased MAR at every skeletal location by 0.5, the average MAR did not change, and remained at 1. Therefore, a typical conclusion of this data would be that the intervention did not alter osteoblast activity because the average MAR did not change, even though the osteoblast activity at every skeletal location was increased. This does not make sense.

The second example given in Fig. 6.2 is similar to above, and serves to illustrate the potentially absurd. Without walking through the example again, we can see that a scenario is possible in which MAR is increased at every skeletal location, but the average MAR decreases.

The regional analysis presented in Chapters 3 and 4 serves two purposes. First, it separates dynamic histomorphometry data by anatomic location. Second, as the pattern of bone formation is strongly conserved with anatomic location, it allowed us to separately analyze

regions of bone that were already forming bone, and regions that were largely quiescent or resorbing. However, a defined anatomical pattern of bone formation may not be present in all instances, yet an investigator may still wish to separately analyze regions with pre-existing bone formation. In such situations, one could administer a fluorescent label several days prior to the intervention, which would label all sites that were forming bone before the start of the experiment. These regions could then be separately analyzed.

For many studies, such a detailed analysis may be unwarranted and not provide additional insight. However, in any scenario where an intervention or treatment alters mineralizing surface, and/or bone modeling, such an analysis method may clarify the data and should be considered. Two such examples are sclerostin antibody treatment as discussed in this dissertation, and mechanical loading studies, both of which stimulate bone formation at new skeletal locations. With the continuing emergence of treatments and skeletal interventions which stimulate new bone formation, consideration of this effect will become increasingly relevant.

Relationship of Sclerostin Expression to Anatomical Location

The regional dynamic histomorphometry data described in chapters 3 and 4 reveal several patterns of bone formation around the femoral mid-diaphyseal cortex. First, the data confirm that cortical drift is strong in rapidly growing animals, with bone formation on the periosteal posterior surface, and endosteal anterior surface. Conversely, the opposing endosteal posterior and periosteal anterior surfaces were either quiescent or resorptive. This general pattern of cortical drift is maintained in adult 6 mo animals, but the formation rates are much lower. In addition, we observed that Scl-Ab was able to consistently stimulate bone formation on quiescent surfaces in adult animals, but the Scl-Ab response on these surfaces was inconsistent in rapidly

growing mice. Among several possible factors, we speculated that sclerostin expression levels around the cortex may be correlated to these findings.

Given that sclerostin is an inhibitor of bone formation via the canonical wnt pathway, we broadly hypothesized that there would be an inverse correlation between regional sclerostin expression and regional patterns of bone formation. That is, regions of cortex characterized by high levels of bone formation would exhibit low sclerostin expression, and vice-a-versa. If true, this could explain several of our findings. For example, as rapidly growing animals have high levels of bone formation relative to adult 6 mo animals, we hypothesized that there would be relatively greater sclerostin expression near sites of bone formation in adult 6 mo animals, compared to rapidly growing mice. By dynamic histomorphometry, we found that sites already high in bone formation in rapidly growing animals were not responsive to Scl-Ab, but sites of pre-existing bone formation in adult animals were able to significantly increase MAR with treatment. One potential explanation for the lack of a Scl-Ab effect in rapidly growing animals is sufficiently low sclerostin expression resulting in no protein for the treatment to inhibit.

Preliminary studies to answer these questions and assess sclerostin expression patterns are underway. Specifically, we have performed immunostaining for sclerostin on 8 week old (rapidly growing) and 6 mo old (adult) WT and Brtl/+ untreated animals, with n=5/group (Fig 6.3). Stained transverse sections were located at a femoral mid-diaphyseal cortex location on transverse sections, identical to those analyzed by dynamic histomorphometry in Chapters 3 and 4.

The data is not definitive at this point, but several initial conclusions can be reached and qualitative observations suggest future research directions. First, and perhaps not surprisingly, sclerostin IF images do not suggest that regional sclerostin levels inversely correlate with local

bone formation rate in a consistent manner. For example, while sclerostin expression does appear lower on the periosteal posterior surface of 6 mo animals (a site of relatively high bone bone formation) when compared to the endosteal posterior surface, sclerostin expression is also very low on the posterior endosteal surface of 8 wk old animals (a site of low bone formation) (Fig 6.3). Although such an inverse correlation does not readily explain our results, initial sclerostin expression data does suggest several consistent patterns, as well as directions for future study, which are outlined below.

There was a large variation in canalicular expression of sclerostin across the cortex, and these relative differences were more apparent than differences in osteocytic expression (Fig 6.3). Moreover, the differences in canalicular expression appear separated by a region of woven bone. This is particularly true in 8 wk old animals. For example, in the posterior region of the femur, canaliculuar sclerostin expression is consistently low on the endosteal side of the woven bone, and relatively high on the periosteal side of the woven bone(Fig 6.3). Whether this is a result of altered sclerostin expression in these regions, or simply an altered canalicular network, remain to be determined. While enumeration of sclerostin positive osteocytes is a standard outcome of such analysis [2], the data presented here suggest that canalicular levels should not be ignored; particularly when the amount of sclerostin reaching cells on the bone surface is of primary importance.

Additionally, we observed localization of sclerostin expression in the periosteum in both rapidly growing and adult animals. The accumulation of an inhibitor of bone formation at a site of bone progenitor cells is intriguing, particularly at an anatomic location with high bone formation rates.

Unique Considerations of Scl-Ab Use in a Rapidly Growing, Pediatric OI Patient

The use of Scl-Ab in an adult OI population will likely be similar to that of osteoporotic patients, for which it is presently in FDA trials [3, 4]. While there will may be differences in effectiveness between OI type, as has been observed with PTH [5], the application of a Scl-Ab treatment regimen should be straightforward.

However, dosing regimen and use of Scl-Ab in a pediatric population will require several unique considerations. These include potential side-effects of Scl-Ab use in a developing skeleton, sequential or co-treatment with a BP, and Scl-Ab dosing regimen as it relates to efficacy over a protracted time period.

Patients with sclerosteosis have too much bone growth, and experience side effects. As these side-effects are thought to manifest during development, there are concerns about the use of Scl-Ab in a developing skeleton. In particular, patients with sclerosteosis can experience intracranial apposition resulting in impaction of the foramina, leading to death [6, 7]. In defense of Scl-Ab use in the developing skeleton, a reasonable argument observes that these side-effects are confined to patients with two non-functioning sclerostin genes. Meanwhile, sclerosteosis "carriers" that have one functioning copy of the *SOST* gene have elevated bone mass, but do not suffer these deleterious side effects [8]. Treatment with an inhibiting antibody is likely analogous to a sclerosteosis "carrier", and complete inhibition of sclerostin by Scl-Ab treatment is unlikely. Regardless, application of sclerostin inhibiting antibodies to a growing skeleton should proceed with caution.

A growing body of literature suggests that the anabolic effect of Scl-Ab is temporary, and bone formation levels, or serum markers of bone formation, revert to pre-treatment levels despite continued injections. This has been demonstrated in adult rats over the course of 12-26 weeks,

and in human clinical trials of post-menopausal women over the course of a year[4, 9]. The duration of an anabolic Scl-Ab effect in the context of a pediatric skeleton is unknown. Moreover, this question is likely impossible to answer in murine models – where the age at puberty is similar or greater than the time the time it takes for an anabolic Scl-Ab effect to subside. Animal models which age slower are necessary to answer this question. But assuming that the anabolic effect subsides with ~1 year of Scl-Ab therapy in a pediatric OI patient, what action should be taken? A simple suggestion might be to halt Scl-Ab therapy for a period of time until it again becomes effective. However, this may be undesirable in a pediatric patient with rapid linear growth, leaving significant regions of new bone without the benefit of therapy. Moreover, Scl-Ab cessation without anti-resorptive treatment, may lead to loss of Scl-Ab induced bone gains.

Presently, bisphosphonates (BP) are commonly used to treat OI and are capable of increasing bone mass, particularly in the axial skeleton. When designing an OI and Scl-Ab clinical trial, it may be viewed as unethical to deny BP and have a true placebo control group. Rather, a combination treatment Scl-Ab+BP treatment strategy not only assuages ethical concerns, but may prove the best for patient outcomes. Combination, and sequential, treatment strategies are currently being explored in animal models of OI.

Perspective: Brtl/+ Scl-Ab Data as it Relates to OI Patient Outcomes

The outcomes observed in this dissertation are impressive, consistent with other Scl-Ab studies. Indeed, after a 5 week treatment period with Scl-Ab, we were able to increase bone mass in adult 6 mo Brtl/+ by over 20% in cortical bone, increase cortical ultimate load by 127%, and trabecular BV/TV by 119%. In a rapidly growing 3 wk Brtl/+ model of Type IV OI, Scl-Ab

treatment "rescued" Brtl/+ femoral strength to a level not significantly different than WT Veh controls. This does not imply that Scl-Ab will have the same effect in humans, and this "rescue" certainly does not imply that Scl-Ab represents a "cure" – even for the specific case of Type IV OI.

Treatment data from mouse models are almost always more impressive than that observed in humans. The bone cells upon which a treatment acts remain of roughly similar size between humans and mice, but the bones of a mouse are orders of magnitude smaller. This makes it easy for bone treatments to induce large gains, on a percentage basis, in murine bone mass. By definition, an identical cellular response between humans and mice will result in different whole bone changes on a percentage basis.

In addition, the body mass differences between Brtl/+ and WT animals confound simple interpretation of the Brtl/+ whole bone phenotype. For example, at 8 weeks of age (Chapter 4), Brtl/+ Veh mice have 23.8% reduced Yield Load and 38.4% less Ultimate Load than WT Veh animals. However, Brtl/+ mice also have 22.4% less body mass than WT at 8 weeks of age. Moreover, with time, both Brtl/+ body mass and whole bone strength approach WT levels. At ~7 months of age, Brtl/+ mice described in Chapter 3 only have an 8.5% reduction in the mean Yield Load, and a 13.5% reduction in Ultimate Load relative to WT Veh. Correspondingly, mean Brtl/+ body mass is only reduced 9.5% at ~7 months of age. Thus, while Brtl/+ bones are certainly weaker, particularly at young animal ages, it is inaccurate to call them less functional without consideration of body weight differences. Indeed, the Brtl/+ mouse does not suffer spontaneous fractures. While some deficits in bone strength and material property still remain in Brtl vs WT after accounting for body mass, the differences are not as large as the whole bone strength data suggest. However, the critical demonstration of these studies is not a "rescue" of

Brtl/+ whole bone strength to WT Veh levels by Scl-Ab. Rather, is it that Scl-Ab was able to stimulate Brtl/+ bone formation and increase cortical bone mass, which led to increase bone strength despite retention of the collagen material defect.

The success of Scl-Ab in OI patients will be explicitly related to its ability to stimulate bone formation in human OI osteoblasts. Moreover, the ability of Scl-Ab to stimulate modeling bone formation in the diaphysis of long bones, particularly on the periosteal surface, will be of critical importance towards improving patient outcomes relative to bisphosphonates. Mild cases of OI, such as Type I, are more likely to benefit from Scl-Ab treatment as moderate increases in bone mass can represent a significant portion of the fracture risk. Consider the severe cases of Type IV OI, or Type III, where patient presentation is severe with progressive limb deformity and bone that can radiologically appear like "popcorn". Even if Scl-Ab is able to stimulate bone formation in these patients, any functional benefit is likely small relative to the severity of OI in the patient. More generally, it is unlikely that any therapy which acts by inhibiting osteoclasts, or increasing osteoblast activity, will ever eliminate OI fracture risk. Continued investigation into therapies which attempt to address the underlying cause of OI (e.g. gene therapy) are paramount to improving OI patient outcomes.

Conclusion

Despite all of the above limitations, Scl-Ab does represent a new candidate therapy for OI. The ability to stimulate bone formation in the Brtl/+ mouse model is encouraging, and mechanistically different from presently available treatment options. Critical to the success of Scl-Ab in OI patients, will be the ability to stimulate bone formation at cortical sites, particularly at the periosteal surface, as was demonstrated in the Brtl/+ mouse.

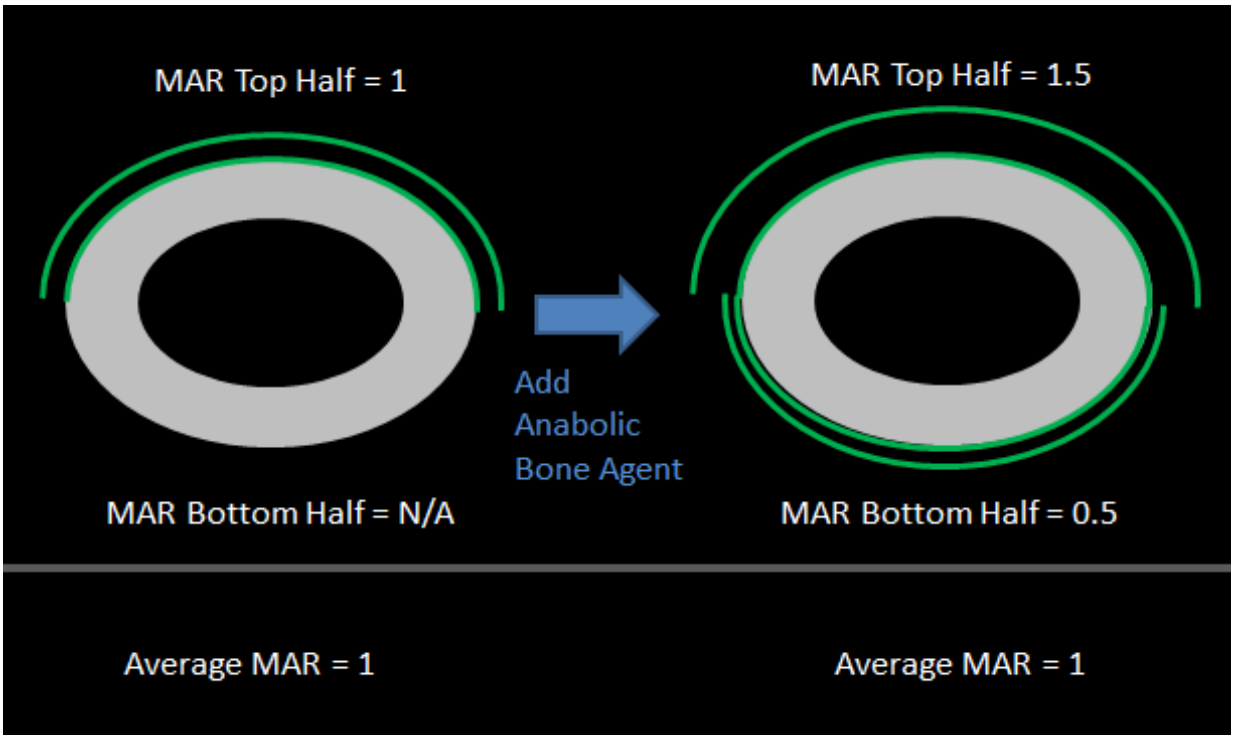

Figure 6.1: Illustration of Confounding Effect of Average MAR. Figure shows the potential effect of stimulating bone formation at a previously queisecent site on the average mineral apposition rate (MAR). Even though bone formation rate increased at every skeletal location, the average MAR did not change.

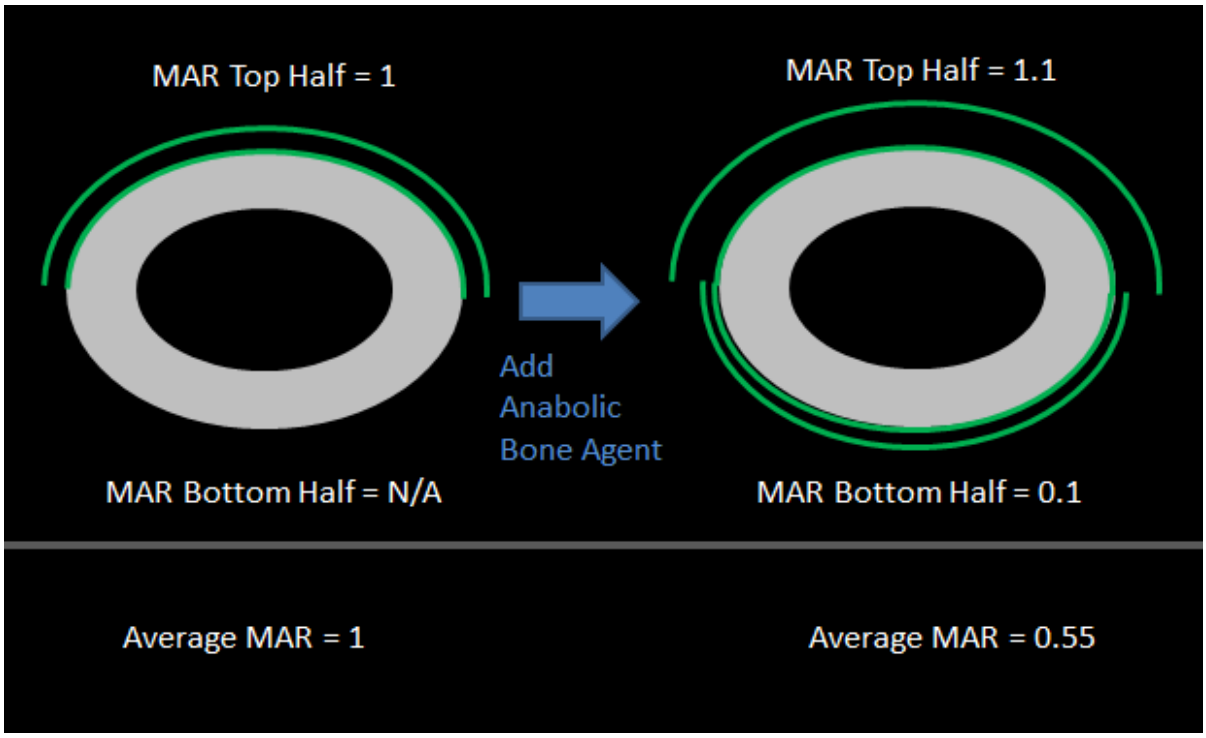

Figure 6.2: Additional Illustration of Confounding Effect of Average MAR. Figures shows the potential effect of stimulating bone formation at a previously queisecent site on the average mineral apposition rate (MAR). Even though bone formation rate increased at every skeletal location, the average MAR decreased.

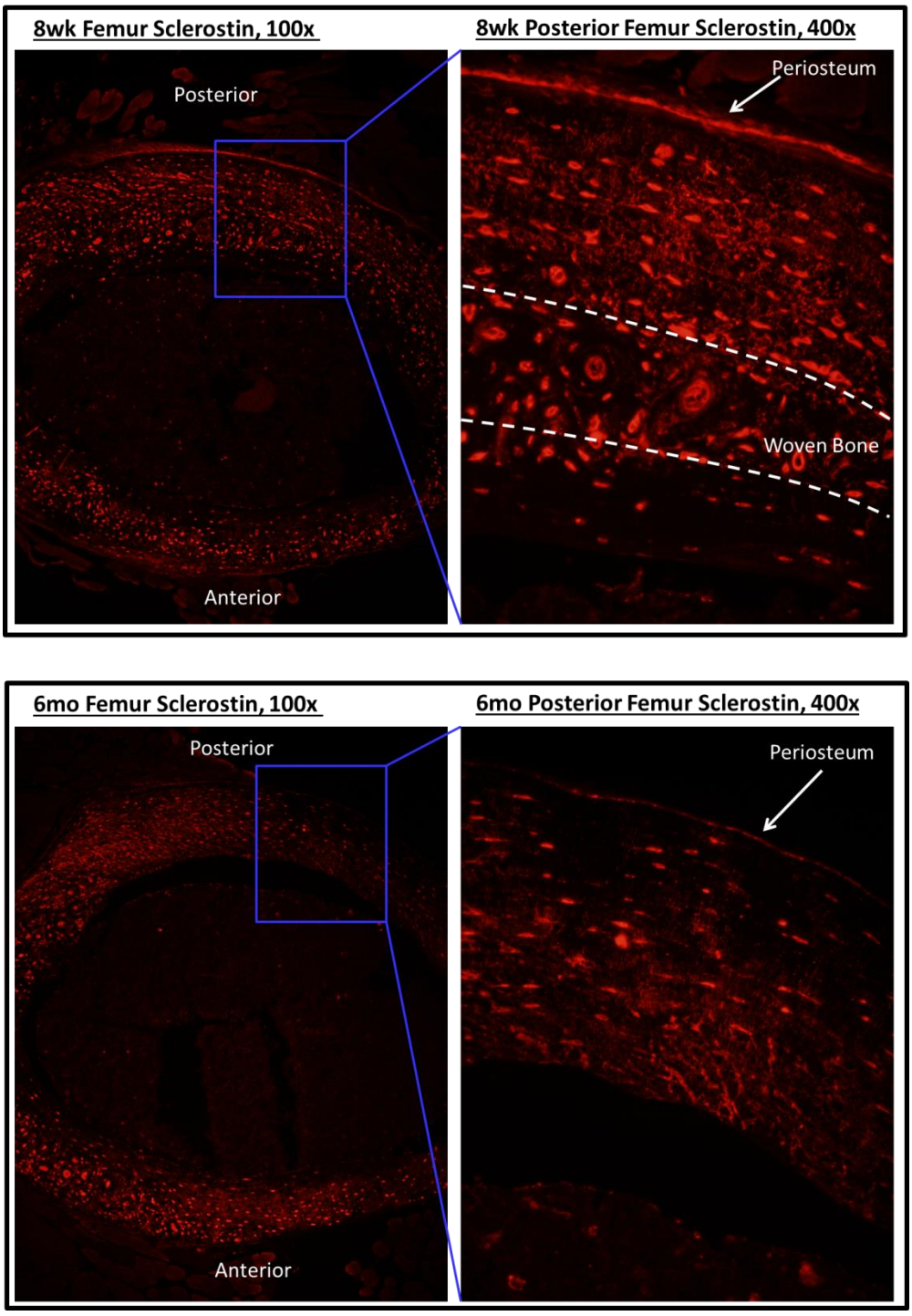

Figure 6.3: Sclerostin Immunofluoresnce Staining at Femoral Mid-Cortex. Images are taken from mid-diaphyseal femur in 8 wk and 6 mo WT animals.

References

1. Dempster DW, Compston JE, Drezner MK, et al. (2013) Standardized nomenclature, symbols, and units for bone histomorphometry: A 2012 update of the report of the ASBMR Histomorphometry Nomenclature Committee. Journal of Bone and Mineral Research 28:2–17. doi: 10.1002/jbmr.1805

2. Robling AG, Niziolek PJ, Baldridge LA, et al. (2008) Mechanical Stimulation of Bone in Vivo Reduces Osteocyte Expression of Sost/Sclerostin. Journal of Biological Chemistry 283:5866 –5875. doi: 10.1074/jbc.M705092200

3. Padhi D, Jang G, Stouch B, et al. (2011) Single-dose, placebo-controlled, randomized study of AMG 785, a sclerostin monoclonal antibody. Journal of Bone and Mineral Research 26:19–26. doi: 10.1002/jbmr.173

4. McClung MR, Grauer A, Boonen S, et al. (2014) Romosozumab in Postmenopausal Women with Low Bone Mineral Density. New England Journal of Medicine 370:412–420. doi: 10.1056/NEJMoa1305224

5. Orwoll ES, Shapiro J, Veith S, et al. (2014) Evaluation of teriparatide treatment in adults with osteogenesis imperfecta. J Clin Invest 124:491–498. doi: 10.1172/JCI71101

6. Epstein S, Hamersma H, Beighton P (1979) Endocrine function in sclerosteosis. S Afr Med J 55:1105–1110.

7. Hamersma H, Gardner J, Beighton P (2003) The natural history of sclerosteosis. Clin Genet 63:192–197.

8. Gardner JC, van Bezooijen RL, Mervis B, et al. (2005) Bone Mineral Density in Sclerosteosis; Affected Individuals and Gene Carriers. J Clin Endocrinol Metab 90:6392–6395. doi: 10.1210/jc.2005-1235

9. Li X, Niu Q-T, Warmington KS, et al. (2012) Short- and Long-term Effects of Sclerostin Antibody in an Ovariectomized Rat Model. J Bone Miner Res 27 (Suppl 1):